NASA Contractor Report 4100

Ultrasonic Characterization of the Nonlinear Elastic Properties of Unidirectional Graphite/Epoxy Composites

William H. Prosser
The Johns Hopkins University
Baltimore, Maryland

Prepared for
Langley Research Center
under Grant NGT 21-001-802

National Aeronautics
and Space Administration

Scientific and Technical
Information Division

1987

Abstract

Because of their high strength and stiffness together with their light weight, fiber reinforced composite materials offer great potential for applications particularly in the aerospace industry. The weight savings translate into increased performance and decreased fuel costs. In addition, the use of these materials avoids the dependence on foreign sources for the critical elements needed in the new exotic metallic alloys that otherwise might be used. Early research has proven the usefulness of these materials, but the need to quantitatively characterize important material properties and develop applicable nondestructive evaluation techniques remains. Important physical properties (i.e. mechanical, thermal, electrical) need to be measured. Moreover, relationships between these physical properties and important engineering properties such as strength, residual strength after impact and fatigue loading, and fiber-matrix interfacial strength need to be examined to provide a basis for quantitative nondestructive evaluation of these materials.

Toward this goal, linear and nonlinear elastic properties have been demonstrated to be important physical properties in conventional materials. In particular, nonlinear properties are important in the nondestructive determination of applied and residual stress (strain) as well as measuring the interatomic bonding forces in crystalline solids. Also, several investigations have established a possible relationship between nonlinear elastic properties and ultimate strength in aluminum and carbon steel.

This work presents the theoretical treatment of linear and nonlinear elasticity in a unidirectionally fiber reinforced composite as well as measurements for a unidirectional graphite/epoxy composite (T300/5208). Linear elastic properties were measured by both ultrasonic and strain gauge measurements. The nonlinear properties were determined by measuring changes in ultrasonic "natural" phase velocity with a pulsed phase locked loop interferometer as a function of stress and temperature. These measurements provide the basis for further investigations into the relationship between

nonlinear elastic properties and other important properties such as strength and fiber-matrix interfacial strength in graphite/epoxy composites.

Acknowledgments

The author would like to thank a number of people without whom this work would not have been possible. In the Materials Science and Engineering Department at Johns Hopkins University, much gratitude is due Dr. R. E. Green, Jr. As my faculty advisor he provided much insight into the technical aspects of this work and was a tremendous source of encouragement and inspiration. Dr. Ron Eby and Dr. Jim Wagner were of technical assistance and provided invaluable comments on the preparation of this essay. Also, the students and staff of this department who provided friendship, assistance, and support are deserving of mention and gratitude.

Numerous people in the Materials Characterization and Instrumentation Section (MCIS) at NASA Langley Research Center are also due thanks. Dr. Joseph S. Heyman, Head of this Section, provided the initial motivation for this research and aided it to completion with generous financial support and technical guidance. Dr. Yost, Sid Allison, Dr. Cantrell, Peter Kushnick, Jerry Clendenin and others at MCIS provided tremendous assistance by sharing their equipment and expertise to make these measurements possible.

Thanks is due to my wife Karen and our families who have provided love, support, and understanding throughout this work.

This research was supported by NASA with a Graduate Student Research Fellowship Training Grant (NGT 21-001-802) as well as the Johns Hopkins Center for Nondestructive Evaluation. Thanks are due Dr. Heyman and Dr. Green respectively in this regard.

TABLE OF CONTENTS

LIST OF FIGURES

LIST OF TABLES

I. INTRODUCTION

The theory of nonlinear elasticity and the measurement of nonlinear elastic properties of materials have been subjects of great interest for many years. Nonlinear elasticity is important in many areas of physical measurements including the characterization of interatomic bonding forces and anharmonic behavior of a crystal lattice, nondestructive measurement of applied and residual stress (strain) using ultrasonic techniques, and stress-strain relations in finite strain of materials. This will be discussed in more detail later.

One of the first successful theoretical treatments of the subject of nonlinear elasticity was presented by Murnaghan [1] in 1937. He extended the theory of infinitesimal elasticity to the general case including strains of any magnitude. Birch [2], in 1938, pointed out the importance of this theory for the case of seismic waves superimposed on the large hydrostatic pressures within the earth. Since that time a number of researchers have presented volumes of material on the subject of nonlinear elasticity. Although a detailed review of this information is beyond the scope of this essay, important work in several areas will be discussed. First, literature discussing the basic property of nonlinear elasticity and its effects on ultrasonic wave propagation will be reviewed. This will be followed by a discussion of some of the literature involving the development of theoretical and measurement techniques as well as some of the applications for nonlinear elastic research. Also, previous measurements of the nonlinear properties of polymers and composites will be discussed.

The study of the mechanical properties of materials is concerned with the deformation of a material upon application of an external force as well as its behavior upon removal of that force. There are three types of mechanical behavior exhibited by materials under loading. These are elastic, anelastic and plastic. In elastic deformation, the material deforms instantaneously upon application of load and returns to its

original shape instantaneously upon removal of load. This behavior can be either linear or nonlinear. This is demonstrated in Figs. 1.1 (a) and 1.1 (b) for the simple case of uniaxial loading where the elongation serves as a measure of the deformation of the material. In anelastic deformation, the material deforms over time upon the application of load and returns to its original shape over time upon the removal of load. This is demonstrated in Fig. 1.2. When a material undergoes plastic deformation, it deforms instantaneously upon application of load but does not return to its original shape upon the removal of the load. Fig. 1.3 shows the load-elongation characteristics of plastic deformation.

However, the behavior of real materials can be a combination of these three types of mechanical behavior and is generally dependent on the amount of load applied. The material may be elastic for small loads but the deformation may be anelastic or plastic at higher loads. Also changes in other parameters such as temperature may affect the response of the material upon loading. The present work is interested in the case of nonlinear elastic behavior where the deformation is recoverable but not linearly related to the applied load.

An understanding of linear and nonlinear elasticity can be gained by considering theories of interatomic bonding in molecules such as the Born [3] and Madelung [4] theories for ionic crystals. In these theories, the total energy of bonding is the energy due to the sum of the attractive and repulsive forces between the atoms multiplied by the distance over which they act. The general shape of such a curve is shown in Fig. 1.4 with the potential energy (E) versus the separation distance (r) plotted. The equilibrium separation distance is r_0 where the potential energy is at a minimum E_0. To move the atoms closer together or further apart raises the energy of the system and thus requires the application of an external force. This force can be determined by taking the derivative of E with respect to separation distance for the curve in Fig. 1.4. The resulting force versus separation distance curve is then a simple analogy on the atomic

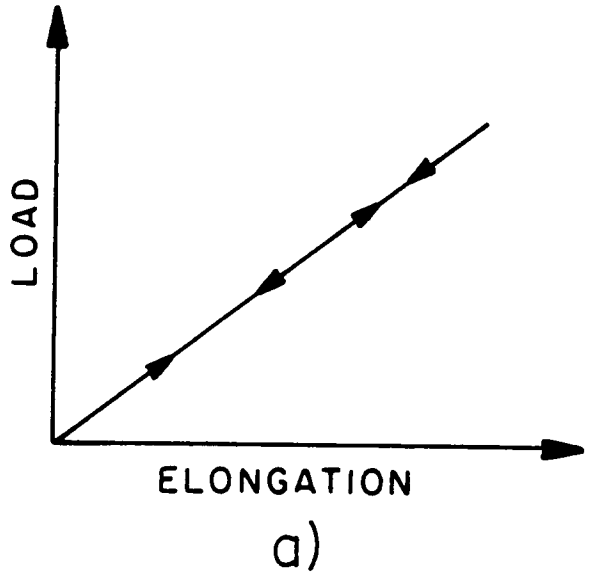

Figure 1.1 - (a) Load-Elongation curve for linear elastic deformation.

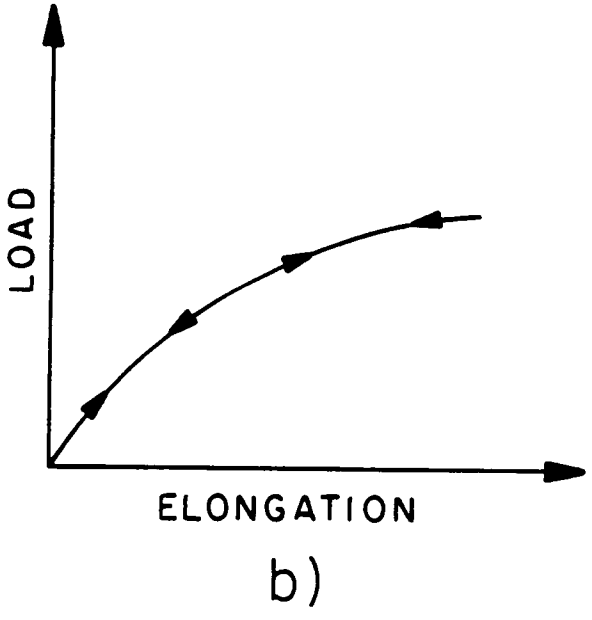

Figure 1.1 - (b) Load-Elongation curve for nonlinear elastic deformation.

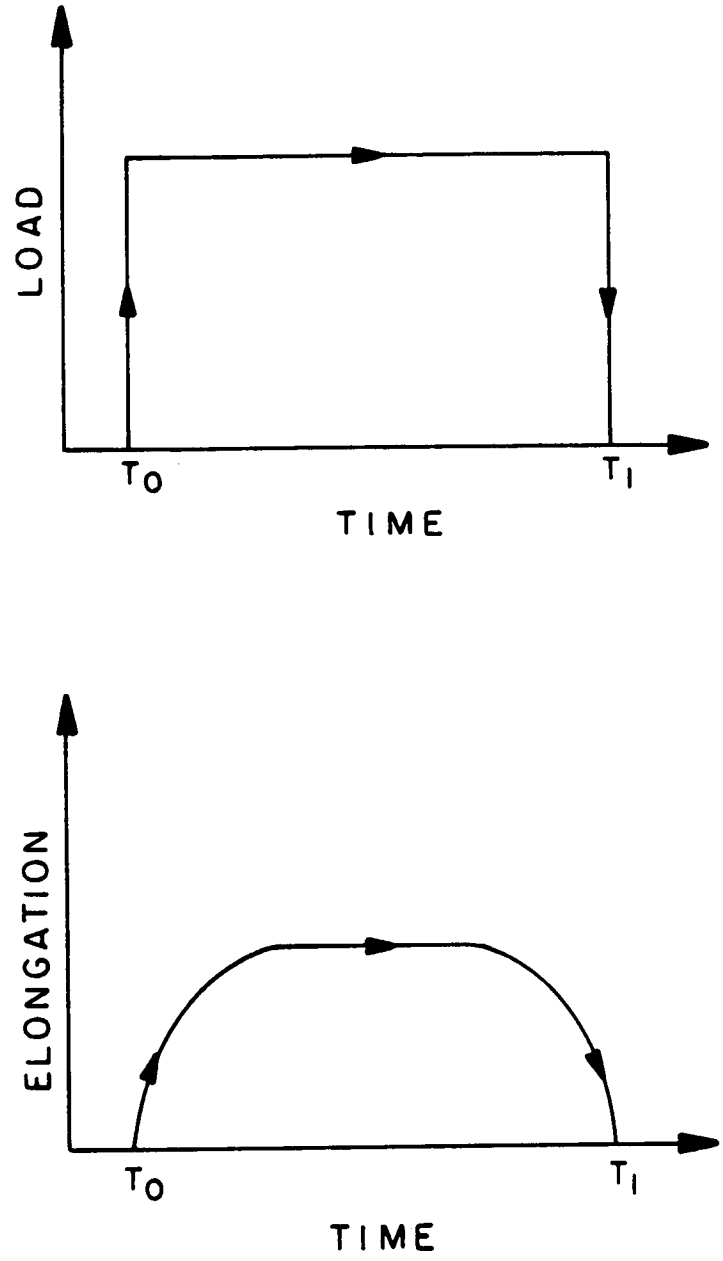

Figure 1.2 - Load-Time and Elongation-Time curves illustrating anelastic deformation.

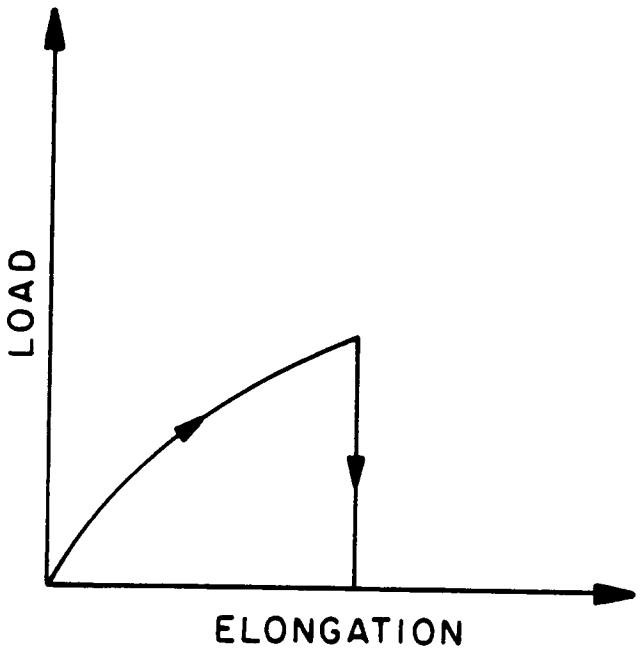

Figure 1.3 - Load-Elongation curve for plastic deformation.

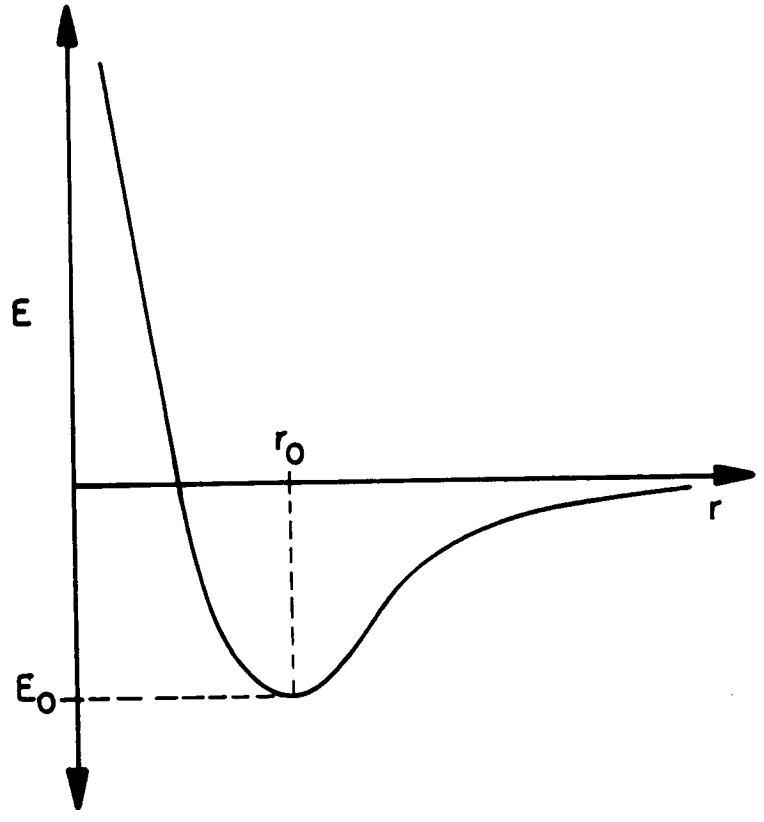

Figure 1.4 - Potential Energy (E) - Separation distance (r) curve for interatomic bonding.

scale to the load-displacement curves discussed earlier.

For small displacements about r_0 , the potential energy curve appears to be and can be approximated as a quadratic function. Therefore its derivative is a linear curve. That is, the relationship between force and separation distance (load and elongation) is linear for small displacements about equilibrium. However, as the amplitude of the displacement becomes larger, the potential energy curve is no longer quadratic. This implies that the force-separation curve is no longer linear which gives rise to nonlinear elasticity.

Another interesting point about Fig. 1.4 is the asymmetry of the potential energy curve about r_0 . This provides a simple explanation for the understanding of thermal expansion in materials. Since the curve is asymmetric, as the material is heated and the atomic lattice vibrations increase, the mean separation distance between atoms changes. For the curve in Fig. 1.4, the mean separation distance increases with increasing amplitude vibrations about r_0 . Thus, in agreement with empirical observations in most materials, expansion occurs as the material is heated.

Because of the small strains (on the order of 10^{-6}) imposed on the sample during ultrasonic wave propagation, nonlinear elastic behavior is generally neglected in the theories of the propagation of ultrasonic waves. However, as pointed out by Green [5], there are three cases where nonlinear elasticity may become important in elastic wave propagation. First, the amplitude of the wave may become large enough to cause finite strains in the material. In the second case, nonlinear behavior may occur when a small amplitude wave is superimposed on a large external static stress. Also, nonlinear effects may be caused by defects in the material which cause localized regions of finite strain.

The effects of nonlinear elasticity on ultrasonic wave propagation were also pointed out by Green [5]. These include the distortion of finite amplitude sinusoidal longitudinal waves. As they propagate, energy from the fundamental frequency is transferred into the harmonics that are generated. The effect has been used by

numerous investigators to measure the nonlinear properties of solids. Measurements on aluminum single crystals as well as NaCl, KCl, LiF and a magnesium aluminum alloy were presented by Gedroĭts and Krasil'Nikov [6] in 1963. Breazeale and Thompson [7] reported measurements of harmonic distortion in polycrystalline aluminum also in 1963 which was followed by numerous other investigations.

Another effect of nonlinear elasticity on ultrasonic wave propagation is that a pure mode nonlinear longitudinal wave may propagate alone, but a nonlinear transverse wave must have a longitudinal component. Also, nonlinear transverse waves do not distort when propagating in a defect free solid.

Nonlinear elastic waves can interact with each other in a solid to produce other waves. This interaction can also take place with thermal phonons to cause energy loss from the elastic wave. The amount of interaction depends on the amplitude of the elastic waves. Interactions of two nonlinear ultrasonic waves to produce a third ultrasonic wave were demonstrated by Rollins [8] in 1963 in fused silica, polycrystalline aluminum and polycrystalline magnesium. Rollins, Taylor and Todd [9] demonstrated this phenomenon again in 1964 and reported the measurements to be correct to within an order of magnitude with predictions based on the measured third order elastic constants of polycrystalline magnesium. Since this time, further examinations of nonlinear wave interactions have followed.

Another effect of nonlinearity in elastic wave propagation is that the velocity of a small amplitude ultrasonic wave superimposed on a large static stress is dependent on the amount of static stress applied. It is this effect which provides the basis for the measurement technique used in this research and will thus be discussed in more detail. The effect can be accounted for by two simple theoretical explanations. In the first, the equation for the velocity of an elastic wave propagating along a long thin rod is recalled to be

$$v = \left(\frac{E}{\rho}\right)^{\frac{1}{2}} \tag{1.1}$$

where v is the ultrasonic phase velocity,

E is Young's modulus

and ρ is the density.

This is based on the assumption that the material is homogeneous, isotropic and behaves in a linear elastic fashion. These assumptions imply that the constitutive equation of the material has the form

$$\sigma = E\epsilon \tag{1.2}$$

where σ is the stress

and ϵ is the strain.

If a nonlinear constitutive equation is used such as

$$\sigma = E_1\epsilon + E_2\epsilon^2, \tag{1.3}$$

it follows that the velocity will now depend on strain and therefore stress.

An alternative approach to understanding this is based on the potential energy theory for interatomic bonding discussed earlier. Since the velocity of ultrasonic waves, together with the density of the medium give a measure of the modulus (second derivative of the potential energy), this modulus can be evaluated as a function of strain (or stress) by measuring the velocity as a function of strain (or stress). Also, since for large displacements (i.e. finite strain), the potential energy function is not a simple quadratic, the modulus and thus the velocity would be expected to change with applied stress. As will be seen later, the relationship between velocity and stress should be linear if terms up to third order in strain are included in the elastic theory.

The theoretical development of the equations relating ultrasonic velocity to stress began with the original work on finite deformation of materials by Murnaghan [1]. This work provided the basis for the theory presented by Hughes and Kelly [10] in 1953 in which they derived wave speeds as a function of stress in homogeneous, isotropic

materials. They considered both uniaxial and hydrostatic compression for different combinations of longitudinal and transverse (shear) mode waves. The following seven equations were presented:

$$\rho_0 v_{x0}^2 = \lambda + 2\mu - \frac{P}{3K_0}(6l + 4m + 7\lambda + 10\mu) \tag{1.3}$$

$$\rho_0 v_{y0}^2 = \mu - \frac{P}{3K_0}(3m - \frac{1}{2}n + 3\lambda + 6\mu) \tag{1.4}$$

$$\rho_0 v_{xx}^2 = \lambda + 2\mu - \frac{P}{3K_0}(2l + \lambda + \frac{\lambda+\mu}{\mu}(4m + 4\lambda + 10\mu)) \tag{1.5}$$

$$\rho_0 v_{yx}^2 = \mu - \frac{P}{3K_0}(m + \frac{\lambda n}{4\mu} + 4\lambda + 4\mu) \tag{1.6}$$

$$\rho_0 v_{xy}^2 = \lambda + 2\mu - \frac{P}{3K_0}(2l - \frac{2\lambda}{\mu}(m + \lambda + 2\mu)) \tag{1.7}$$

$$\rho_0 v_{yy}^2 = \mu - \frac{P}{3K_0}(m + \frac{\lambda n}{4\mu} + \lambda + 2\mu) \tag{1.8}$$

$$\rho_0 v_{yz}^2 = \mu - \frac{P}{3K_0}(m - (\frac{\lambda+\mu}{2\mu})n - 2\lambda) \tag{1.9}$$

where λ,μ are the second order linear elastic moduli of Lame' for a homogeneous, isotropic material,

l,m,n are the third order elastic moduli for a homogeneous, isotropic material as defined by Murnaghan,

ρ_0 is the density of the unstressed material,

K_0 is the bulk modulus,

P is the uniaxial or hydrostatic compression,

and v is the velocity of an ultrasonic wave propagating along the x axis. The first subscript on v refers to the direction of polarization, while the second gives the direction of loading. 0 for the second subscript implies hydrostatic loading.

They made measurements of the nonlinear constants of polystyrene, Armco Iron and Pyrex. Toupin and Bernstein [11] followed this work with an extension of the theory to include a material of arbitrary crystal symmetry. This work was published in 1961.

The next major theoretical developments were presented in a series of papers by Brugger [12,13] and Thurston and Brugger [14] in 1964 and 1965. These papers provided the formulation and notation for most of the research presented in following years on the topic. In the first paper by Brugger [12], a formal thermodynamic definition of the higher order elastic constants of a solid was given. The relationships between his definition and those used by Murnaghan [1] and other authors were also presented. In the paper of Thurston and Brugger [14], the concept of an ultrasonic "natural" velocity was introduced. The "natural" velocity was defined as the initial (unstressed) path length divided by the time of flight of the elastic wave. The concept of "natural" velocity is of great importance in the measurement of nonlinear properties because it requires that the change in only one parameter, the time of flight, be monitored as a function of stress in the experiments. In determining normal ultrasonic phase velocity changes, the time of flight as well as the propagation distance must be measured making the experimental measurements more difficult and uncertain. Also presented in this paper were general equations for the relationship between the "natural" velocity changes and applied stress for different crystal symmetries, wave modes, and stress conditions. In the final paper by Brugger [13], explicit equations were presented for these relations for a number of crystal symmetries, wave modes and stress conditions. These equations allow the calculation of all of the third order elastic coefficients for all of the crystal point groups.

Thus, based on the theory of Thurston and Brugger [14], measurements need only be made of the change in "natural" velocity (i.e. changes in time of flight) of ultrasonic waves as a function of stress to determine the third order elastic coefficients. However, the changes involved are generally quite small and require very accurate ultrasonic

techniques. Several such techniques have been developed over the years which make these measurements possible. Early measurements by Hughes et al. [15] in 1950 used a simple pulse transmission technique. A voltage spike was used to excite a piezoelectric ultrasonic transducer which launched an ultrasonic wave into the sample. A receiving transducer on the opposite side of the sample converted the elastic wave into an electrical signal which was displayed on an oscilloscope. The time of flight was measured directly on the scope with an uncertainty reported to be +/− 0.03 μs. This led to fractional uncertainties of larger than one part in 10^3 for samples with a 20 μs travel time.

Improvements in the ability to measure more accurately the ultrasonic wave time of flight followed rapidly. In 1953, McSkimin [16,17] reported on a phase comparison ultrasonic technique. This technique was a pulse-echo technique which used the same transducer as a generator and receiver of the elastic waves. A tone-burst (burst of several cycles of high frequency sinusoidal waves) was used to excite the transducer and thus generate the ultrasonic pulse. The elastic pulse traveled through the sample and reflected off of the other side. This occurred a number of times producing an oscilloscope pattern of a number of decaying amplitude pulses which were all similar except for the exponential decrease in their amplitude. In McSkimin's technique he amplified and rectified the received echos and displayed them on the oscilloscope. The time of flight was determined by varying the frequency of the tone-burst to find frequencies where the received echos were all in phase. For this condition the time of flight was given by

$$t = \frac{n - \frac{\gamma}{360}}{fn} \qquad (1.10)$$

where t was the time of flight,

n was an integer,

f was the frequency of the tone-burst

and γ was a phase angle, in degrees, correcting for phase shifts at the specimen-transducer interface.

The integer n was determined by measuring two sequential values of the frequency for the "in phase" condition. In this case, n was given by

$$n = \frac{f_1}{\Delta f} \tag{1.11}$$

where f_1 and f_2 were the two measured values of frequency and Δf was the difference between the two measured values.

An expression for the phase angle γ based on standard equivalent electrical transmission line theory was presented. It was calculated from known material properties (mechanical impedances of specimen and transducer and resonant frequency of transducer). The overall uncertainty in measuring velocity was reported to be 0.14 %.

In 1957 Williams and Lamb [18] reported a technique using a pair of ultrasonic bursts and a through transmission technique. The first burst was launched through the sample and reflected multiple times through the specimen. The second burst was launched through the same transducer a short time later so that the first arrival of the second pulse at the receiving transducer would coincide with the arrival of the first echo of the first pulse. The excitation frequency was then adjusted so that there was cancellation between the two signals. Analysis was then presented which allowed calculation of the travel time in the specimen from the frequency which included corrections for phase shifts at the specimen-transducer interface. Analysis of the phase angle also included the effect of the coupling medium between the transducer and specimen. The measured velocity was considered to be accurate to one part in 10^4 .

Other techniques developed later such as the pulse superposition method (McSkimin [19]) in 1961 and the pulse echo overlap technique (May [20] and Papadakis [21]) increased absolute accuracy of velocity measurements under certain conditions to several parts per million according to Papadakis [22]. He also reported that changes in

time of flight could be measured accurate to parts in 10^7 using these techniques. Details of the pulse echo overlap technique will be discussed later.

The final technique discussed was reported by Heyman [23,24] in 1980. It allowed changes in "natural" velocity accurate to one part in 10^7 to be measured. The technique uses an ultrasonic instrument known as a pulsed phase locked loop (P2L2) which measures changes in resonant frequency of the specimen, transducer, bond composite resonator system as a function of some other parameter such as stress or temperature. This can be shown to be equivalent to measuring changes in "natural" velocity (W) as follows. Since

$$W = \frac{L_0}{t} \tag{1.12}$$

where L_0 is the initial length of propagation which is a constant

and t is the time of flight,

then

$$\Delta W = \frac{(t\Delta L_0 - L_0\Delta t)}{t^2} \tag{1.13}$$

which reduces to

$$\Delta W = -\frac{L_0\Delta t}{t^2} \tag{1.14}$$

since

$$\Delta L_0 = 0. \tag{1.15}$$

Therefore,

$$\frac{\Delta W}{W} = -\frac{\Delta t}{t}. \tag{1.16}$$

The normal phase velocity (v) is given by

$$v = \frac{L}{t} \tag{1.17}$$

where L is the length of propagation which is not a constant.

Therefore,

$$\frac{\Delta W}{W} = -\frac{\Delta t}{t} = \frac{\Delta v}{v} - \frac{\Delta L}{L}. \tag{1.18}$$

However the resonant frequency of the test system is given by

$$F_n = \frac{nv}{2L} \tag{1.19}$$

where n is an integer denoting the number of the harmonic.

Therefore,

$$\frac{\Delta F}{F} = \frac{\Delta v}{v} - \frac{\Delta L}{L}, \tag{1.20}$$

and thus,

$$\frac{\Delta F}{F} = \frac{\Delta W}{W} = -\frac{\Delta t}{t}. \tag{1.21}$$

The way in which the P2L2 measures changes in resonant frequency will be discussed in a later section as it is the instrument used for the nonlinear measurements in this work.

Although most of the work discussed thus far deals with the development of theory and measurement techniques for nonlinear behavior of materials, much work in the literature points out the importance of nonlinear measurements and their applications. One of the first applications of nonlinear elasticity was in the area of materials characterization. Nonlinear elastic constants, through their representation in terms of interatomic potentials in crystalline solids, provide much information about the nature of the bonding of atoms in a crystal. Einspruch and Manning [25] pointed out the importance of nonlinear and anharmonic phenomena in solid materials in relation to

other important material properties such as thermal coefficients of expansion, Grüneisen constants and ultrasonic attenuation. They also pointed out the need for a nonlinear description of elasticity in theories dealing with regions of high stress or finite strain in solids such as around dislocations.

One of the most useful and important applications of nonlinear elasticity, however, has been in the field of nondestructive evaluation of applied and residual stress (strain) in materials. This application is based on the fact that ultrasonic wave speeds are a function of the stress state of a material due to nonlinear effects. Thus, if the relationship between stress and velocity is previously measured for a given material, theoretically, the state of stress in the material can be monitored by measuring the ultrasonic velocity. A variation of this is called the acoustoelastic effect or acoustical birefringence. The acoustoelastic effect arises from the fact that two shear waves, one polarized parallel to stress and the other perpendicular to stress, have a difference in velocity proportional to the applied stress. Again this is due to nonlinear effects. Acoustical birefringence is similar to optical birefringence or the photoelastic effect which has been used to determine strain in transparent materials for many years. As early as 1959 the acoustoelastic effect was being touted for the measurement of residual stress. Benson and Raelson [26] stated that acoustoelasticity could be as effective as photoelastic methods with the additional benefit of applications to opaque materials.

However, in the years since, problems have plagued the application of acoustical birefringence for the measurement of residual stress. The effect of velocity difference between the shear waves due to material anisotropy is often much larger than changes observed due to stress making residual stress measurements difficult. Another problem involves energy flux deviation. In an anisotropic body, the energy flux vector (the direction of the flow of energy per unit time per unit area) of an elastic wave does not in general coincide with the wave normal. This refraction of the wave is different for the two shear waves which means the two waves do not follow the same path through the

material. It also depends on the degree of anisotropy and may also change as a function of stress. These factors make velocity measurements for acoustoelastic determination of stress extremely difficult. Also, as pointed out by Hsu [27], although there are analogies between the photoelastic effect and the acoustoelastic effect, a comparison of the important parameters (i.e. wavelengths, frequencies, velocity changes, etc.) for both acoustical and optical wave propagation shows that the acoustic technique is not as efficient as the optical technique.

Nevertheless, numerous investigators are still attempting to overcome these problems. Theory has been developed to attempt to account for the effect of special textures which has met with limited success in applications. Also, as noted earlier, measurement technology in ultrasonics has progressed substantially. The progress in acoustoelasticity was reviewed in detail by Pao et al. [28]. The general problem of the experimental determination of residual stress using ultrasonic methods has yet to be solved. However, the detection of applied stress has been successfully reported by numerous authors [24,29,30].

Nonlinear elastic material properties may also be important in the nondestructive evaluation of important engineering properties of materials. For engineering applications, it is important to determine material properties such as strength and residual strength after impact or fatigue loading and thermal cycling. However, most nondestructive measurements yield only physical properties such as modulus, density or coefficient of thermal expansion. To determine the important engineering properties relationships must be developed between the measured physical quantities and the desired engineering properties. Nonlinear properties may be useful in this respect as they are parameters which are significant in large deformations (i.e. near failure strains) of materials. To examine this, Heyman et al. [31] studied the relationship between the Stress Acoustic Constant (SAC) which is a measure of a mixture of second and third order elastic moduli and carbon content in carbon steels. They found the SAC not only

seemed to be related to the carbon content but to the strength of the material as well. In aluminum, Heyman and Chern [32] examined the relationship between the SAC and heat treatment. They found that while the second order moduli were insensitive to the different heat treatments used, the SAC was able to differentiate them. Thus, a simple test method for detecting improperly heat treated and thus inferior strength aluminum was demonstrated based on measurements of nonlinear elastic properties.

Although previous discussion has considered primarily only metallic and non-metallic crystalline solids, numerous studies have presented measurements of nonlinear phenomena in polymeric and composite materials. In 1950, Hughes et al. [15] reported changes in wave speed as a function of pressure and temperature for polyethylene, polystyrene and Lucite. In 1953, Hughes and Kelly [10] presented the three third order elastic constants for polystyrene. In 1959, Singh and Nolle [33] measured the velocity as a function of hydrostatic pressure and temperature for polyisobutylene. Assay et al. [34,35] presented the change in velocity for polymethylmethacrylate as a function of stress and temperature. The relationship between stress and velocity became nonlinear at high pressures indicating higher order nonlinear effects. Lamberson [36], in 1969, reported on the temperature and hydrostatic pressure dependence of velocity in polystyrene and two composite materials. One of the composites was carbon phenolic while the other was a tape wound silica phenolic. He also reported nonlinear stress-velocity curves for these materials at high pressures. Zarembo and Shklovskaya [37] reported harmonic generation data for polystyrene, plexiglass and rubber in 1971. They also examined the effect of hydrostatic and uniaxial stress on harmonic generation in these materials. Other authors [38,39] have reported nonlinear measurements on different polymeric materials since this time.

The present work deals with the measurement of the linear and nonlinear elastic properties of a graphite/epoxy composite material. More specifically, measurements were made on unidirectional laminates of T300/5208 (Thornel 300 graphite fibers in a

Narmco 5208 epoxy resin). The choice of a unidirectional lay up was made because it offers the highest elastic symmetry and therefore is the least complex orientation to analyze. The elastic symmetry of unidirectional fiber reinforced composites is usually taken to be that of transverse isotropy if the fibers are randomly distributed in the plane perpendicular to the fiber axis. A transversely isotropic material is one which has a preferred axis, perpendicular to which is a plane in which the material behaves in an elastically isotropic fashion. In the case of a unidirectional composite, the fiber axis is the preferred axis having a much larger elastic stiffness, and the isotropic plane is the plane perpendicular to the fiber axis with a much lower stiffness.

For a transversely isotropic material there are five linear elastic (second order) moduli. This is the same as for the case of a hexagonal single crystal. However, there are only nine nonlinear (third order) moduli for transverse isotropy as opposed to either ten or twelve for the different point group symmetries of hexagonal single crystals. In the present work, the five linear (second order) elastic stiffness moduli for the unidirectional composites were computed from ultrasonic velocity measurements. These values were then compared with available data from the literature as well as checked for consistency with the assumption of transverse isotropy. From the linear elastic stiffness moduli, the compliance moduli were calculated and compared with those obtained by strain gauge measurements. These were also compared with reported values for a similar material. Measurements were then made to determine the change in "natural" wave velocity as a function of applied stress and temperature. A variety of combinations of propagation direction and loading configurations were used with longitudinal and transverse waves. This data was also checked for consistency with the predictions of transverse isotropy. Then the velocity-stress data was used to calculate some of the nonlinear coefficients of this material.

II. LINEAR ELASTICITY

II.A. Introduction

In order to determine the nonlinear elastic moduli, the linear elastic stiffness and compliance moduli must first be measured. In this chapter, measurements of these properties in a unidirectional graphite/epoxy composite will be discussed. Definitions of the terms used in linear elastic theory will be presented first, followed by a theoretical explanation of the methods used. Then, the measurements will be reported and compared with theoretically predicted and previously measured values for this material.

II.B. Theory

As discussed earlier, the theoretical basis for linear elasticity shows that it is only applicable for small or infinitesimal deformations. This permits the use of simplifying assumptions in the definition of strain for linear elasticity. The coordinates of a point of material in an undeformed body are defined to be a_i with respect to the origin in an orthogonal coordinate system (Note: Einstein convention of summation over repeated indices is assumed throughout this paper). The same point of material defined by a_i will be displaced to a new position x_i in the material after deformation. The displacement is a vector defined by

$$\vec{u} = \vec{x} - \vec{a} \tag{2.1}$$

having components u_i. The strain can now be defined in two ways. The Lagrangian strain tensor which provides a measure of the deformation with respect to the undeformed material coordinates is defined by

$$\eta_{ij} = \frac{1}{2}\left(\frac{\partial u_i}{\partial a_j} + \frac{\partial u_j}{\partial a_i} + \frac{\partial u_k}{\partial a_i}\frac{\partial u_k}{\partial a_j}\right) \tag{2.2}$$

In the Eulerian formulation of strain, the strain is described in reference to the deformed state and is given by

$$e_{ij} = \frac{1}{2}\left(\frac{\partial u_i}{\partial x_j} + \frac{\partial u_j}{\partial x_i} + \frac{\partial u_k \partial u_k}{\partial a_i \partial a_j}\right). \tag{2.3}$$

The Lagrangian formulation is often referred to as a material description of strain while the Eulerian is called the spatial description. The Lagrangian is more often used in solid mechanics and the Eulerian in fluid mechanics. The assumption of infinitesimal deformation can now be applied. This assumption means that since

$$\frac{\partial u_i}{\partial a_j} \text{ and } \frac{\partial u_j}{\partial a_i} \ll 1 \tag{2.4}$$

for infinitesimal deformations, then the quadratic term $\left(\frac{\partial u_k \partial u_k}{\partial a_i \partial a_j}\right)$ is much smaller than the linear terms and can be dropped from the expression. Thus the small or infinitesimal strain tensor is defined by

$$\epsilon_{ij} = \frac{1}{2}\left(\frac{\partial u_i}{\partial a_j} + \frac{\partial u_j}{\partial a_i}\right). \tag{2.5}$$

The small strain assumption also means that

$$\epsilon_{ij} = \frac{1}{2}\left(\frac{\partial u_i}{\partial a_j} + \frac{\partial u_j}{\partial a_i}\right) = \frac{1}{2}\left(\frac{\partial u_i}{\partial x_j} + \frac{\partial u_j}{\partial x_j}\right) \tag{2.6}$$

or that there is no difference between the Lagrangian and Eulerian formulations for strain. It can also be seen from the definition of the small strain tensor that it is a symmetric tensor (i.e. $\epsilon_{ij} = \epsilon_{ji}$).

The physical description of the components ϵ_{11}, ϵ_{22}, and ϵ_{33} is that they are the normal strains which provide the measure of the normalized change in length of the body along the respective coordinate axis. For example, if l_0 is the unstrained length along axis x_1 and l_1 is the strained length along x_1 , then

$$\epsilon_{11} = \frac{(l_1 - l_0)}{l_0}. \tag{2.7}$$

The remaining strain components are the shear strains which are a measure of the change in angle between two originally orthogonal axes in the undeformed medium. This is demonstrated in Fig. 2.1 where the strain is given by

$$\epsilon_{12} = \frac{\Delta x_1}{x_2} = \tan(\theta) \approx \theta \quad \text{(for small strain)}. \tag{2.8}$$

The stress tensor (σ_{ij}) provides a measure of the applied forces on the body. It is defined by

$$\sigma_{ij} = \frac{\text{force on the i'th face in the j'th direction}}{\text{cross sectional area of the i'th face}}. \tag{2.9}$$

A diagram of the nine components of the stress tensor is shown in Fig. 2.2. The engineering or nominal stress is used where the cross sectional area is that measured in the unstressed state. The true stress uses the instantaneous cross sectional area which is much more difficult to measure. The components σ_{11}, σ_{22} and σ_{33} are the normal stress components while the remainder are shear stress components. Laws of statics can be used to show that if a body is to be in rotational equilibrium, the stress tensor must also be symmetric.

Having defined both stress and strain, the relationship between the two can now be discussed. For linear elasticity, the generalized Hooke's law is used. This expresses the relationship between stress and strain as

$$\sigma_{ij} = c_{ijkl}\epsilon_{kl} \tag{2.10}$$

where c_{ijkl} is the fourth rank linear elastic stiffness tensor. In the most general form this tensor has eighty-one components. However, because the stress and strain tensors are both symmetric, the following relations are valid

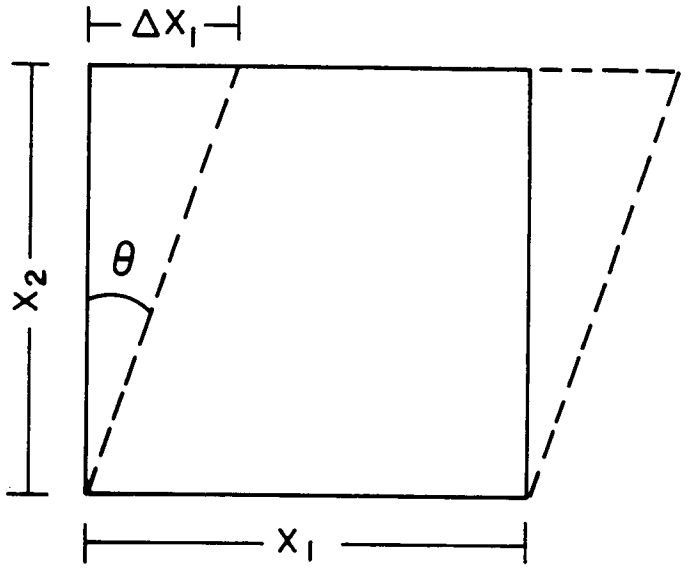

Figure 2.1 - Two dimensional representation of shear strain, solid line represents undeformed medium while dashed line is deformed medium.

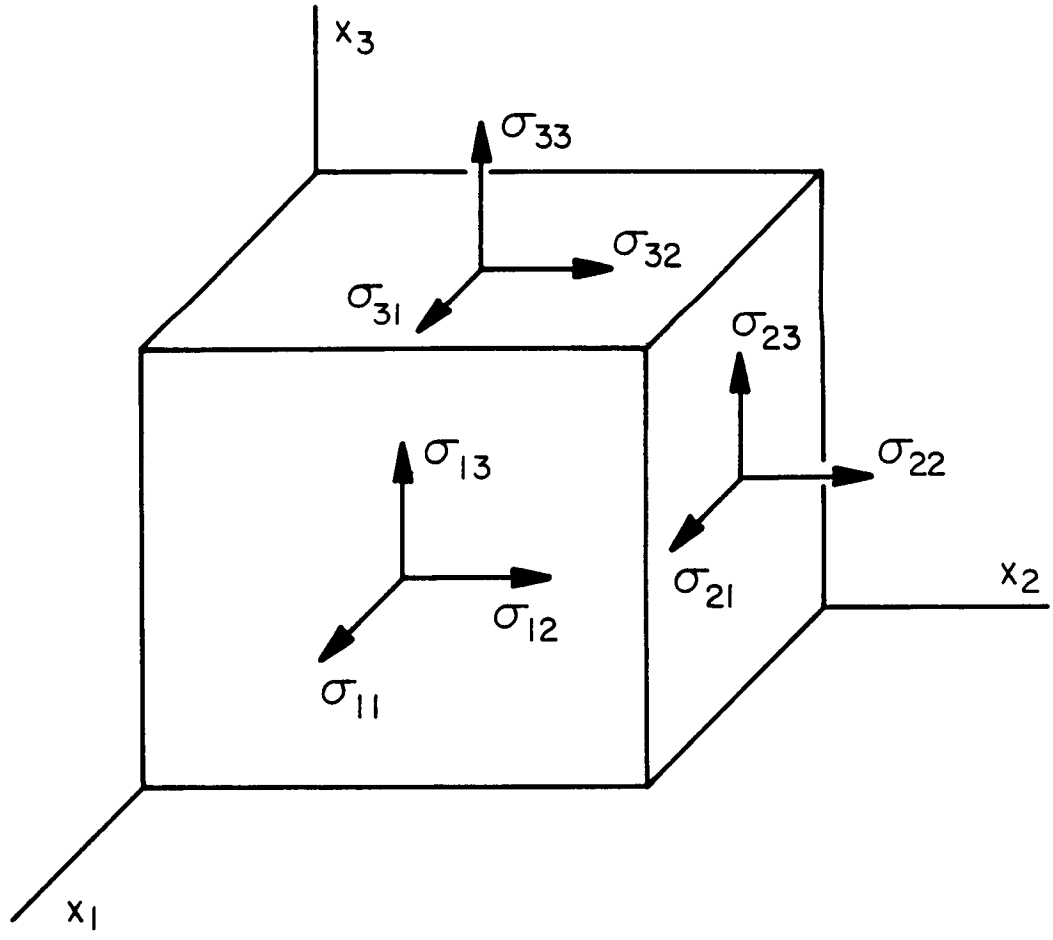

Figure 2.2 - Diagram of the nine stress tensor components.

$$c_{ijkl} = c_{jikl} \tag{2.11}$$

and

$$c_{ijkl} = c_{ijlk}. \tag{2.12}$$

This reduces the number of independent components to thirty-six. The assumed existence of a strain energy density function (ϕ) which for the case of linear elasticity has the form

$$\phi = \frac{1}{2} c_{ijkl} \epsilon_{ij} \epsilon_{kl} \tag{2.13}$$

provides further reduction of the number of independent elastic coefficients. It must be true that

$$\phi = \frac{1}{2} c_{ijkl} \epsilon_{ij} \epsilon_{kl} = \frac{1}{2} c_{ijkl} \epsilon_{kl} \epsilon_{ij}. \tag{2.14}$$

Equating this expression term by term with respect to strain yields the relation

$$c_{ijkl} = c_{klij}. \tag{2.15}$$

This reduces the number of independent coefficients to twenty-one. At this point, the Voigt notation can be used to simplify things somewhat. For each pair of indices on stress, strain and elastic moduli, the following substitutions are made

$$\begin{array}{llll} 11 \rightarrow 1 & & 23 \rightarrow 4 \\ 22 \rightarrow 2 & & 31 \rightarrow 5 \\ 33 \rightarrow 3 & & 12 \rightarrow 6 \end{array} \tag{2.16}$$

Using this notation, the generalized Hooke's law can be rewritten as

$$\sigma_A = c_{AB} \epsilon_B \tag{2.17}$$

where capital subscripts are summed from one to six. The elastic stiffness moduli can

now be written in matrix form for the most general anisotropic solid as

$$c_{AB} = \begin{bmatrix} c_{11} & c_{12} & c_{13} & c_{14} & c_{15} & c_{16} \\ c_{12} & c_{22} & c_{23} & c_{24} & c_{25} & c_{26} \\ c_{13} & c_{23} & c_{33} & c_{34} & c_{35} & c_{36} \\ c_{14} & c_{24} & c_{34} & c_{44} & c_{45} & c_{46} \\ c_{15} & c_{25} & c_{35} & c_{45} & c_{55} & c_{56} \\ c_{16} & c_{26} & c_{36} & c_{46} & c_{56} & c_{66} \end{bmatrix} \tag{2.18}$$

The reduction in the number of independent elastic constants can be carried further if material symmetries are taken into consideration. This is accomplished by examining the effect on the strain energy density function of a rotation of the material which places the material in an elastically equivalent condition due to symmetries of the material. Due to the scalar nature of the strain energy density function, it should have the same value in both configurations. An example of this procedure is now given. The strain energy density function is written out in terms of the twenty-one independent coefficients as

$$\phi = \frac{1}{2}(c_{11}\epsilon_1^2 + c_{22}\epsilon_2^2 + c_{33}\epsilon_3^2 + c_{44}\epsilon_4^2 + c_{55}\epsilon_5^2 + c_{66}\epsilon_6^2) + c_{12}\epsilon_1\epsilon_2$$

$$+ c_{13}\epsilon_1\epsilon_3 + c_{14}\epsilon_1\epsilon_4 + c_{15}\epsilon_1\epsilon_5 + c_{16}\epsilon_1\epsilon_6 + c_{23}\epsilon_2\epsilon_3 + c_{24}\epsilon_2\epsilon_4 + c_{25}\epsilon_2\epsilon_5$$

$$+ c_{26}\epsilon_2\epsilon_6 + c_{34}\epsilon_3\epsilon_4 + c_{35}\epsilon_3\epsilon_5 + c_{36}\epsilon_3\epsilon_6 + c_{45}\epsilon_4\epsilon_5 + c_{46}\epsilon_4\epsilon_6 + c_{56}\epsilon_5\epsilon_6 \tag{2.19}$$

In an isotropic material any rotation is elastically equivalent. Assuming an isotropic material, a rotation of 180 degrees around the x_3 axis is chosen and is shown in Fig. 2.3. The transformation matrix or direction cosine matrix $[a_{ij}]$ is found by taking the cosine of the angle between the rotated and original axes. For this rotation it is given by

$$[a_{ij}] = \begin{bmatrix} -1 & 0 & 0 \\ 0 & -1 & 0 \\ 0 & 0 & 1 \end{bmatrix}. \tag{2.20}$$

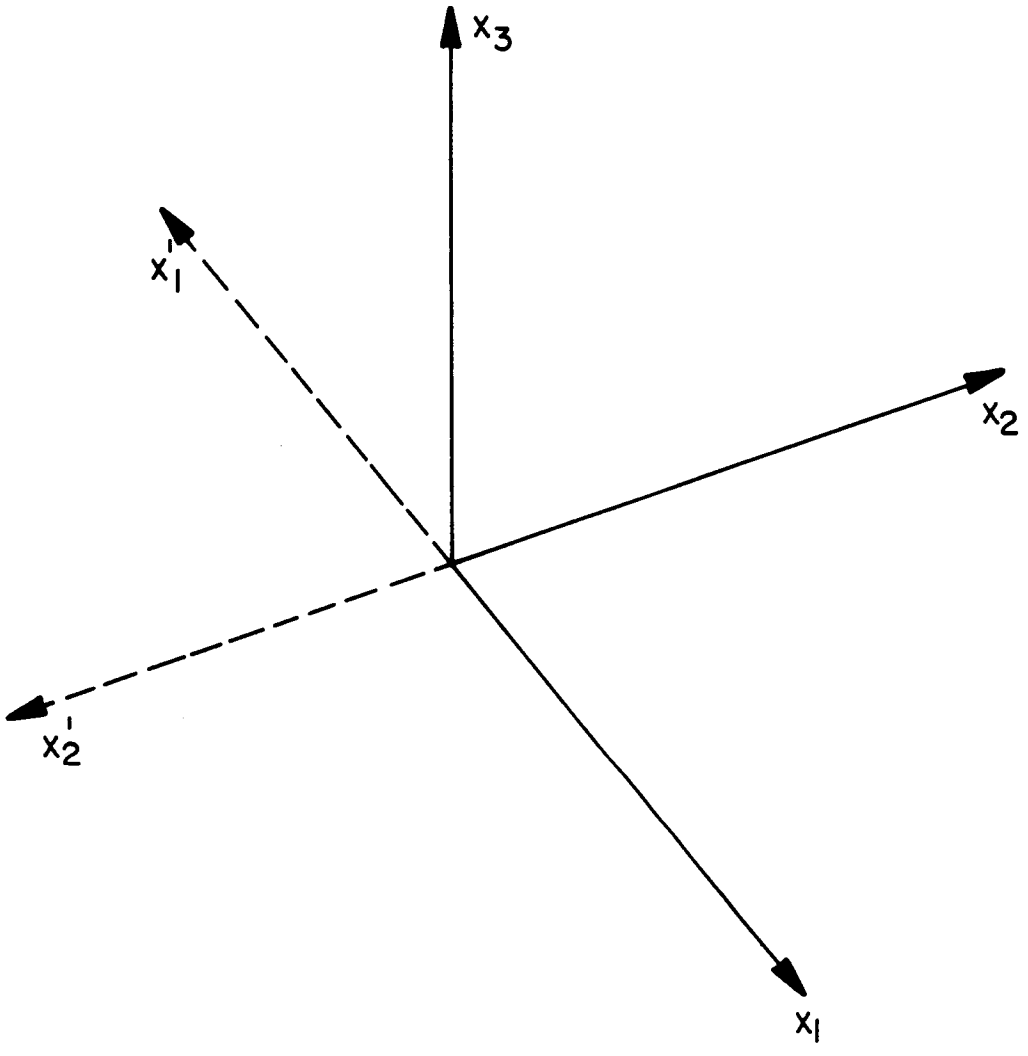

Figure 2.3 - Diagram of the rotation of axes 180 degrees around the x_3 axis (primed axes are the rotated axes).

The effect of this rotation on the strain tensor is given by

$$\epsilon'_{ij} = a_{ik}a_{jl}\epsilon_{kl}. \tag{2.21}$$

Thus

$$\begin{aligned}
\epsilon'_{11} &= \epsilon_{11} & \epsilon'_1 &= \epsilon_1 \\
\epsilon'_{22} &= \epsilon_{22} & \epsilon'_2 &= \epsilon_2 \\
\epsilon'_{33} &= \epsilon_{33} & \epsilon'_3 &= \epsilon_3 \\
\epsilon'_{23} &= -\epsilon_{23} \quad \text{or} & \epsilon'_4 &= -\epsilon_4 \\
\epsilon'_{31} &= -\epsilon_{31} & \epsilon'_5 &= -\epsilon_5 \\
\epsilon'_{12} &= \epsilon_{12} & \epsilon'_6 &= \epsilon_6
\end{aligned} \tag{2.22}$$

The rotated strain energy density function can be written after substituting equation (2.22) as

$$\begin{aligned}
\phi' = \frac{1}{2}(&c_{11}\epsilon_1^2 + c_{22}\epsilon_2^2 + c_{33}\epsilon_3^2 + c_{44}\epsilon_4^2 + c_{55}\epsilon_5^2 + c_{66}\epsilon_6^2) + c_{12}\epsilon_1\epsilon_2 \\
&+ c_{13}\epsilon_1\epsilon_3 - c_{14}\epsilon_1\epsilon_4 - c_{15}\epsilon_1\epsilon_5 + c_{16}\epsilon_1\epsilon_6 + c_{23}\epsilon_2\epsilon_3 - c_{24}\epsilon_2\epsilon_4 - c_{25}\epsilon_2\epsilon_5 \\
&+ c_{26}\epsilon_2\epsilon_6 - c_{34}\epsilon_3\epsilon_4 - c_{35}\epsilon_3\epsilon_5 + c_{36}\epsilon_3\epsilon_6 + c_{45}\epsilon_4\epsilon_5 - c_{46}\epsilon_4\epsilon_6 - c_{56}\epsilon_5\epsilon_6).
\end{aligned} \tag{2.23}$$

Evaluating term by term the relation

$$\phi' = \phi \tag{2.24}$$

yields

$$\begin{aligned}
c_{14} &= -c_{14} \\
c_{15} &= -c_{15} \\
c_{24} &= -c_{24} \\
c_{25} &= -c_{25} \\
c_{34} &= -c_{34} \\
c_{35} &= -c_{35} \\
c_{46} &= -c_{46} \\
c_{56} &= -c_{56} \\
\text{all other } c_{ij} &= c_{ij}.
\end{aligned} \tag{2.25}$$

If equations (2.25) are to be true, then

$$c_{14} = c_{15} = c_{24} = c_{25} = c_{34} = c_{35} = c_{46} = c_{56} = 0. \tag{2.26}$$

Application of further symmetry operations will show that for an isotropic material, the number of independent elastic coefficients reduces to two. The matrix then appears as

$$[c_{AB}] = \begin{bmatrix} c_{11} & c_{12} & c_{12} & 0 & 0 & 0 \\ c_{12} & c_{11} & c_{12} & 0 & 0 & 0 \\ c_{13} & c_{12} & c_{11} & 0 & 0 & 0 \\ 0 & 0 & 0 & \frac{c_{11} - c_{12}}{2} & 0 & 0 \\ 0 & 0 & 0 & 0 & \frac{c_{11} - c_{12}}{2} & 0 \\ 0 & 0 & 0 & 0 & 0 & \frac{c_{11} - c_{12}}{2} \end{bmatrix}, \tag{2.27}$$

For a transversely isotropic material, the number of independent coefficients is five while for an orthotropic material it is nine. The derivation of the independent coefficients as well as their final matrix forms for these two elastic symmetries which are important for unidirectional fiber reinforced composites is shown in Appendix A.

The relationship between strain and stress is given by

$$\epsilon_{ij} = s_{ijkl}\sigma_{kl}. \tag{2.28}$$

The moduli s_{ijkl} form the linear elastic compliance tensor. The conditions of symmetry for the stiffness tensor also apply to the compliance tensor. The relations between the compliance and stiffness moduli for a given symmetry can be determined by inverting the stiffness matrix.

The value of the elastic moduli are also dependent upon the conditions (isothermal or adiabatic) in which they are measured. Isothermal moduli are measured at constant temperature (T) while adiabatic moduli are measured at constant entropy (S). The work by Brugger [12] provides a precise thermodynamic definition of the elastic

moduli and the relationship between adiabatic and isothermal coefficients. In terms of the free energy (F), the isothermal stiffness moduli are defined by

$$c^{T}_{ijkl} = \rho_0 \left(\frac{\partial^2 F}{\partial \eta_{ij} \partial \eta_{kl}} \right)_T \tag{2.29}$$

where ρ_0 is the unstrained density.

The adiabatic stiffness moduli are

$$c^{S}_{ijkl} = \rho_0 \left(\frac{\partial^2 U}{\partial \eta_{ij} \partial \eta_{kl}} \right)_S \tag{2.30}$$

where U is the internal energy.

The adiabatic and isothermal compliances are defined in terms of the enthalpy (H) and the Gibbs function (G) respectively and the thermodynamic tensions (t_{ij}) which are

$$t_{ij} = \rho_0 \left(\frac{\partial U}{\partial \eta_{ij}} \right)_S = \rho_0 \left(\frac{\partial F}{\partial \eta_{ij}} \right)_T . \tag{2.31}$$

The compliance moduli are

$$s^{S}_{ijkl} = - \rho_0 \left(\frac{\partial^2 H}{\partial t_{ij} \partial t_{kl}} \right)_S \tag{2.32}$$

and

$$s^{T}_{ijkl} = - \rho_0 \left(\frac{\partial^2 G}{\partial t_{ij} \partial t_{kl}} \right)_T . \tag{2.33}$$

The relationship between adiabatic and isothermal compliance moduli was given in matrix form by Hankey and Schule [40] as

$$s^{T}_{AB} = s^{S}_{AB} + \left(\frac{T}{\rho_0 c_p} \right) \alpha_A \alpha_B \tag{2.34}$$

where c_p is the specific heat at constant pressure,

and α_A is the linear coefficient of thermal expansion defined by

$$\alpha_A = \frac{\partial \eta_A}{\partial T}. \tag{2.35}$$

The difference between adiabatic and isothermal moduli is usually quite small and often less than experimental uncertainty.

The determination of the adiabatic linear elastic stiffness moduli can be made by measuring the density and the ultrasonic wave velocity. The derivation of the equations of motion for the propagation of linear elastic waves in an anisotropic medium provides the theoretical basis for this technique. This subject has been treated by a number of authors among the earliest being Love [41] and it is reviewed in detail by Green [5]. In deriving the wave equations, a number of initial assumptions about the propagation medium are made. It is assumed to be unbounded, homogeneous and continuous. Next, an infinitesimal volume element of the medium is examined and the net unbalanced forces acting on it are determined. This is accomplished by finding the resultant of the variation of stress across the element for each direction and multiplying this by the respective cross sectional area. Fig. 2.4 shows the variation of stress along the x_1 direction for the infinitesimal volume element with sides of length δx_1, δx_2 and δx_3. If there were no variation of stress and thus no net unbalanced forces, there would be no wave motion. The net unbalanced force along x_1 is given by

$$[(\sigma_{11} + \frac{\partial \sigma_{11}}{\partial x_1}\delta x_1) - \sigma_{11}]\delta x_2 \delta x_3 + [(\sigma_{21} + \frac{\partial \sigma_{21}}{\partial x_2}\delta x_2) - \sigma_{21}]\delta x_1 \delta x_3$$

$$+ [(\sigma_{31} + \frac{\partial \sigma_{31}}{\partial x_3}\delta x_3) - \sigma_{31}]\delta x_1 \delta x_2. \tag{2.36}$$

This can be reduced to

$$\left(\frac{\partial \sigma_{11}}{\partial x_1} + \frac{\partial \sigma_{21}}{\partial x_2} + \frac{\partial \sigma_{31}}{\partial x_3}\right)\delta x_1 \delta x_2 \delta x_3. \tag{2.37}$$

Similar expression can be written for the net unbalanced force along x_2 and x_3 . According to Newton's second law these unbalanced forces must equal $m\ddot{u}_i$ where m is the mass

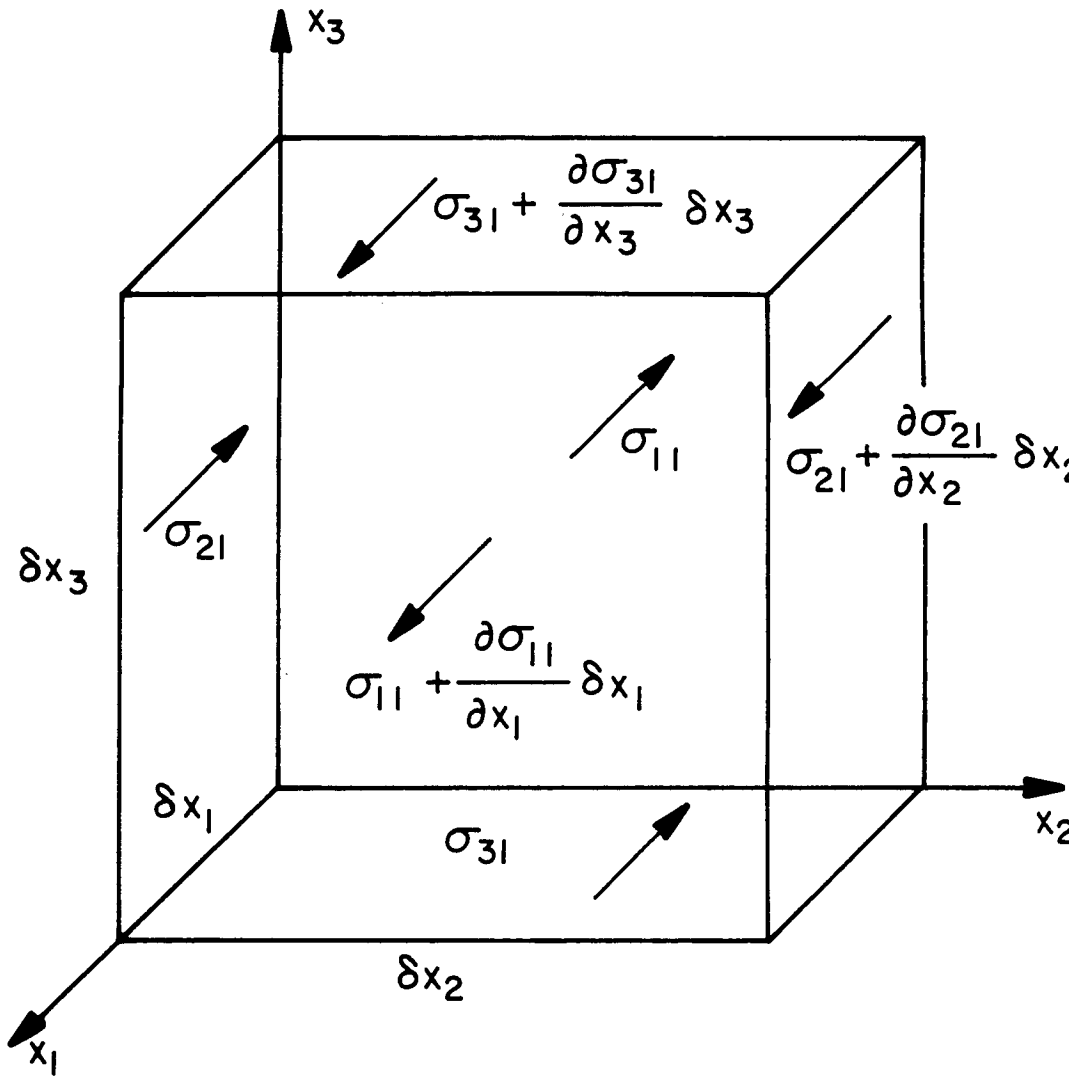

Figure 2.4 - Illustration of the variation of stress on a volume element of material along the x_1 direction.

of the element and $\ddot{u}_i$ are the second time derivatives of the displacements which are the acceleration components. Actually, to be more exact, it is pointed out that Newton's second law states that the force is equal to the time derivative of the momentum p_i . However,

$$p_i = m\dot{u}_i \tag{2.38}$$

and therefore

$$\dot{p}_i = m\ddot{u}_i + \dot{m}\dot{u}_i. \tag{2.39}$$

Since the mass of the element is assumed to be constant in time the forces are simply given by $m\ddot{u}_i$. Therefore the balance of forces can be written in component form as

$$m\ddot{u}_i = \left(\frac{\partial \sigma_{ij}}{\partial x_j}\right)\delta x_1 \delta x_2 \delta x_3. \tag{2.40}$$

It is noted that the body forces are neglected in this equation. The mass can be rewritten in terms of the density ρ_0 and the volume (V) which is given by

$$V = \delta x_1 \delta x_2 \delta x_3 \tag{2.41}$$

as

$$m = \rho_0 \delta x_1 \delta x_2 \delta x_3. \tag{2.42}$$

Substituting (2.42) into (2.40) and canceling appropriate terms yields

$$\rho_0 \ddot{u}_i = \left(\frac{\partial \sigma_{ij}}{\partial x_j}\right). \tag{2.43}$$

To rewrite this in terms of only density and displacement, the stress is first rewritten in terms of the strain using Hooke's law (2.10). Then the strain definition (2.6) is used to produce the expression for stress in terms of displacement as

$$\sigma_{ij} = c_{ijkl}\left[\frac{1}{2}\left(\frac{\partial u_k}{\partial x_l} + \frac{\partial u_l}{\partial x_k}\right)\right]. \tag{2.44}$$

The symmetry of the elastic coefficients (2.12) is applied to further simplify (2.44) to yield

$$\sigma_{ij} = \frac{1}{2}c_{ijkl}\left(\frac{\partial u_k}{\partial x_l}\right) + \frac{1}{2}c_{ijlk}\left(\frac{\partial u_l}{\partial x_k}\right) \tag{2.45}$$

and therefore

$$\sigma_{ij} = c_{ijkl}\left(\frac{\partial u_k}{\partial x_l}\right). \tag{2.46}$$

This is now put back into equation (2.43) to yield the final form of the equation of motion for linear elastic wave propagation in an anisotropic medium which is

$$\rho_0 \ddot{u}_i = c_{ijkl}\left(\frac{\partial^2 u_k}{\partial x_l \partial x_j}\right). \tag{2.47}$$

Now that the equation of motion has been derived, the next step is to choose a solution for the displacements as a function of time and space. For a plane wave, a solution can be written as

$$u_i(x_k,t) = A_0\alpha_i e^{i(\omega t - k_m x_m)} \tag{2.48}$$

where A_0 is the amplitude of the wave,

α_i are the direction cosines of the particle displacement vector,

t is the time,

ω is the angular frequency

and k_m are the components of the wave vector.

The wave vector components (k_m) are related to the direction cosines of the wave normal (l_m) and the wavelength (λ) by the expression

$$k_m = \left(\frac{2\pi}{\lambda}\right) l_m = k l_m \tag{2.49}$$

where k is the wave number.

The solution for the displacement can now be substituted into the equation of motion. This will lead to the following expression

$$c_{ijkl} k^2 l_l l_j \alpha_k = \rho_0 \omega^2 \alpha_i \tag{2.50}$$

which can be rewritten as

$$(c_{ijkl} l_l l_j - \rho_0 v^2 \delta_{ik}) \alpha_k = 0 \tag{2.51}$$

where v is the phase velocity of the elastic wave and is given by

$$v = \frac{\omega}{k}. \tag{2.52}$$

In equation (2.51), it is noted that α_k is arbitrary and therefore not necessarily equal to zero. In order for this equation to have nontrivial solutions, it must be true that the determinant of the matrix of coefficients must equal zero. That is

$$\left| c_{ijkl} l_l l_j - \rho_0 v^2 \delta_{ik} \right| = 0. \tag{2.53}$$

To more conveniently write this equation, a matrix $[\lambda_{ik}]$ is defined by

$$\lambda_{ik} = c_{ijkl} l_l l_j. \tag{2.54}$$

Therefore, equation (2.53) becomes

$$\left| \lambda_{ik} - \rho_0 v^2 \delta_{ik} \right| = 0. \tag{2.55}$$

This is a characteristic equation which when expanded forms a cubic expression in terms of $\rho_0 v^2$. Since λ_{ik} is a symmetric matrix, the three solutions for $\rho_0 v^2$ must all be real. The physical significance of this is that for any arbitrary direction in an anisotropic

medium, three plane waves may be propagated. The velocity of each of these waves depends on the density, the elastic constants and the direction cosines of the wave normal. Thus, if the ultrasonic wave velocities are measured for a number of directions in an anisotropic medium with known density and elastic symmetry, the linear elastic stiffness moduli can be determined. Although not formally designated as such in the preceding equations, these moduli will be the adiabatic stiffnesses.

The particle displacement vector direction cosines can be determined for each of the three waves propagating along a given direction. This is accomplished by solving for the eigenvectors for each eigenvalue ($\rho_0 v^2$) using the equation

$$\rho_0 v^2 \alpha_i = \lambda_{ik} \alpha_k, \tag{2.56}$$

and also applying the fact that

$$\alpha_i \alpha_i = 1. \tag{2.57}$$

These direction cosines determine the mode of the wave. If they are the same as the wave normal direction cosines, that is

$$\alpha_i = l_i, \tag{2.58}$$

then the particle displacement of the elastic wave lies along the direction of propagation of the wave. A wave of this type is referred to as a pure mode longitudinal (compressional) wave. If the particle displacement is perpendicular to the propagation direction and therefore

$$\alpha_i l_i = 0, \tag{2.59}$$

then the wave is called a pure mode transverse (shear) wave. Illustrations of longitudinal and transverse mode waves are given in Figs. 2.5 a) and b).

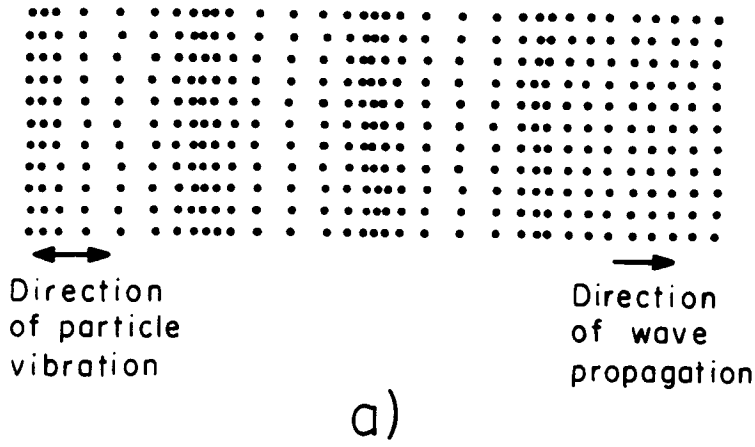

Figure 2.5 - (a) Illustration of a longitudinal (compressional) elastic wave demonstrating directions of particle vibration and propagation.

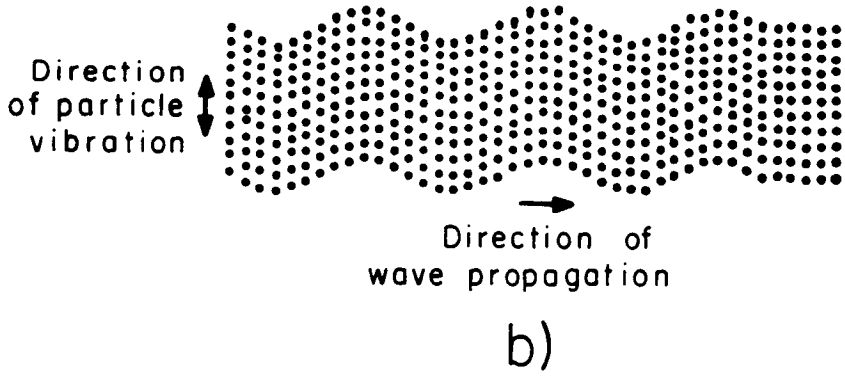

Figure 2.5 - (b) Illustration of a transverse (shear) wave.

However, in general the wave need not be pure mode. It can be either quasilongitudinal or quasitransverse depending on which type of particle motion is more dominant. Of the three waves propagating along a given direction, one is longitudinal or quasilongitudinal while the other two are transverse or quasitransverse.

Another consideration of linear elastic wave propagation in an anisotropic medium is that the direction of the energy flux of the wave may not in general be the same as the direction of the wave front normal. That is, there may be a refraction of the wave because of the anisotropy of the medium. The energy flux vector is defined as the direction of the flow of energy per unit time per unit area. A diagram of the energy flux deviation of a quasitransverse wave is shown in Fig. 2.6. Equations for expressing the energy flux vector and its deviation from the direction of the wave normal are reviewed by Green [5] and are presented here.

First, the expressions for the kinetic energy (K) and the potential energy (P) which is contained in the wave field are given by

$$K = \frac{1}{2}\int \rho \dot{u}_i^2 d\tau \tag{2.60}$$

and

$$P = \frac{1}{2}\int \sigma_{ij}\epsilon_{ij} d\tau \tag{2.61}$$

where $d\tau$ is a volume element of the wave field.

The sum of K and P yields the total elastic energy Ξ contained in the wave field which is

$$\Xi = \frac{1}{2}\left(\int \rho \dot{u}_i^2 d\tau + \int \sigma_{ij}\epsilon_{ij} d\tau\right). \tag{2.62}$$

The time derivative of Ξ is then given by

$$\frac{\partial \Xi}{\partial t} = \int \rho \dot{u}_i \ddot{u}_i d\tau + \frac{1}{2}\int \frac{\partial}{\partial t}(\sigma_{ij}\epsilon_{ij}) d\tau. \tag{2.63}$$

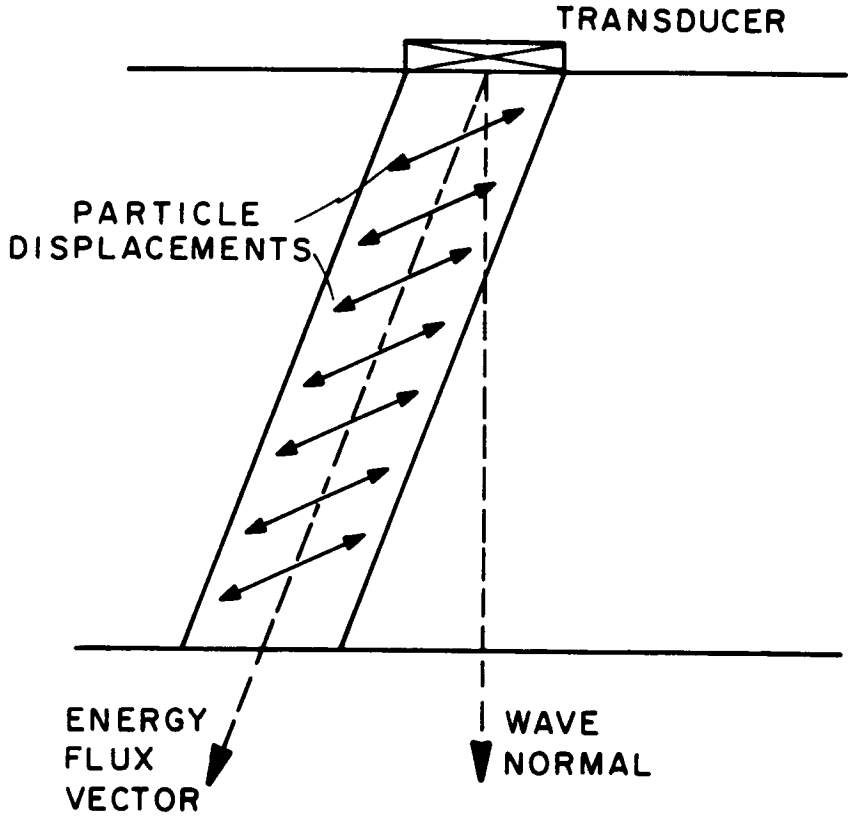

Figure 2.6 - Diagram of a quasitransverse elastic wave undergoing energy flux deviation illustrating the directions of particle displacements, wave normal, and energy flux vector.

To simplify this expression the term under the second integral is now considered. It can be rewritten as

$$\frac{\partial}{\partial t}(\sigma_{ij}\epsilon_{ij}) = \dot{\sigma}_{ij}\epsilon_{ij} + \sigma_{ij}\dot{\epsilon}_{ij}. \tag{2.64}$$

Hooke's law (2.10) can now be substituted into this equation to express $\frac{\partial}{\partial t}(\sigma_{ij}\epsilon_{ij})$ in terms of the elastic moduli and the strains as

$$\frac{\partial}{\partial t}(\sigma_{ij}\epsilon_{ij}) = c_{ijkl}\dot{\epsilon}_{kl}\epsilon_{ij} + c_{ijkl}\epsilon_{kl}\dot{\epsilon}_{ij}. \tag{2.65}$$

Because of the symmetry of the elastic moduli, equation (2.65) can be rewritten as

$$\frac{\partial}{\partial t}(\sigma_{ij}\epsilon_{ij}) = c_{klij}\dot{\epsilon}_{kl}\epsilon_{ij} + c_{ijkl}\epsilon_{kl}\dot{\epsilon}_{ij}. \tag{2.66}$$

Again using Hooke's law this becomes

$$\frac{\partial}{\partial t}(\sigma_{ij}\epsilon_{ij}) = \sigma_{kl}\dot{\epsilon}_{kl} + \sigma_{ij}\dot{\epsilon}_{ij} \tag{2.67}$$

which can be rewritten as

$$\frac{\partial}{\partial t}(\sigma_{ij}\epsilon_{ij}) = 2\sigma_{ij}\dot{\epsilon}_{ij} \tag{2.68}$$

after the dummy indices k and l are summed out of the equation. The time derivative of the strain in equation (2.68) can be rewritten in terms of the displacements using the definition of strain as

$$\dot{\epsilon}_{ij} = \frac{1}{2}\left(\frac{\partial \dot{u}_i}{\partial x_j} + \frac{\partial \dot{u}_j}{\partial x_i}\right). \tag{2.69}$$

This is substituted into equation (2.68) resulting in

$$\frac{\partial}{\partial t}(\sigma_{ij}\epsilon_{ij}) = \sigma_{ij}\left(\frac{\partial \dot{u}_i}{\partial x_j} + \frac{\partial \dot{u}_j}{\partial x_i}\right), \tag{2.70}$$

which because of the symmetry of the stress tensor is

$$\frac{\partial}{\partial t}(\sigma_{ij}\epsilon_{ij}) = 2\sigma_{ij}\frac{\partial \dot{u}_i}{\partial x_j}. \tag{2.71}$$

Equation (2.71) is now put back into equation (2.63) to give the time derivative of the total energy of the elastic wave field as

$$\frac{\partial \Xi}{\partial t} = \int \rho \dot{u}_i \ddot{u}_i d\tau + \int \sigma_{ij}\frac{\partial \dot{u}_i}{\partial x_j} d\tau. \tag{2.72}$$

Since

$$\frac{\partial}{\partial x_j}(\sigma_{ij}\dot{u}_i) = \sigma_{ij}\frac{\partial \dot{u}_i}{\partial x_j} + \dot{u}_i\frac{\partial \sigma_{ij}}{\partial x_j}, \tag{2.73}$$

or

$$\sigma_{ij}\frac{\partial \dot{u}_i}{\partial x_j} = \frac{\partial}{\partial x_j}(\sigma_{ij}\dot{u}_i) - \dot{u}_i\frac{\partial \sigma_{ij}}{\partial x_j}, \tag{2.74}$$

the second integral in equation (2.72) can be rewritten as

$$\int \sigma_{ij}\frac{\partial \dot{u}_i}{\partial x_j} d\tau = \int \frac{\partial}{\partial x_j}(\sigma_{ij}\dot{u}_i) d\tau - \int \dot{u}_i\frac{\partial \sigma_{ij}}{\partial x_j} d\tau. \tag{2.75}$$

Gauss's theorem can now be applied to the first integral of equation (2.75) to rewrite it as a surface integral of the form

$$\int \frac{\partial}{\partial x_j}(\sigma_{ij}\dot{u}_i) d\tau = \int \sigma_{ij}\dot{u}_i dS. \tag{2.76}$$

This can be substituted into equation (2.75) which is then inserted into equation (2.72) which gives

$$\frac{\partial \Xi}{\partial t} = \int \left(\rho \ddot{u}_i - \frac{\partial \sigma_{ij}}{\partial x_j}\right)\dot{u}_i d\tau + \int \sigma_{ij}\dot{u}_i dS. \tag{2.77}$$

The first integral equals zero because of the equation of motion (2.47). Therefore, it remains that

$$\frac{\partial \Xi}{\partial t} = \int \sigma_{ij} \dot{u}_i dS. \tag{2.78}$$

This equation represents the energy flow into the volume element τ through the surface S. The energy flux vector with components E_j can be formed which gives the energy flux flowing outward from the volume τ through S by

$$E_j = - \sigma_{ij} \dot{u}_i. \tag{2.79}$$

If the time averaged values E of the energy flux vector over one cycle of the elastic wave are computed and it is defined that

$$E_T^2 = E_1^2 + E_2^2 + E_3^2, \tag{2.80}$$

then the direction cosines of the energy flux vector (E_i') can be formed by

$$E_i' = \frac{E_i}{E_T}. \tag{2.81}$$

If

$$E_i' = l_i, \tag{2.82}$$

then the wave propagates along the direction of the wave normal and there is no energy flux deviation. Otherwise, the angle (δ) of deviation of the energy flux from the wave normal can be determined by

$$\delta = \cos^{-1}(E_i' l_i). \tag{2.83}$$

Therefore, to determine the elastic moduli by using ultrasonic velocity measurements, a number of considerations must be examined. First, the elastic symmetry and

thus the form of the elastic stiffness matrix must be known. Then a direction of propagation must be chosen and the solutions for the velocities of the three waves that propagate along this direction must be calculated in terms of the density and the elastic moduli. Also, any energy flux deviation of the three wave modes must be determined. This is repeated for a number of different directions until enough independent equations are derived to calculate all of the elastic moduli from the corresponding velocity measurements. Usually, an attempt is usually made to choose directions which propagate waves which are pure mode and suffer no energy flux deviations to make the measurements as easy as possible. Unfortunately, this can not always be accomplished. Brugger [42] published an equation which can be used to determine the pure mode directions for the various elastic symmetries. In general form this equation is

$$\epsilon_{ijk} c_{jlrs} l_k l_l l_r l_s = 0 \tag{2.84}$$

where ϵ_{ijk} is the permutation tensor.

It is defined by

$$\epsilon_{ijk} = \begin{cases} 0 & \text{if any i,j,k are equal} \\ 1 & \text{if i,j,k are in cyclic order} \\ -1 & \text{if i,j,k are in acyclic order} \end{cases} \tag{2.85}$$

Also presented are the pure mode wave directions for the various elastic symmetries.

The specific case of elastic wave propagation in a unidirectionally graphite fiber reinforced composite will now be discussed. First, the applicability of the previously derived wave equations to a composite material must be considered with respect to the heterogeneous nature of the medium. This violates one of the initial assumptions that the medium be homogeneous. However, it is generally assumed that if the wavelength of the elastic waves is much larger than the size of the inhomogeneity, then the material is macroscopically homogeneous and the wave equations are applicable. In the materials studied, the size of the inhomogeneity is given by the diameter of the fibers which is

on the order of seven μm . In the frequency range used ($\approx$ 2.25MHz) , the wavelengths for the different wave modes and directions of propagation ranged from about 700μm to almost 5000μm . Therefore, the previously stated assumptions are valid as are the wave equations.

Another important question is the use of Hooke's law because of the viscoelastic nature of most polymeric materials. However, epoxies and their composites, because of the high degree of crosslinking along the molecular chains, generally exhibit little viscoelastic behavior. This is especially true at the temperatures at which these measurements were made (room temperature). Measurements of the wave speeds and thus the moduli as a function of frequency demonstrated no viscoelastic effects. Therefore the application of Hooke's law appeared to be valid.

The appropriate elastic symmetry model for a unidirectionally fiber reinforced graphite/epoxy composite must now be chosen in order to derive the specific solutions for the velocities of ultrasonic wave propagation. The most common symmetry model used for unidirectional composities is that of transverse isotropy. In a transversely isotropic material, there exists a preferred axis perpendicular to which there exists a plane in which the material behaves isotropically. In unidirectional graphite/epoxy, the fiber direction (x_3) is the preferred axis while the x_1x_2 plane is the plane of isotropy as shown in Fig. 2.7. Transversely isotropic behavior of unidirectional composites is based on the assumption of a random distribution of fibers in the x_1x_2 plane as well as alignment of the fibers along the x_3 axis. The symmetry conditions for such a material are that it be elastically insensitive to twofold (180 degree) rotations about each of the three axes as well as insensitive to any rotation around the x_3 axis. Application of these symmetry conditions as shown in Appendix A demonstrates that there are only five independent elastic moduli. The matrix form of the elastic stiffness moduli for a transversely isotropic material is then given by

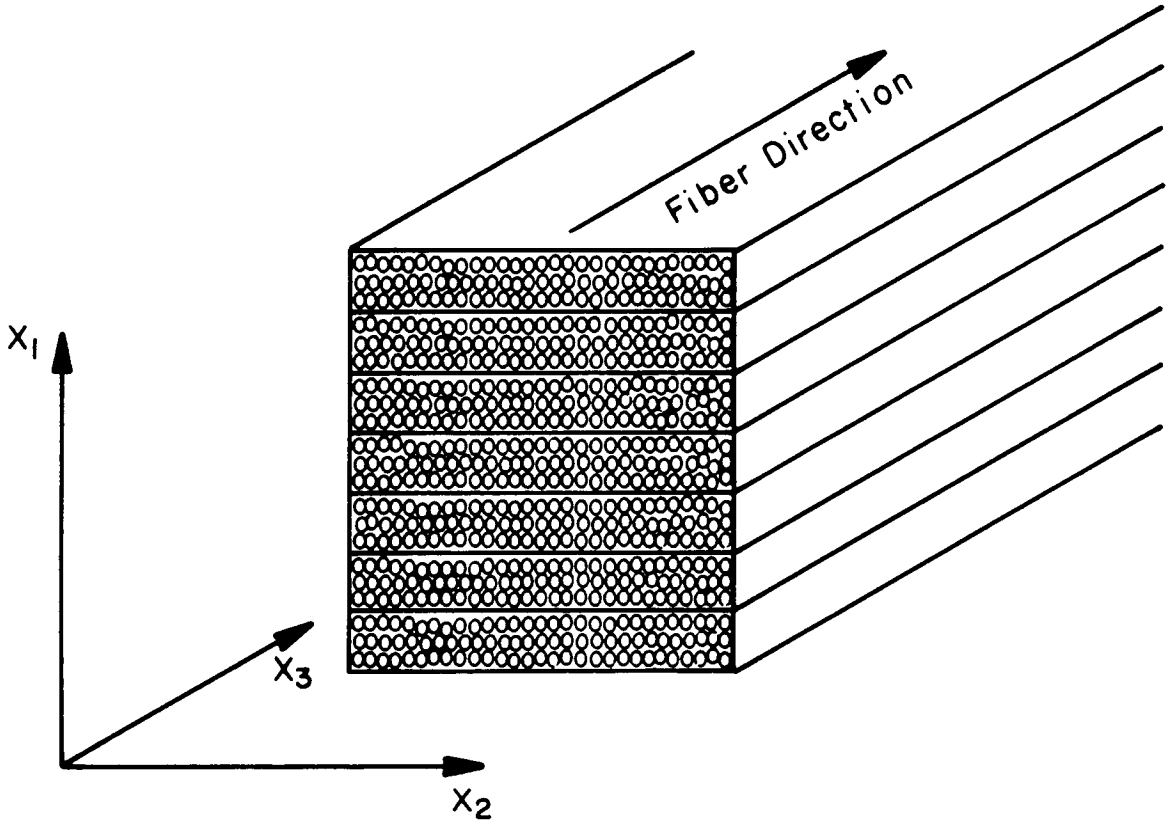

Figure 2.7 - Illustration of axis designation in a unidirectional fiber reinforced composite with respect to the fiber direction and the lamina stacking direction.

$$[c_{AB}] = \begin{bmatrix} c_{11} & c_{12} & c_{13} & 0 & 0 & 0 \\ c_{12} & c_{11} & c_{13} & 0 & 0 & 0 \\ c_{13} & c_{13} & c_{33} & 0 & 0 & 0 \\ 0 & 0 & 0 & c_{44} & 0 & 0 \\ 0 & 0 & 0 & 0 & c_{44} & 0 \\ 0 & 0 & 0 & 0 & 0 & \frac{c_{11} - c_{12}}{2} \end{bmatrix} \quad (2.86)$$

However, if for some reason the fibers are not randomly spaced in the x_1x_2 plane, this plane will no longer be elastically isotropic. In this case, the material will possess an orthotropic symmetry. This might occur if because of the lay up process of manufacture there was a resin rich layer between each lamina as shown in Fig. 2.8 or if some of the laminae were misoriented. The resulting orthotropic material would now have only the two fold symmetries about each of the three axes as is the case with cross ply or angular ply composite lay ups. For this symmetry the number of independent linear elastic moduli increases to nine as shown in Appendix A. The matrix form of the moduli is then

$$[c_{AB}] = \begin{bmatrix} c_{11} & c_{12} & c_{13} & 0 & 0 & 0 \\ c_{12} & c_{22} & c_{23} & 0 & 0 & 0 \\ c_{13} & c_{23} & c_{33} & 0 & 0 & 0 \\ 0 & 0 & 0 & c_{44} & 0 & 0 \\ 0 & 0 & 0 & 0 & c_{55} & 0 \\ 0 & 0 & 0 & 0 & 0 & c_{66} \end{bmatrix} \quad (2.87)$$

Ultrasonic velocity data can be compared with the equations derived for both models to determine which gives the best fit to the data. The derivations of the equations for the velocity as a function of density and elastic moduli for a number of different directions and pure wave modes for transversely isotropic and orthotropic symmetries are presented in Appendix B. However a summary of the results is presented in

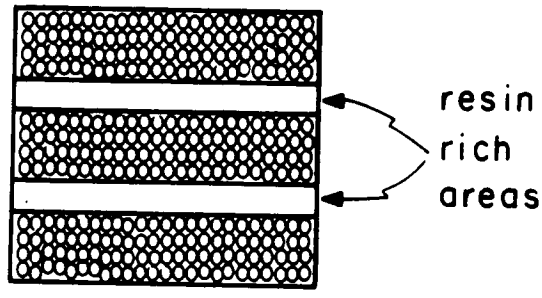

Figure 2.8 - Illustration of unidirectional composite with resin rich regions between laminae causing the material to have orthotropic elastic symmetry.

Table 2.1. To determine all of the elastic moduli for the two models, several nonpure mode waves must be used. The results for these waves are presented in Table 2.2.

II.C. Experiment

In most of the ultrasonic velocity measurements made in this study, a pulse echo overlap velocity measurement system was used. This system was briefly discussed in the Introduction. However, the details of its operation will now be discussed. Figure 2.9 shows a block diagram of the entire pulse echo overlap system. A Matec model 6600 pulse modulator and receiver was used to generate an electrical tone burst of variable amplitude and frequency. This was used to excite an ultrasonic transducer (typically undamped crystals of quartz or PZT with fundamental resonances of approximately 2.25 MHz.) which excited ultrasonic waves into the graphite/epoxy samples. The resulting echoes from the back surface of the specimen were detected by the same transducer and converted back into electrical signals. The received signals were input into the receiver and amplified. After amplification, they were displayed on a Hewlitt Packard (H.P.) 1743A dual trace oscilloscope. A typical pulse echo pattern is shown in Fig. 2.10. The echoes appear identical to the generating signal (main bang) except for an exponential decrease in amplitude due to attenuation in the sample.

To have the pulse echo pattern appear stable on the oscilloscope, the Matec generator and the H.P. 1743A oscilloscope must be triggered simultaneously. This was accomplished by using the triggering components of the pulse echo overlap system. The signal from a continuous wave (c.w.) oscillator (Matec model 110) was input into a Matec 122B decade divider and dual delay generator. The Matec 122B divided the original signal by a preset amount (typically 1000) and then generated a trigger signal at the divided frequency. This is demonstrated for frequency division by five in Fig. 2.11.

Table 2.1 - Equations for pure mode linear elastic wave propagation in transversely isotropic and orthotropic media.

Propagation Direction Cosines	Particle Displacement Direction Cosines	Wave Mode	Transversely Isotropic Model	Orthotropic Model
$l_1 = 1$	$\alpha_1 = 1 \quad \alpha_2 = 0 \quad \alpha_3 = 0$	PL	$\rho_0 v^2 = c_{11}$	$\rho_0 v^2 = c_{11}$
$l_2 = 0$	$\alpha_1 = 0 \quad \alpha_2 = 1 \quad \alpha_3 = 0$	PT	$\rho_0 v^2 = \frac{1}{2}(c_{11} - c_{12})$	$\rho_0 v^2 = c_{66}$
$l_3 = 0$	$\alpha_1 = 0 \quad \alpha_2 = 0 \quad \alpha_3 = 1$	PT	$\rho_0 v^2 = c_{44}$	$\rho_0 v^2 = c_{55}$
$l_1 = 0$	$\alpha_1 = 1 \quad \alpha_2 = 0 \quad \alpha_3 = 0$	PT	$\rho_0 v^2 = \frac{1}{2}(c_{11} - c_{12})$	$\rho_0 v^2 = c_{66}$
$l_2 = 1$	$\alpha_1 = 0 \quad \alpha_2 = 1 \quad \alpha_3 = 0$	PL	$\rho_0 v^2 = c_{11}$	$\rho_0 v^2 = c_{22}$
$l_3 = 0$	$\alpha_1 = 0 \quad \alpha_2 = 0 \quad \alpha_3 = 1$	PT	$\rho_0 v^2 = c_{44}$	$\rho_0 v^2 = c_{44}$
$l_1 = 0$	$\alpha_1 = 1 \quad \alpha_2 = 0 \quad \alpha_3 = 0$	PT	$\rho_0 v^2 = c_{44}$	$\rho_0 v^2 = c_{55}$
$l_2 = 0$	$\alpha_1 = 0 \quad \alpha_2 = 1 \quad \alpha_3 = 0$	PT	$\rho_0 v^2 = c_{44}$	$\rho_0 v^2 = c_{44}$
$l_3 = 1$	$\alpha_1 = 0 \quad \alpha_2 = 0 \quad \alpha_3 = 1$	PL	$\rho_0 v^2 = c_{33}$	$\rho_0 v^2 = c_{33}$

Table 2.2 - Equations for non pure mode, off axis linear elastic wave propagation in transversely istotropic and orthotropic media.

Transverse Isotropy		
Propagation Direction Cosines	Wave Mode	$\rho_0 v^2$
$l_1 = \frac{1}{\sqrt{2}}$	QL	$\frac{1}{4}\left[c_{11} + 2c_{44} + c_{33} + \sqrt{(c_{11} - c_{33})^2 + 4(c_{13} + c_{44})^2}\right]$
$l_2 = 0$	PT	$\frac{1}{2}\left[\frac{1}{2}(c_{11} - c_{12}) + c_{44}\right]$
$l_3 = \frac{1}{\sqrt{2}}$	QT	$\frac{1}{4}\left[c_{11} + 2c_{44} + c_{33} - \sqrt{(c_{11} - c_{33})^2 + 4(c_{13} + c_{44})^2}\right]$
$l_1 = 0$	QL	Same as QL above
$l_2 = \frac{1}{\sqrt{2}}$	PT	Same as PT above
$l_3 = \frac{1}{\sqrt{2}}$	QT	Same as QT above
$l_1 = \frac{1}{\sqrt{2}}$	PL	c_{11}
$l_2 = \frac{1}{\sqrt{2}}$	PT	c_{44}
$l_3 = 0$	PT	$\frac{1}{2}(c_{11} - c_{12})$

Table 2.2 - (Continued)

Orthotropy		
Propagation Direction Cosines	Wave Mode	$\rho_0 v^2$
$l_1 = \frac{1}{\sqrt{2}}$	QL	$\frac{1}{4}\left[c_{11} + 2c_{55} + c_{33} + \sqrt{(c_{11} - c_{33})^2 + 4(c_{13} + c_{55})^2}\right]$
$l_2 = 0$	PT	$\frac{1}{2}(c_{44} + c_{66})$
$l_3 = \frac{1}{\sqrt{2}}$	QT	$\frac{1}{4}\left[c_{11} + 2c_{55} + c_{33} - \sqrt{(c_{11} - c_{33})^2 + 4(c_{13} + c_{55})^2}\right]$
$l_1 = 0$	QL	$\frac{1}{4}\left[c_{22} + 2c_{44} + c_{33} + \sqrt{(c_{22} - c_{33})^2 + 4(c_{23} + c_{44})^2}\right]$
$l_2 = \frac{1}{\sqrt{2}}$	PT	$\frac{1}{2}(c_{55} + c_{66})$
$l_3 = \frac{1}{\sqrt{2}}$	QT	$\frac{1}{4}\left[c_{22} + 2c_{44} + c_{33} - \sqrt{(c_{22} - c_{33})^2 + 4(c_{23} + c_{44})^2}\right]$
$l_1 = \frac{1}{\sqrt{2}}$	QL	$\frac{1}{4}\left[c_{11} + 2c_{66} + c_{22} + \sqrt{(c_{11} - c_{22})^2 + 4(c_{12} + c_{66})^2}\right]$
$l_2 = \frac{1}{\sqrt{2}}$	PT	$\frac{1}{2}(c_{44} + c_{55})$
$l_3 = 0$	QT	$\frac{1}{4}\left[c_{11} + 2c_{66} + c_{22} - \sqrt{(c_{11} - c_{22})^2 + 4(c_{12} + c_{66})^2}\right]$

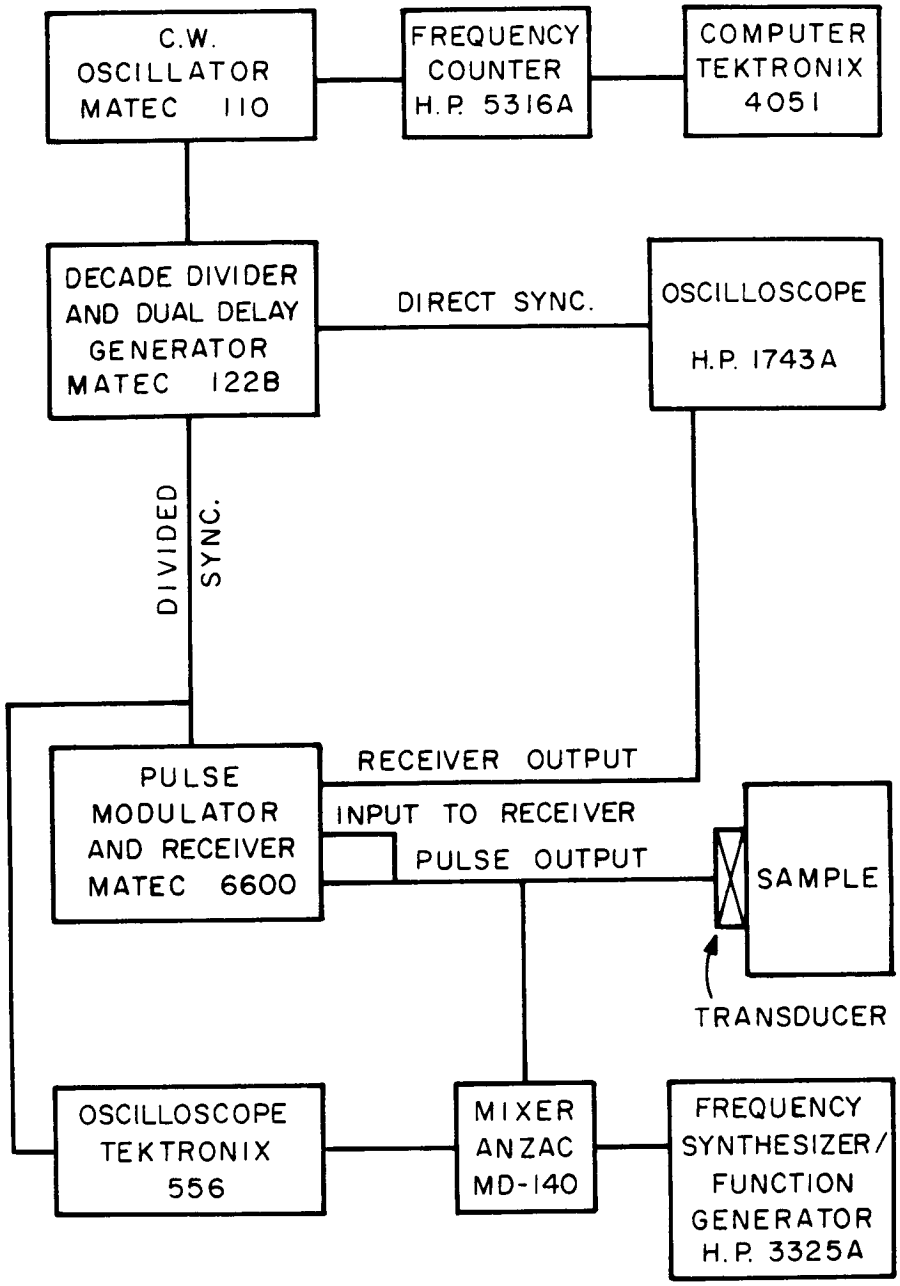

Figure 2.9 - Block diagram of pulse echo overlap system.

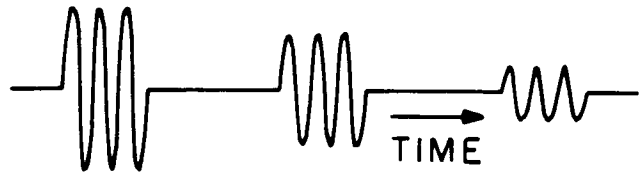

Figure 2.10 - Illustration of a typical pulse echo pattern demonstrating voltage versus time.

The trigger signal was then used to trigger both the Matec model 6600 and the oscilloscope. The Matec model 122B also generated a dual strobe which was input into the z axis of the scope. This had the effect of intensifying two chosen regions of the oscilloscope trace. The width and spacing of the strobes was variable.

The high accuracy in measuring the time between two echoes needed to compute the velocity arises because of a special triggering technique. First, the echo pattern was set up as previously described. The strobes were set so that two echoes were intensified on the trace and the scope intensity control was adjusted so that only these two echoes remained visible on the trace. Then, using another output of the Matec model 122B, a trigger signal was applied to the oscilloscope which was at the original rate of the Matec oscillator which was typically 1000 times faster than the trigger rate of the Matec model 6600. This caused an oscilloscope trace to be drawn out 1000 times during the single pulse echo cycle of the Matec 6600. The effect of this, because of the persistence of the oscilloscope screen, was to make the two echoes appear together on the screen as shown in Fig. 2.12. If the trigger frequency was adjusted, the two echoes could be caused to coincide on the screen or "overlapped" as shown in Fig. 2.13. The frequency (f) of the Matec c.w. oscillator at which this occurred was related to the time between echoes (t) by

$$t = \frac{n}{f} \tag{2.88}$$

where n was an integer.

By measuring two successive overlap frequencies (f_1,f_2), the integer n could be taken out of the equation and the time of flight then given by

$$t = \left(\frac{1}{f_2 - f_1} \right) \tag{2.89}$$

A number of overlap frequencies were measured and the results averaged to get a more reliable value for t. The main uncertainties of the measurement of t were the

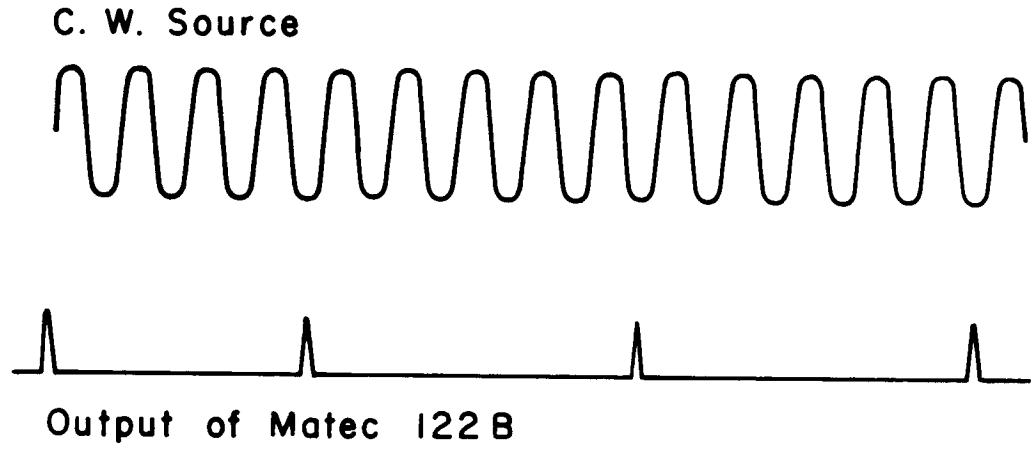

Figure 2.11 - Illustration of frequency division of a continuous wave (c.w.) source by the Matec model 122B by a factor of five.

Figure 2.12 - Illustration of an oscilloscope trace of two echoes during the pulse echo overlap technique where the echoes are not properly overlapped.

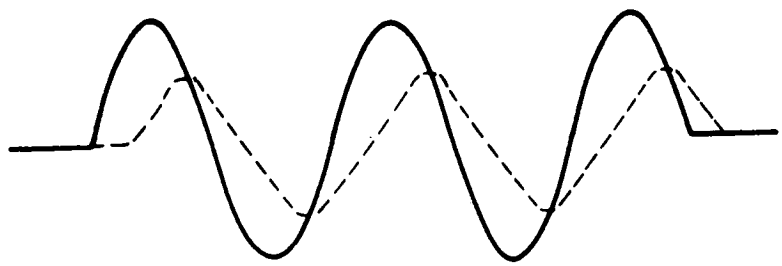

Figure 2.13 - Illustration of two properly overlapped echoes.

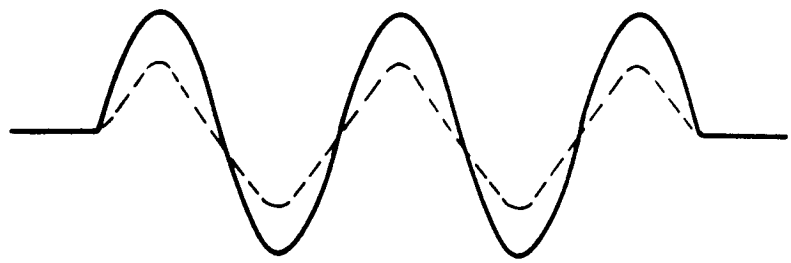

uncertainty in the operator's visual ability to detect the overlapped condition and the uncertainty in the measurement of the c.w. oscillator frequency.

Because of time delays of the ultrasonic pulse in the bond and phase shifts at the specimen-transducer interface, corrections had to be made to determine the true time of flight (δ) from the measured time (t). The theory for these corrections was presented by McSkimmin [19] and is outlined in Appendix C. In this theory it is necessary to determine the frequency of the ultrasonic pulse. This was accomplished by inputting the tone burst into a mixer (Anzac MD-40) along with the signal from a H.P. 3325A frequency synthesizer/function generator. The output of the mixer was then input into a Tektronix 53C oscilloscope. The output of the mixer was the sum and difference frequencies of the tone burst and the H.P. c.w. source. If they were of the same frequency, the output of the mixer was a constant voltage (0 Hz) dependent on the phase difference between the two signals. This phase difference was variable each time the Matec 6600 was triggered and thus a series of parallel lines was generated on the scope trace. This is shown in Fig. 2.14. If the frequencies were different, then the output would have the difference frequency again phase shifted on each new trace. Therefore, the frequency of the tone burst from the Matec 6600 could be monitored by the frequency of the H.P. frequency synthesizer.

The remaining equipment was used to collect data. A Tektronix 4051 computer was used to read the trigger frequency values and calculate the time of flight which was used to calculate the velocities and the moduli. The program used to control the pulse echo overlap data acquisition and analysis is shown in Appendix D.

There were a number of factors which affected the size and geometry of the samples used. They had to have parallel sides to be used in the pulse echo technique. Also, the thicker the specimen, the more accurately its time of flight could be measured. However, because of the high ultrasonic attenuation of graphite/epoxy composites, especially for shear waves, there were limits on the maximum thickness. Also, limits on

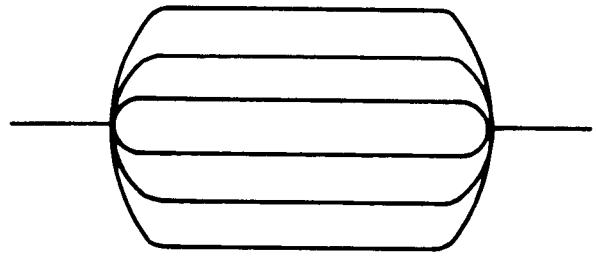

Figure 2.14 - Illustration of the oscilloscope trace of the output of a mixer when the input c.w. and pulse sources are of the same frequency.

sample thickness occurred because of the desire to have the wavefront remain planar. The distance (d) over which the wavefront remains planar was given by Mason [43] as

$$d \approx \frac{R^2}{2\lambda} \tag{2.90}$$

where R is the radius of the transducer

and λ is the wavelength of the ultrasonic wave.

However limitations on the thickness because of the large attenuation usually occurred before this requirement became important. There were also restrictions on the lateral dimensions of the samples. The equation of motion are based on the assumption of a wave propagating through a unbounded medium. However, ultrasonic velocities have been shown by Tu et al. [44] to be independent of lateral dimensions if the sample was at least two and one half times the acoustic wavelength.

The above constraints provided the basis for the choice of the sample geometries used. Ideally, the measurements of the elastic moduli would be made using only one sample to avoid any problems with sample to sample variations in the elastic properties. These problems are especially prevalent in polymer composite materials where elastic property variations may occur not only from batch to batch due to different curing procedures but also within a given batch because of regional variation of fiber content, void content and other important parameters. However, because of the above constraints and the necessity to use off axis non pure mode wave propagation to determine some of the moduli, several samples were required. These samples were all cut from a 150 ply laminate of T300/5208 unidirectional graphite/epoxy that was nominally 12 X 15 X 0.9 in. (30.5 X 38.1 X 2.3 cm.) after cure. This panel was designated MCIS 1 and layed up and cured at NASA, Langley Research Center. The finished panel was ultrasonically C-scanned by the Materials Characterization and Instrumentation Section at NASA Langley for the presence of gross voids or delaminations. None were found to be present. A number of tensile and compression samples were then cut and machined

from this panel. Those used for the ultrasonic testing were MCIS 1.10A, 1.8A, 1.10B, 1.7A, 1.5 A,B,E and F and 1.6A. whose dimensions are listed in Tables 2.3 and 2.4. The samples were generally flat and parallel to +/- 0.0003 in. (0.00076 cm.) or better. Samples MCIS 1.10A, 1.8A, 1.10B and 1.7A were all rectangular parallelepipeds with their faces oriented perpendicular to the three coordinate axes. The densities for each are also given in Table 2.3 which show some sample to sample variation. The remaining samples were cut to allow wave propagation in a direction that was 45 degrees between two of the axes and perpendicular to the third. These samples were used to propagate the waves listed in Table 2.2. The sample dimensions are given in Table 2.4. The densities of these samples were not measured but the value of 1.54 g/cm^3 was used for all calculations involving these specimen.

Measurements of the pure mode longitudinal wave speeds along each of the three coordinate axes were made using specimen MCIS 1.10A. Specimen MCIS 1.8A, 1.10B and 1.7A were used to determine the six different combinations of polarization and propagation directions for the pure mode shear waves along the three axes. The velocities and the product $\rho_0 v^2$ for each of these waves are shown in Table 2.5. The uncertainties for the shear wave velocities were larger than those of the longitudinal velocities because of the much higher attenuation of shear waves. Even using the thinner specimen for the shear waves did not overcome the high attenuation. This resulted in a much smaller amplitude second echo which was difficult to reproducibly overlap. The uncertainty in the longitudinal velocity along x_3 was also large because of the high velocity and thus the short time of flight along this direction.

The measured values were then compared with theory to check for transversely isotropic behavior. The products $\rho_0 v^2$ calculated using the longitudinal waves along x_1 and x_2 in sample MCIS 1.10A should be equal as should the products calculated from the two shear waves propagating along x_3 in sample MCIS 1.8A. Comparisons for the other similar products were not valid because they were obtained on different samples.

Table 2.3 - Sample dimensions and densities for samples used for pure mode elastic wave propagation.

Sample Number	Dimensions (in.) x_1	x_2	x_3	Density (g/cm^3)
1.10A	0.8001	0.7999	0.8002	1.5404 +/− 0.0004
1.10B	0.7999	0.5002	0.7996	1.5460 +/− 0.0006
1.8A	0.8002	0.8000	0.5002	1.5384 +/− 0.0005
1.7A	0.5001	0.8001	0.7999	1.5411 +/− 0.0005

Table 2.4 - Sample dimensions for samples used for off axis, non pure mode wave propagation.

Sample Number	Dimension (in.) along axis 45 degrees between axes		Dimension (in.) along axis	
1.5A	0.4499	x_1, x_3	0.9	x_2
1.5B	0.5000	x_1, x_3	0.9	x_2
1.5E	0.4491	x_2, x_3	0.9	x_1
1.5F	0.4993	x_2, x_3	0.9	x_1
1.6A	0.5001	x_1, x_2	0.9	x_3

Table 2.5 - Data for pure mode linear elastic wave propagation.

Sample Number	Propagation Direction	Polarization Direction	Velocity (10^5cm/s)	$\rho_0 v^2$ (GPa)
1.10A	x_1	x_1	3.0467 +/- 0.0005	14.295 +/- 0.005
1.10A	x_2	x_2	3.0390 +/- 0.0008	14.226 +/- 0.006
1.10A	x_3	x_3	8.390 +/- 0.007	108.4 +/- 0.1
1.7A	x_1	x_2	1.557 +/- 0.002	3.736 +/- 0.007
1.7A	x_1	x_3	1.849 +/- 0.003	5.27 +/- 0.01
1.10B	x_2	x_1	1.558 +/- 0.003	3.75 +/- 0.01
1.10B	x_2	x_3	1.850 +/- 0.003	5.29 +/- 0.01
1.8A	x_3	x_1	1.850 +/- 0.002	5.265 +/- 0.008
1.8A	x_3	x_2	1.851 +/- 0.002	5.271 +/- 0.008

In the first comparison, the difference was larger than experimental error. However, it was still quite small and thus the deviation from transversely isotropic elastic behavior was small. In the comparison of the shear wave products, the difference is smaller than experimental uncertainty. Thus, overall the elastic behavior of the material was very nearly transversely isotropic for linear elasticity.

Using the data presented in Table 2.5, four of the transversely isotropic moduli can be calculated using the equations from Table 2.1. Also, six of the nine orthotropic moduli can be calculated. However, to determine the transversely isotropic c_{13} and the orthotropic c_{12},c_{13}, and c_{23} , off axis quasilongitudinal and quasishear mode waves had to be used. The samples used for these measurements were MCIS 1.5 A,B,E and F and 1.6A. As pointed out by Kriz and Stinchcomb [45], these wave modes suffer energy flux deviations as large as 43 degrees which impose further specimen size requirements. The basic requirements are that the sample was thick enough to allow the two quasi-mode waves to separate into distinct wave forms and thin enough so that the deviation of the wave did not cause it to impinge on the side of the specimen. The energy flux deviation and large attenuation also prevented the use of the pulse echo method for the velocity measurements. For these measurements, two transducers were used in a through transmission arrangement. The time of flight was first measured through a fused quartz delay line. Then it was measured through the delay line and the specimen for the different wave modes. The difference between the two was taken to be the time of flight and used to calculate the velocity. The uncertainty of this method is much larger than the pulse echo overlap method resulting in much reduced accuracy. The results are shown in Table 2.6 which show large scatter due to uncertainty in the measurement as well as material variations.

Using the data from Tables 2.5 and 2.6 with the equations from Tables 2.1 and 2.2, the independent elastic moduli were determined for both the transverse isotropy and orthotropy models. The results are presented in Table 2.7. Where possible, the

multiple results were averaged except for c_{13} and c_{23} where there was a wide range of values. This wide range was due to the large uncertainty in the measurements which propagates into an even larger uncertainty in the calculated values. The values presented for c_{13} and c_{23} were calculated using the quasishear data because the quasi-longitudinal data yielded complex values for the moduli.

The values for the transversely isotropic model can be compared with those reported by Kriz and Stinchcomb [45]. They reported data for the moduli of T300/5208 graphite/epoxy measured ultrasonically as well as the values theoretically predicted from the properties of the fibers and matrix. The theoretical values are derived for an assumed volume fraction of fibers of 0.67. These are all presented in Table 2.8. The values all compare favorably except for c_{33} which was much lower in the present study. The lower density of the samples used in the present experiments implies that there may be a lower fiber content and/or a higher void content. This would account for some of the discrepancy in the value of c_{33} . There may also be some misalignment of the fibers along the x_3 axis which would also lower the value of c_{33} although there is no other confirming evidence of this fact. The values of Kriz and Stinchcomb also show much more scatter demonstrating sample to sample variations.

To calculate the nonlinear elastic moduli, the isothermal linear elastic compliance moduli are also needed. The adiabatic compliance moduli can be obtained by inverting the stiffness matrix. Corrections for differences in adiabatic versus isothermal moduli can then be applied if they are larger than the uncertainties of the inverted values. For the case of transverse isotropy the compliances are given by the following equations,

$$s_{11} = \frac{c_{11}c_{33} - c_{13}^2}{c_{33}(c_{11}^2 - c_{12}^2) + 2c_{13}^2(c_{12} - c_{11})}, \tag{2.91}$$

$$s_{33} = \frac{c_{11} + c_{12}}{c_{33}(c_{11} + c_{12}) - 2c_{13}^2}, \tag{2.92}$$

Table 2.6 - Data for off axis, non pure mode linear elastic wave propagation.

Sample Number	Propagation Direction		Wave Mode	Velocity (10^5cm/s)	$\rho_0 v^2$ (GPa)
	Perpendicular to	45 degrees between			Assuming $\rho_0 = 1.54$g/cm^3
1.5A	x_2	x_1, x_3	QL	5.78	51.4
1.5A	x_2	x_1, x_3	QT	2.47	9.40
1.5B	x_2	x_1, x_3	QL	5.73	50.6
1.5B	x_2	x_1, x_3	QT	2.38	8.72
1.5E	x_1	x_2, x_3	QL	6.00	55.44
1.5E	x_1	x_2, x_3	QT	2.42	9.01
1.5F	x_1	x_2, x_3	QL	5.86	52.9
1.5F	x_1	x_2, x_3	QT	2.40	8.87
1.6A	x_3	x_1, x_2	QL	3.043	14.26
1.6A	x_3	x_1, x_2	QT	1.558	3.74

Table 2.7 - Measured linear elastic moduli for transversely isotropic and orthotropic symmetries.

Transversely Isotropic Modulus	Value (GPa)	Orthotropic Modulus	Value (GPa)
c_{11}	14.26	c_{11}	14.295
c_{12}	6.78	c_{12}	6.78
c_{13}	3.0 - 8.9	c_{13}	3.3 - 9.0
c_{33}	108.4	c_{33}	108.4
c_{44}	5.27	c_{44}	5.28
		c_{22}	14.226
		c_{23}	6.6 - 7.7
		c_{55}	5.27
		c_{66}	3.74

Table 2.8 - Comparison of measured transversely isotropic stiffness data with that presented by Kriz and Stinchcomb [45].

Modulus	Present Work (GPa)	Kriz and Stinchcomb	
		Experiment	Theory
c_{11}	14.26	15.0 - 15.7	14.5
c_{12}	6.78	7.10 - 7.58	7.24
c_{13}	3.0 - 8.9	6.96 - 9.09	6.50
c_{33}	108.4	154	161
c_{44}	5.27	7.84	7.10

$$s_{12} = \frac{-(c_{12}c_{33} - c_{13}^2)}{c_{33}(c_{11}^2 - c_{12}^2) + 2c_{13}^2(c_{12} - c_{11})}, \tag{2.93}$$

$$s_{13} = \frac{c_{13}(c_{12} - c_{11})}{c_{33}(c_{11}^2 - c_{12}^2) + 2c_{13}^2(c_{12} - c_{11})} \tag{2.94}$$

and

$$s_{44} = \frac{1}{c_{44}}. \tag{2.95}$$

Because of the large uncertainty in c_{13} , there is a variation in the possible values for the compliance moduli. The values for the compliances for the two extreme values of c_{13} are given in Table 2.9. The wide variation in the values of c_{13} has little effect except on the modulus s_{13} .

The inversion of the orthotropic stiffness moduli yields the following equations

$$s_{11} = \frac{c_{22}c_{33} - c_{23}^2}{c_{11}(c_{22}c_{33} - c_{23}^2) - c_{12}(c_{12}c_{33} - 2c_{13}c_{23}) - c_{13}^2c_{22}}, \tag{2.96}$$

$$s_{22} = \frac{c_{11}c_{33} - c_{13}^2}{c_{11}(c_{22}c_{33} - c_{23}^2) - c_{12}(c_{12}c_{33} - 2c_{13}c_{23}) - c_{13}^2c_{22}}, \tag{2.97}$$

$$s_{33} = \frac{c_{11}c_{22} - c_{12}^2}{c_{11}(c_{22}c_{33} - c_{23}^2) - c_{12}(c_{12}c_{33} - 2c_{13}c_{23}) - c_{13}^2c_{22}}, \tag{2.98}$$

$$s_{44} = \frac{1}{c_{44}}, \tag{2.99}$$

$$s_{55} = \frac{1}{c_{55}}, \tag{2.100}$$

$$s_{66} = \frac{1}{c_{66}}, \tag{2.101}$$

$$s_{12} = \frac{-(c_{12}c_{33} - c_{13}c_{23})}{c_{11}(c_{22}c_{33} - c_{23}^2) - c_{12}(c^{12}c_{33} - 2c_{13}c_{23}) - c_{13}^2c_{22}}, \tag{2.102}$$

$$s_{13} = \frac{c_{12}c_{23} - c_{13}c_{22}}{c_{11}(c_{22}c_{33} - c_{23}^2) - c_{12}(c_{12}c_{33} - 2c_{13}c_{23}) - c_{13}^2c_{22}} \tag{2.103}$$

Table 2.9 - Calculated linear elastic compliance values using ultrasonic stiffness data for transversely isotropic and orthotropic symmetries.

Compliance Moduli $(GPa)^{-1}$		
Transverse Isotropy		
Modulus	$c_{13} = 3.0$	$c_{13} = 8.9$
s_{11}	0.091	0.093
s_{12}	-0.043	-0.041
s_{13}	-0.0013	-0.0042
s_{33}	0.0093	0.0099
s_{44}	0.19	0.19
Orthotropy $(c_{23} = 7.2)$		
Modulus	$c_{13} = 3.3$	$c_{13} = 9.0$
s_{11}	0.090	0.093
s_{22}	0.093	0.092
s_{33}	0.0095	0.0098
s_{44}	0.19	0.19
s_{55}	0.19	0.19
s_{66}	0.27	0.27
s_{12}	-0.043	-0.042
s_{13}	0.00011	-0.0049
s_{23}	-0.0049	-0.0026

and

$$s_{23} = \frac{-(c_{11}c_{23} - c_{13}c_{12})}{c_{11}(c_{22}c_{33} - c_{23}^2) - c_{12}(c_{12}c_{33} - 2c_{13}c_{23}) - c_{13}^2c_{22}}. \quad (2.104)$$

The calculated values for these moduli are also presented in Table 2.9. Again there was a narrow range of values except in the constants s_{13} and s_{23} because of the large uncertainty in c_{13} and c_{23} .

The isothermal correction for these adiabatic compliance moduli can be calculated using equation (2.34). The temperature of these measurements was nominally 24 C and the density was 1.54 g/cm^3 . The coefficients of thermal expansion for similar unidirectional carbon/epoxy composites were given by Hull [46] as $\alpha_1 = \alpha_2 = 30 \cdot 10^{-6}$/C and $\alpha_3 = -0.2 \cdot 10^{-6}$/C and the specific heat was given by as $c_p = 2.1$ J/gC (unpublished data from C. Welsh, 1986). Using these values, the maximum correction term was only about $7 \cdot 10^{-6}$ GPa^{-1} which was much smaller than the uncertainty of the calculated values. Thus the difference between the adiabatic and the isothermal values for the compliance moduli was negligible.

Some of the elastic compliance moduli were also measured using static compressive loading with bonded strain gauges to measure the strain. The theory for this is based on Hooke's law. If a unidirectional stress is applied, for example, along the x_1 axis, the strain can be written as

$$\epsilon_1 = s_{11}\sigma_1, \quad (2.105)$$

$$\epsilon_2 = s_{12}\sigma_1, \quad (2.106)$$

$$\epsilon_3 = s_{13}\sigma_1 \quad (2.107)$$

and

$$\epsilon_4 = \epsilon_5 = \epsilon_6 = 0. \quad (2.108)$$

Therefore the moduli can be rewritten as

$$s_{1A} = \frac{d\epsilon_A}{d\sigma_1} \tag{2.109}$$

or in more general form as

$$s_{AB} = \frac{d\epsilon_B}{d\sigma_A}, \tag{2.110}$$

for a unidirectional stress along the A axis. Therefore the stress and strain can be measured and the slope of the stress-strain curve will provide the moduli.

The samples used in these measurements were cubes nominally 0.7 in. (1.8 cm.) on a side oriented with faces perpendicular to the coordinate axes. They were also cut from the panel MCIS 1 and were designated MCIS 1.8D and E. The load was applied with a MTS 810 load frame in compression and the calibrated output of the load cell was input into a H.P. 3478A digital multimeter. To insure that the load remained unidirectional, a fixture was designed and inserted into the load frame that placed the upper compression plate on a ball bearing. This allowed the compression plate to compensate for any slight lack of parallelism in the specimen. Fig 2.15 illustrates this fixture. The strains were measured with Measurements Group Inc. 350Ω strain gauges. The surfaces of the samples were cleaned according to manufacturer's instructions and the strain gauges were then bonded onto the samples. A conventional Wheatstone Bridge circuit was used with a H.P. 6002A power supply providing a five volt input and a H.P. 3478A voltmeter measuring the output voltage. A Tektronix 4051 computer was used to read the data from the voltmeters and calculate stress, strain and the resulting modulus. The control program is shown in Appendix E. Fig 2.16 shows the block diagram for the experimental set up. During each test, a unidirectional stress was applied and the corresponding strain was measured in two directions. One direction was parallel to the direction of applied stress while the other was perpendicular. Then

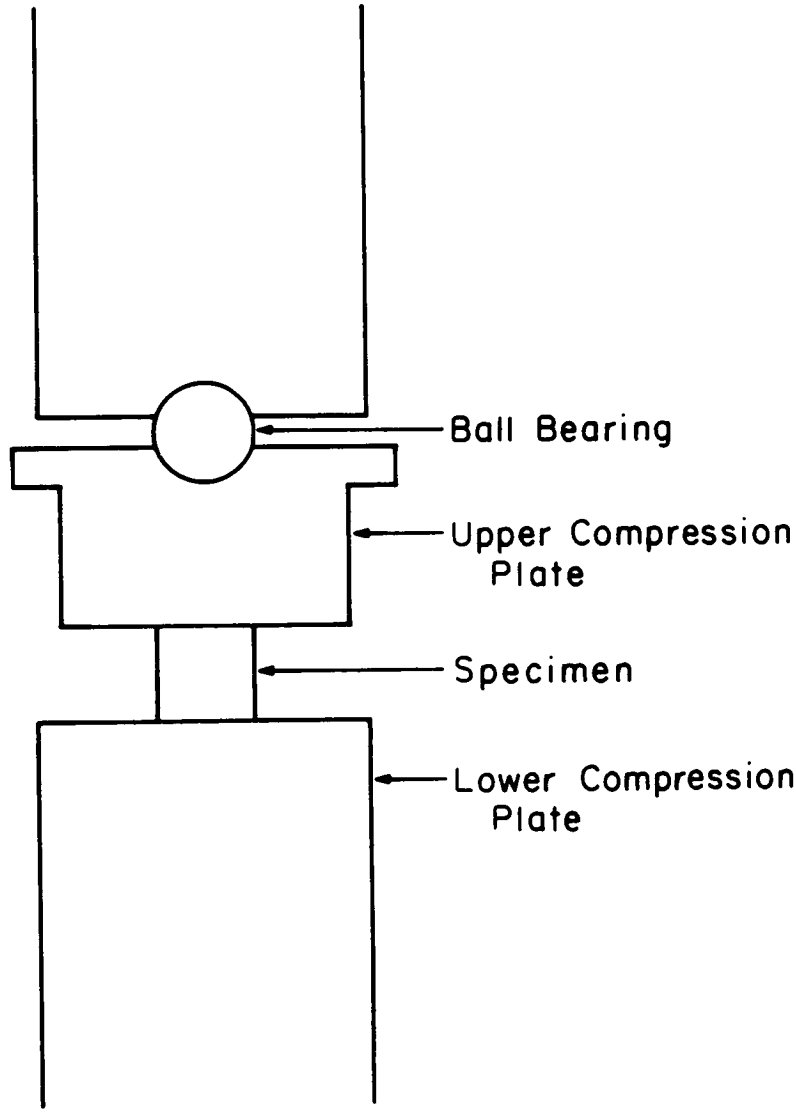

Figure 2.15 - Diagram of the compression fixture used during the static loading for the measurement of the elastic compliance moduli and the uniaxial stress acoustic constants.

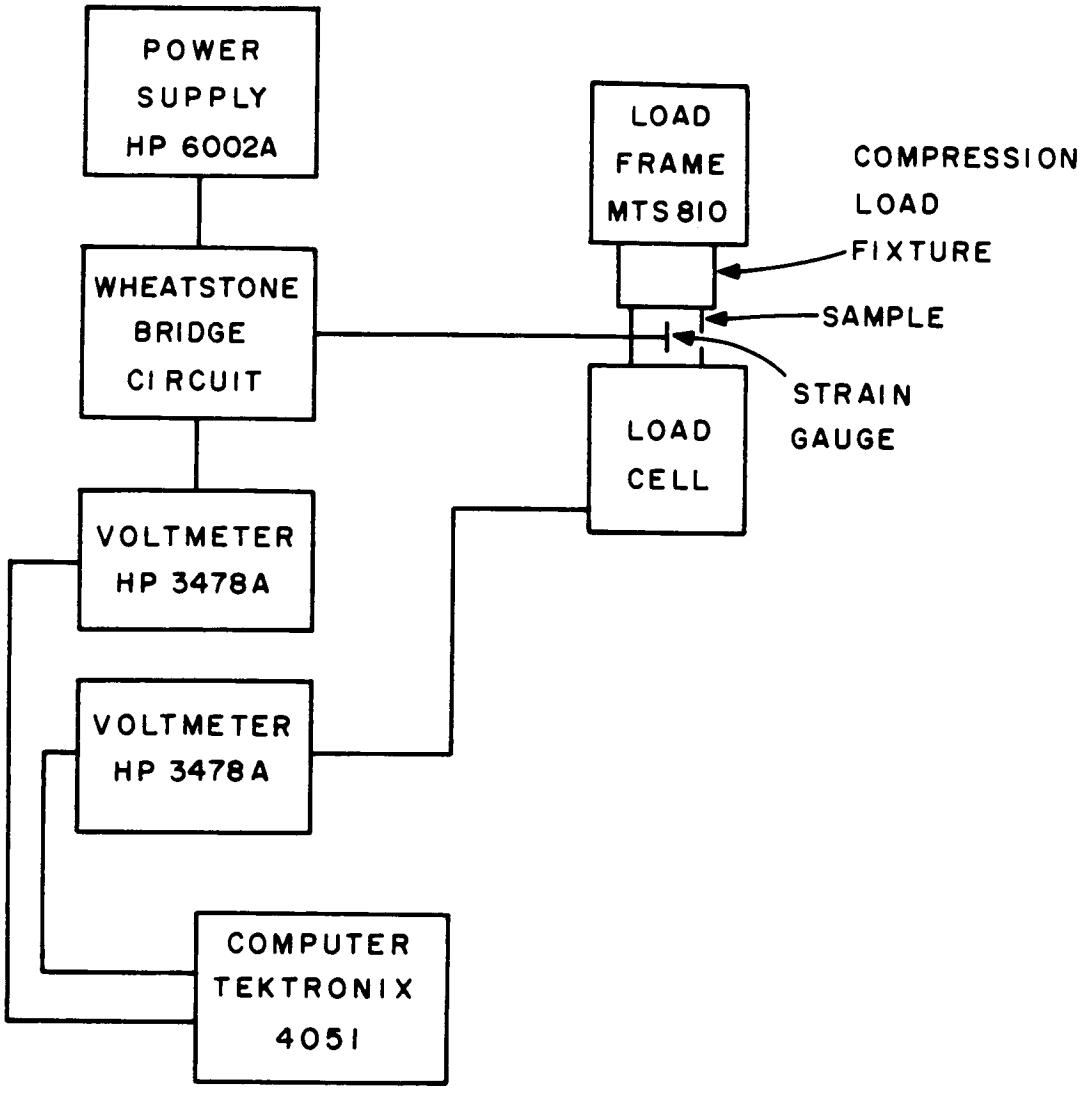

Figure 2.16 - Block diagram of the apparatus used for static measurement of the linear elastic compliance moduli.

the sample was reoriented to apply stress in a different direction.

The resulting values for the compliance moduli are given in Table 2.10. The shear moduli s_{44}, s_{55} and s_{66} were not measured by this technique. Again the deviation from transversely isotropic behavior is quite small as demonstrated by the good agreement between s_{11} and s_{22} and between s_{13} and s_{23} for the orthotropic moduli. These values compare favorably with the values obtained from the inversion of the ultrasonic data except for the value of s_{12} . This discrepancy could be caused by error accumulation in the inversion of the stiffness moduli of it could be due to inaccuracy of the static measurement. Ledbetter and Read [47] also compared static measurements to ultrasonic measurements for a NbTi fiber reinforced Cu composite and reported discrepancies in the off diagonal moduli. The measured values can also be compared to those presented by Garber [48] which are listed in Table 2.11. His measurements were made in tension on thin laminates of T300/5208. Because thin laminates were used, s_{12} was not measured. The values compare favorably except for s_{33} . This is consistent with the lower value of c_{33} reported earlier for the material in the present study.

II.D. Conclusion

The linear elastic stiffness and compliance moduli of a unidirectional graphite/epoxy composite have been measured by ultrasonic and static measurements. These measurements demonstrate a measurable deviation from transversely isotropic behavior. However, the deviation is very small, especially when compared to material variations from sample to sample, and thus the assumption of transverse isotropy for the linear elastic behavior of this material is valid.

Comparisons of the present data with that presented in the literature for similar materials are favorable except for the values of c_{33} and s_{33} . The difference in these

Table 2.10 - Measured linear elastic compliance values for transversely isotropic and orthotropic symmetries.

Transversely Isotropic Modulus	Value $(GPa)^{-1}$	Orthotropic Modulus	Value $(GPa)^{-1}$
s_{11}	0.089	s_{11}	0.0890
s_{12}	-0.063	s_{12}	-0.0626
s_{13}	-0.0021	s_{13}	-0.00208
s_{33}	0.00935	s_{33}	0.00935
		s_{22}	0.0891
		s_{23}	-0.00215

Table 2.11 - Comparison of measured compliance values with those presented by Garber [49].

Modulus	Present Work	Garber $(GPa)^{-1}$
s_{11}	0.089	0.0921
s_{12}	-0.063	not measured
s_{13}	-0.0021	-0.0025
s_{33}	0.00935	0.0078

moduli together with a lower measured density may indicate a lower fiber volume content or a higher void content in the material of the present study. It also may indicate either a poor alignment of the fibers or a waviness of the fibers along the fiber axis.

The comparisons of the ultrasonic and static data are good except for the modulus s_{12} . The difference may be an artifact of the measurement or the calculations used in the comparisons. Because of the higher accuracy of ultrasonic measurements, the values used in the computation of the nonlinear moduli in the next chapter are those obtained by ultrasonic measurements except in the case of s_{13} where large uncertainties exist.

III. NONLINEAR ELASTICTIY

III.A. Introduction

Using the linear elastic stiffness and compliance moduli presented in the previous chapter, the nonlinear elastic moduli can be calculated from measurements of the stress dependence of the ultrasonic "natural" velocity. In this chapter, the theory of how this is accomplished will be presented along with actual measurements and calculations for the unidirectional graphite/epoxy composites being studied.

III.B. Theory

The theory for nonlinear elasticity differs in several respects from the theory of linear elasticity which was presented earlier. The first major difference is that the assumption of infinitesimal deformation is no longer valid. Therefore, the strain tensor must be defined using either the Lagrangian or Eulerian definitions. In this work the Lagrangian formulation will be used. The constitutive equation (i.e. relation between stress and strain) must be extended to include higher order terms. Also the strain energy function must be extended. It is given by Brugger [12] as

$$\phi = \frac{1}{2}c_{ijkl}\eta_{ij}\eta_{kl} + \frac{1}{6}c_{ijklmn}\eta_{ij}\eta_{kl}\eta_{mn} + \cdots . \tag{3.1}$$

The numerical coefficient for each of the terms is $\frac{1}{n!}$ where n is the order of strain for that term. The Voigt reduced notation can be used to rewrite this equation as

$$\phi = \frac{1}{2}\sum_{A} c_{AA}\eta_A^2 + \sum_{A<B} c_{AB}\eta_A\eta_B + \frac{1}{6}\sum_{A} c_{AAA}\eta_A^3$$

$$+ \frac{1}{2}\sum_{A\neq B} c_{AAB}\eta_A^2\eta_B + \sum_{A<B<D} c_{ABD}\eta_A\eta_B\eta_d + \cdots \tag{3.2}$$

where no sum is implied except where indicated and the capital indices range from 1 to 6.

The definitions for the elastic moduli are similar to those of linear elastic theory. The higher order adiabatic and isothermal moduli were defined by Brugger [12] as

$$c^{S}_{ijklmn\ldots} = \rho_0 \left(\frac{\partial^n U}{\partial \eta_{ij} \partial \eta_{kl} \partial \eta_{mn} \cdots} \right)_S, \tag{3.3}$$

$$c^{T}_{ijklmn\ldots} = \rho_0 \left(\frac{\partial^n F}{\partial \eta_{ij} \partial \eta_{kl} \partial \eta_{mn} \cdots} \right)_T, \tag{3.4}$$

$$s^{S}_{ijklmn\ldots} = -\rho_0 \left(\frac{\partial^n H}{\partial t_{ij} \partial t_{kl} \partial t_{mn} \cdots} \right)_S \tag{3.5}$$

and

$$s^{T}_{ijklmn\ldots} = -\rho_0 \left(\frac{\partial^n G}{\partial t_{ij} \partial t_{kl} \partial t_{mn} \cdots} \right)_T. \tag{3.6}$$

However, in this research, the third order moduli were obtained by measuring the stress derivative (isothermal) of the ultrasonic velocity (adiabatic). Therefore the resulting moduli were the "mixed" third order moduli as defined by Brugger [12] as

$$c^{M}_{ijklmn} = \left(\frac{\partial c^{S}_{ijkl}}{\partial \eta_{mn}} \right)_T \tag{3.7}$$

or in reduced notation

$$c^{M}_{ABD} = \left(\frac{\partial c^{S}_{AB}}{\partial \eta_D} \right)_T. \tag{3.8}$$

They are related to the pure adiabatic third order moduli by

$$c^{S}_{ijklmn} = c^{M}_{ijklmn} + \frac{T}{\rho_0 C_T} c^{S}_{mnop} \alpha_{op} \left[c_{ijklqr} \alpha_{qr} - \left(\frac{\partial c^{S}_{ijkl}}{\partial T} \right)_T \right] \tag{3.9}$$

or

$$c^S_{ABD} = C^M_{ABD} + \frac{T}{\rho_0 C_T} C^S_{DE} \alpha_E \left[c^M_{ABF} \alpha_F - \left(\frac{\partial c^S_{AB}}{\partial T} \right)_T \right] \qquad (3.10)$$

However, again the differences are usually small and therefore less than experimental uncertainty.

Using the same arguments based on symmetry of the stress and strain tensors and the existence of the strain energy function, the number of independent third order elastic moduli can be reduced to 56 for the most general anisotropic material. Further considerations of the symmetry of the material reduces the number to 20 for an orthotropic material and 9 for a transversely isotropic material as shown in Appendix F. For the orthotropic case the independent moduli are c_{111}, c_{112}, c_{113}, c_{122}, c_{123}, c_{133}, c_{144}, c_{155}, c_{166}, c_{222}, c_{223}, c_{233}, c_{244}, c_{255}, c_{266}, c_{333}, c_{344}, c_{355}, c_{366} and c_{456} . All other moduli are equal to zero. The independent moduli for transverse isotropy are c_{111}, c_{112}, c_{113}, c_{123}, c_{133}, c_{144}, c_{155}, c_{333} and c_{344} with the following relations for the other moduli

$$\begin{aligned}
&c_{222} = c_{111}, \quad c_{355} = c_{344} \\
&c_{223} = c_{113}, \quad c_{166} = c_{266} = \frac{1}{4}(c_{111} - c_{112}) \\
&c_{255} = c_{144}, \quad c_{233} = c_{133} \\
&c_{244} = c_{155}, \quad c_{366} = \frac{1}{2}(c_{113} - c_{123}) \\
&c_{122} = c_{112}, \quad c_{456} = \frac{1}{2}(c_{155} - c_{144})
\end{aligned} \qquad (3.11)$$

with all remaining $c_{ABD} = 0$.

As mentioned previously, these moduli can be obtained from measurements of the stress derivative of the ultrasonic "natural" velocity. The theoretical basis for this was presented by Thurston and Brugger [14]. They rederived the equation of motion for a small amplitude elastic wave propagating in a homogeneously stressed medium using the following notation. The coordinates a_i refer to the position of a point of material in the "natural" or unstressed state. X_i are coordinates of the homogeneously stressed material

or the material in the initial state while x_i refer to the material in the stressed state deformed by the small amplitude elastic wave. The vector components u_i are the components of displacement from the initial state due to the elastic wave and are given by

$$u_i = x_i - X_i. \tag{3.12}$$

U_i are the components of displacement referred to the natural state and are related to u_i by

$$u_i = \left(\frac{\partial X_i}{\partial a_q}\right) U_q. \tag{3.13}$$

The wave equation was then presented as

$$\rho_0 \ddot{u}_j = \tilde{A}^S_{jkpm} \frac{\partial^2 u_k}{\partial a_p a_m} \tag{3.14}$$

where $\tilde{}$ refers to values in the initial state

and $\tilde{A}^S_{jkpm}$ is given by

$$\tilde{A}^S_{jkpm} = \delta_{jk}\tilde{t}_{pm} + \frac{\partial X_j \partial X_k}{\partial a_q \partial a_i}\tilde{c}^S_{pqmi}. \tag{3.15}$$

A solution in terms of the "natural" velocity was chosen of the form

$$u_j = A_j e^{i\omega(t - a_i N_i/W)} \tag{3.16}$$

where $\mathbf{N}$ is a unit normal in the natural state.

This solution implies that a wave with a wave front which is a material plane with unit normal $\mathbf{N}$ moves from the plane $\mathbf{N} \cdot \vec{a} = 0$ to $\mathbf{N} \cdot \vec{a} = L_0$ in the time L_0/W . Substitution of this solution yielded the propagation conditions

$$\rho_0 W^2 U_j = \omega_{jk} U_k \tag{3.17}$$

where ω_{jk} is given by

$$\omega_{jk} = N_r N_s(\delta_{jk}\tilde{t}_{rs} + (\delta_{qk} + 2\tilde{\eta}_{qk})\tilde{c}^{S}_{jrqs}). \tag{3.18}$$

The eigenvector $\mathbf{U}$ is normalized so that its components are the direction cosines of the particle displacement with respect to the natural state. Differentiating equation (3.17) with respect to pressure (p) and evaluating at zero pressure yields

$$(\rho_0 W^2)'_{p=0} = (U_j \omega'_{jk} U_k)_{p=0} \tag{3.19}$$

which was reduced to the following forms for the conditions of hydrostatic pressure and uniaxial compressive stress. For hydrostatic loading,

$$-(\rho_0 W^2)'_{p=0} = 1 + 2wF_{HC} + G_{HC} \tag{3.20}$$

where $F_{HC} = s^{T}_{aars} U_r U_s$, (3.21)

$G_{HC} = s^{T}_{aauv} c_{uvprqs} N_p N_q U_r U_s$, (3.22)

and $w = (\rho_0 W^2)_0 = (\rho v^2)_0 = c^{S}_{prqs} N_p N_q U_r U_s$. (3.23)

For uniaxial loading the equation reduced to

$$-(\rho_o W^2)'_{p=0} = 2wF_{uc} + G_{uc}, \tag{3.24}$$

where F_{uc} and G_{uc} are given by

$$F_{uc} = s^{T}_{abrs} M_a M_b U_r U_s \tag{3.25}$$

and

$$G_{uc} = s^{T}_{abuv} c_{uvprqs} M_a M_b N_p N_q U_r U_s \tag{3.26}$$

and M_i are the components of a unit vector in the direction of stress.

It is assumed for the uniaxial case that the direction of propagation is always perpendicular to the direction of stress.

These equations provide relationships between the linear elastic stiffness and compliance moduli, the third order elastic moduli and the derivative of the "natural" velocity with respect to stress. However, the measurements made in this study were of the Stress Acoustic Constants (H) which were defined by Heyman [31] and Cantrell [49] to be

$$H = \left(\frac{\frac{\Delta W}{W}}{\Delta \sigma} \right) = \frac{(\rho_0 W^2)'_{p=0}}{(2\rho_0 W^2)}. \tag{3.27}$$

Since there were a number of different orientations of stress and propagation and polarization directions, the different SAC's were designated with three subscripts as H_{ijk} . The first subscript gave the direction of applied stress which was limited to one of the three axes for these experiments. A zero for the first subscript implies hydrostatic loading. The second and third subscripts were the directions of propagation and polarization of the ultrasonic wave respectively. These again were limited to being pure mode waves along the three axes.

Using this notation, the equations for the SAC's were derived for both the models of transverse isotropy and orthotropy. The results for the 27 cases considered are given in table 3.1.

III.C. Experiment

The measurements of the stress derivatives of the "natural" velocity were carried out using some of the samples that were used in the previously described ultrasonic velocity measurements. Sample MCIS 1.10A was used for the measurements of the longitudinal velocity derivatives while samples MCIS 1.8A, 1.10B and 1.7A were used in the shear wave measurements.

Table 3.1 - Stress Acoustic Constant Equations for transversely isotropic and orthotropic media.

Transverse Isotropy
$H_{011} = -\left[\dfrac{1 + 2c_{11}(s_{11} + s_{12} + s_{13}) + (s_{11} + s_{12} + s_{13})(c_{111} + c_{112}) + (2s_{13} + s_{33})c_{113}}{2c_{11}}\right]$
$H_{022} = H_{011}$
$H_{033} = -\left[\dfrac{1 + 2c_{33}(2s_{13} + s_{33}) + 2(s_{11} + s_{12} + s_{13})c_{133} + (2s_{13} + s_{33})c_{333}}{2c_{33}}\right]$
$H_{031} = -\left[\dfrac{1 + 2c_{44}(s_{11} + s_{12} + s_{13}) + (s_{11} + s_{12} + s_{13})(c_{144} + c_{155}) + (2s_{13} + s_{33})c_{344}}{2c_{44}}\right]$
$H_{032} = H_{031}$
$H_{012} = -\left[\dfrac{1 + (c_{11} - c_{12})(s_{11} + s_{12} + s_{13}) + \frac{1}{2}((s_{11} + s_{12} + s_{13})(c_{111} - c_{112})}{(c_{11} - c_{12})}\right] - \left[\dfrac{(2s_{13} + s_{33})(c_{113} - c_{123})}{(c_{11} - c_{12})}\right]$
$H_{021} = H_{012}$
$H_{013} = -\left[\dfrac{1 + 2c_{44}(2s_{13} + s_{33}) + (s_{11} + s_{12} + s_{13})(c_{144} + c_{155}) + (2s_{13} + s_{33})c_{344}}{2c_{44}}\right]$
$H_{023} = H_{013}$
$H_{133} = -\left[\dfrac{2c_{33}s_{13} + (s_{11} + s_{12})c_{133} + s_{13}c_{333}}{2c_{33}}\right]$
$H_{233} = H_{133}$
$H_{122} = -\left[\dfrac{2c_{11}s_{12} + s_{11}c_{112} + s_{12}c_{111} + s_{13}c_{113}}{2c_{11}}\right]$
$H_{211} = H_{122}$
$H_{311} = -\left[\dfrac{2c_{11}s_{13} + s_{13}(c_{111} + c_{112}) + s_{33}c_{113}}{2c_{11}}\right]$
$H_{322} = H_{311}$

Table 3.1 - Continued

Transverse Isotropy (Continued)
$H_{123} = -\left[\frac{2c_{44}s_{13} + s_{11}c_{144} + s_{12}c_{155} + s_{13}c_{344}}{2c_{44}}\right]$
$H_{213} = H_{123}$
$H_{121} = -\left[\frac{(c_{11} - c_{12}) + 1/4(s_{11} + s_{12})(c_{111} - c_{112}) + 1/2s_{13}(c_{113} - c_{123})}{(c_{11} - c_{12})}\right]$
$H_{212} = H_{121}$
$H_{312} = -\left[\frac{(c_{11} - c_{12})s_{13} + \frac{1}{2}s_{13}(c_{111} - c_{112}) + \frac{1}{2}s_{33}(c_{133} - c_{123})}{(c_{11} - c_{12})}\right]$
$H_{321} = H_{312}$
$H_{313} = -\left[\frac{2c_{44}s_{33} + s_{13}(c_{144} + c_{155}) + s_{33}c_{344}}{2c_{44}}\right]$
$H_{323} = H_{313}$
$H_{131} = -\left[\frac{2c_{44}s_{11} + s_{11}c_{155} + s_{12}c_{144} + s_{13}c_{344}}{2c_{44}}\right]$
$H_{232} = H_{131}$
$H_{132} = -\left[\frac{2c_{44}s_{12} + s_{11}c_{144} + s_{12}c_{155} + s_{13}c_{344}}{2c_{44}}\right]$
$H_{231} = H_{231}$

Table 3.1 - Continued

Orthotropy
$H_{011} = -\left[\frac{1 + 2c_{11}S_1 + S_1c_{111} + S_2c_{112} + S_3c_{113}}{2c_{11}}\right]$
$H_{022} = -\left[\frac{1 + 2c_{22}S_2 + S_1c_{122} + S_2c_{222} + S_3c_{223}}{2c_{22}}\right]$
$H_{033} = -\left[\frac{1 + 2c_{33}S_3 + S_1c_{133} + S_2c_{233} + S_3c_{333}}{2c_{33}}\right]$
$H_{031} = -\left[\frac{1 + 2c_{55}S_1 + S_1c_{155} + S_2c_{255} + S_3c_{355}}{2c_{55}}\right]$
$H_{032} = -\left[\frac{1 + 2c_{44}S_2 + S_1c_{144} + S_2c_{244} + S_3c_{344}}{2c_{55}}\right]$
$H_{012} = -\left[\frac{1 + 2c_{66}S_2 + S_1c_{166} + S_2c_{266} + S_3c_{366}}{2c_{66}}\right]$
$H_{021} = -\left[\frac{1 + 2c_{66}S_1 + S_1c_{166} + S_2c_{266} + S_3c_{366}}{2c_{66}}\right]$
$H_{013} = -\left[\frac{1 + 2c_{55}S_3 + S_1c_{155} + S_2c_{255} + S_3c_{355}}{2c_{55}}\right]$
$H_{023} = -\left[\frac{1 + 2c_{44}S_3 + S_1c_{144} + S_2c_{244} + S_3c_{355}}{2c_{44}}\right]$
$H_{133} = -\left[\frac{2c_{33}s_{13} + s_{11}c_{133} + s_{12}c_{233} + s_{13}c_{333}}{2c_{33}}\right]$
$H_{233} = -\left[\frac{2c_{33}s_{23} + s_{12}c_{133} + s_{22}c_{233} + s_{23}c_{333}}{2c_{33}}\right]$
$H_{122} = -\left[\frac{2c_{22}s_{12} + s_{11}c_{122} + s_{12}c_{222} + s_{13}c_{223}}{2c_{22}}\right]$
$H_{211} = -\left[\frac{2c_{11}s_{12} + s_{12}c_{111} + s_{22}c_{112} + s_{23}c_{113}}{2c_{11}}\right]$

where $S_1 = s_{11} + s_{12} + s_{13}$

$S_2 = s_{12} + s_{22} + s_{23}$

and $S_3 = s_{13} + s_{23} + s_{33}$

Table 3.1 - Continued

Orthotropy
$H_{322} = -\left[\frac{2c_{22}s_{23} + s_{13}c_{122} + s_{23}c_{222} + s_{33}c_{223}}{2c_{22}}\right]$
$H_{311} = -\left[\frac{2c_{11}s_{13} + s_{13}c_{111} + s_{23}c_{112} + s_{33}c_{113}}{2c_{11}}\right]$
$H_{121} = -\left[\frac{2c_{66}s_{11} + s_{11}c_{166} + s_{12}c_{266} + s_{13}c_{366}}{2c_{66}}\right]$
$H_{212} = -\left[\frac{2c_{66}s_{22} + s_{12}c_{166} + s_{22}c_{266} + s_{23}c_{366}}{2c_{66}}\right]$
$H_{312} = -\left[\frac{2c_{66}s_{23} + s_{13}c_{166} + s_{23}c_{266} + s_{33}c_{366}}{2c_{66}}\right]$
$H_{321} = -\left[\frac{2c_{66}s_{13} + s_{13}c_{166} + s_{23}c_{266} + s_{33}c_{366}}{2c_{66}}\right]$
$H_{123} = -\left[\frac{2c_{44}s_{13} + s_{11}c_{144} + s_{12}c_{244} + s_{13}c_{344}}{2c_{44}}\right]$
$H_{213} = -\left[\frac{2c_{55}s_{23} + s_{12}c_{155} + s_{22}c_{255} + s_{23}c_{355}}{2c_{55}}\right]$
$H_{323} = -\left[\frac{2c_{44}s_{33} + s_{13}c_{144} + s_{23}c_{244} + s_{33}c_{344}}{2c_{44}}\right]$
$H_{313} = -\left[\frac{2c_{55}s_{33} + s_{13}c_{155} + s_{23}c_{255} + s_{33}c_{355}}{2c_{55}}\right]$
$H_{131} = -\left[\frac{2c_{55}s_{11} + s_{11}c_{155} + s_{12}c_{255} + s_{13}c_{355}}{2c_{55}}\right]$
$H_{232} = -\left[\frac{2c_{44}s_{22} + s_{12}c_{144} + s_{22}c_{244} + s_{23}c_{344}}{2c_{44}}\right]$
$H_{132} = -\left[\frac{2c_{44}s_{12} + s_{11}c_{144} + s_{12}c_{244} + s_{13}c_{344}}{2c_{44}}\right]$
$H_{231} = -\left[\frac{2c_{55}s_{12} + s_{12}c_{155} + s_{22}c_{255} + s_{23}c_{355}}{2c_{55}}\right]$

The change in "natural" velocity was measured using a pulsed phase locked loop (P2L2) interferometer. The theory of the measurement of the change in resonant frequency and it's relationship to the change in "natural" velocity was presented earlier. Now the theory of the operation of the P2L2 which is shown in Fig. 3.1 will be discussed.

The heart of the P2L2 is a voltage controlled oscillator (VCO) which generates a continuous wave signal of a frequency that is controlled by a D.C. input signal. A portion of the signal from the VCO is gated out into a tone burst and is then used to excite the ultrasonic transducer. The resulting elastic wave is launched into the sample and is then detected either by the same transducer in the pulse echo mode or another transducer in the through transmission mode. The received signal is input into the P2L2 where it is phase compared with the signal from the VCO at a preselected phase point using a sample and hold. The sampled voltage from the phase detector is then used to drive the VCO to a condition of quadrature. The acoustic phase shift (θ) given by

$$\theta = 2\pi ft \tag{3.28}$$

is then maintained as a constant by the feedback loop and therefore

$$\Delta\theta = 0 = 2\pi(t\Delta f + f\Delta t) \tag{3.29}$$

and

$$\frac{\Delta\theta}{\theta} = 0 = \frac{\Delta f}{f} + \frac{\Delta t}{t}. \tag{3.30}$$

Thus, as stated earlier,

$$\frac{\Delta f}{f} = \frac{\Delta W}{W} = -\frac{\Delta t}{t}. \tag{3.31}$$

Therefore, by monitoring the change in the frequency of the P2L2, the change in "natural" velocity is also monitored.

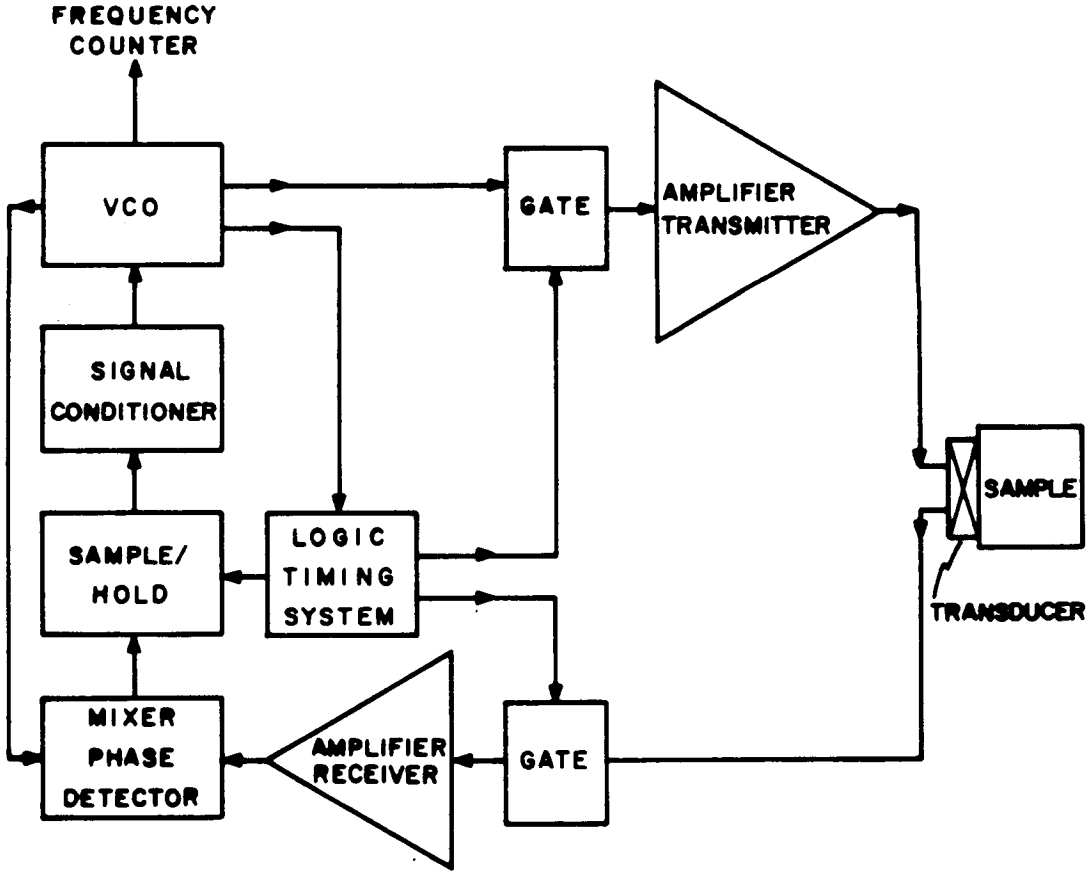

Figure 3.1 - Block diagram of the pulsed phase locked loop ultrasonic interferometer.

A block diagram of the experimental apparatus used for the uniaxial SAC measurements is shown in Fig. 3.2. The uniaxial compressive load was applied as in the strain gauge measurements with a MTS 810 load frame. The calibrated output of the load cell was monitored by the H.P. 3478A digital multimeter. The tone burst from the P2L2 was used to excite a conventional damped broad band 2.25 MHz transducer. Because broad band transducers were used, phase shifts at the transducer specimen interface were assumed to be negligible. The P2L2 was used in a pulse echo mode with the reflected echos input back into the instrument for phase comparison. A Tektronix 2445 oscilloscope was used to view the ultrasonic signal, the phase signal and the sample and hold position. It was triggered by a reference sync from the P2L2. The frequency was monitored by a H.P. 5316A universal counter. The voltage and frequency values were read by a Tektronix 4051 computer and converted to stress and normalized frequency shift. The program listed in Appendix G also computed the slope of the curve by linear regression as well as plotted and stored the data.

The value for each uniaxial SAC was determined by averaging the values from ten measurements. A spring loaded clamping device was used to maintain constant pressure of the transducer on the specimen in order to hold the bond thickness constant during the measurement. Variations in the bond thickness would cause phase shifts which introduced errors into the measurement. These errors which have less effect on thick samples made initial measurements on thin laminates impossible and placed another constraint on minimum specimen thickness. The transducer was also rebonded onto the specimen three or four times during the ten measurements to determine the effect of slight variations in initial bond thicknesses. After each rebonding, the specimen was ramped through the load cycle several times to settle the bond. Then, the sample was allowed to remain at rest approximately 15 minutes to bring the sample to equilibrium temperature. This was necessary because the handling of the sample during rebonding increased the temperature slightly which could significantly affect the results.

C-2

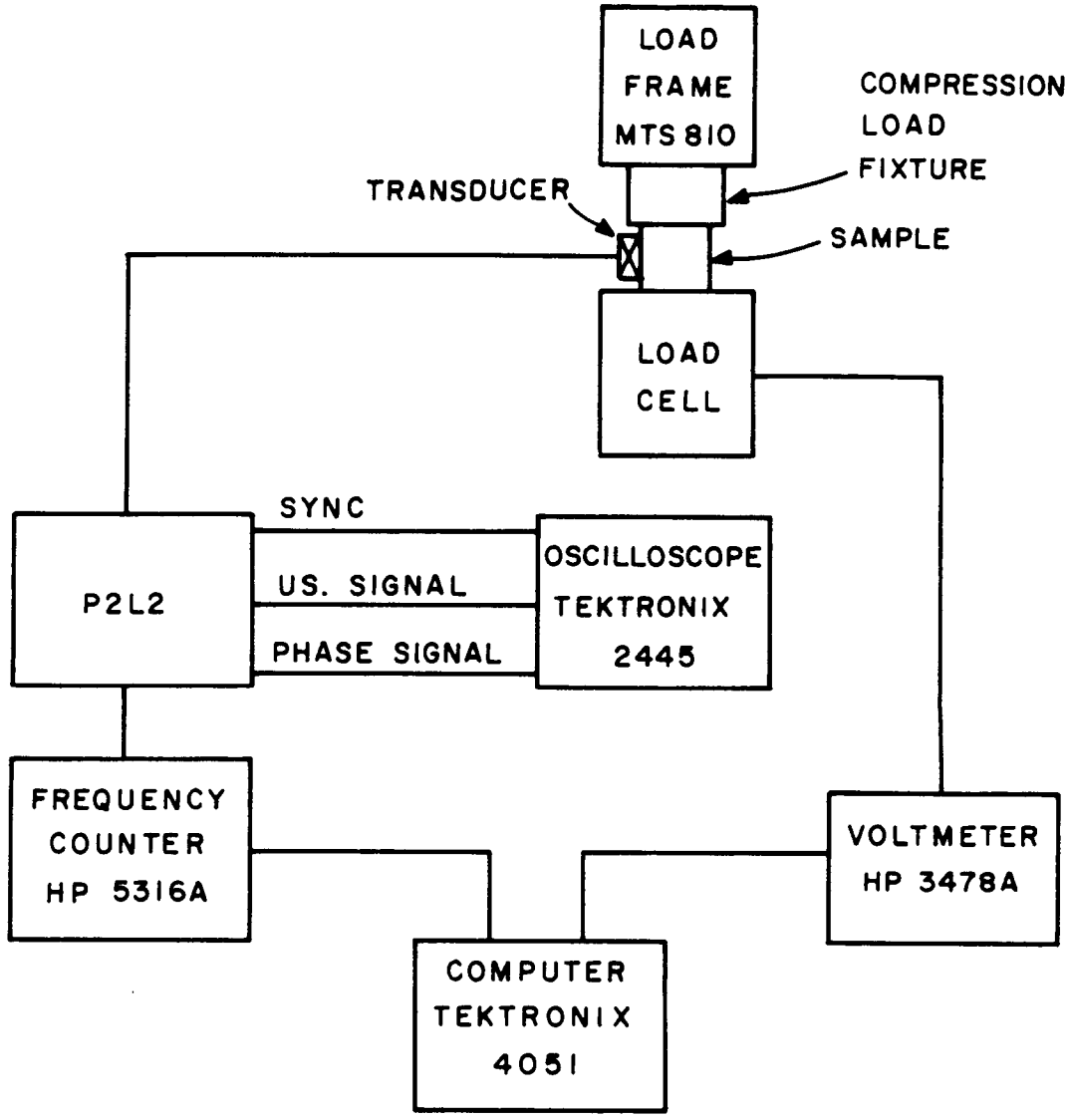

Figure 3.2 - Block diagram of uniaxial stress acoustic constant measurement apparatus.

Another concern in these measurements was again the presence of viscoelastic effects in these materials. The loading rate was varied considerably to examine this effect. The specimen were loaded to between 80 and 100 MPa in times ranging from 10 sec. to over three minutes with no observed effects. The measurements were made for both increasing and decreasing load with no measurable differences. The effect of temperature variations due to thermoelastic heating was also considered. Theory assumes these measurements to be made under isothermal conditions. At these loading rates which were very nearly isothermal, the effect of thermoelastic heating was calculated to be much less than experimental uncertainty. The basis of these calculations was the temperature derivative of velocity data to be presented later.

The previously mentioned constraints on the choices of stress, propagation and polarization directions allows for 18 measurements to be made. The average values from the ten measurements of each and their standard deviations are presented in Table 3.2. The uncertainties were typically less than five percent of the measured values for these measurements. The values were consistently positive indicating increasing frequency as a function of increasing compressive stress except for H_{323} and H_{313} . A few of the wave modes exhibited nonlinear (quadratic) curves indicating higher than third order nonlinear effects. These are designated by an * in the table and the SAC values for these are the linear coefficients of a quadratic fit to the data. Typical curves for the uniaxial SAC measurements are shown in Figs. 3.3 - 3.20.

As with the linear elastic measurements, some of these measurements can be used to check for consistency with transversely isotropic behavior. The SAC pairs $(H_{122}, H_{211},)$ (H_{311}, H_{322}) , (H_{133}, H_{233}) , (H_{131}, H_{232}) , and (H_{132}, H_{231}) should all have equal values. Other pairs that should have equal values were not compared as they were measured on different specimens making comparisons invalid because of sample to sample variations. The values of some of these pairs compare well within experimental uncertainty. However, H_{133} and H_{233} differ by more than the uncertainty of the

Table 3.2 - Measured values for the Uniaxial Stress Acoustic Constants.

Uniaxial Stress Acoustic Constants	
SAC	Value $(GPa)^{-1}$
H^{*}_{122}	0.0490 +/- 0.0009
H^{*}_{211}	0.0427 +/- 0.0010
H_{322}	0.00116 +/- 0.00007
H_{311}	0.00123 +/- 0.00001
H_{121}	0.0887 +/- 0.0007
H_{212}	0.0741 +/- 0.0010
H_{312}	0.00279 +/- 0.00010
H_{321}	0.00299 +/- 0.00010
H^{*}_{123}	0.068 +/- 0.002
H^{*}_{213}	0.0572 +/- 0.0010
H_{323}	-0.00993 +/- 0.0004
H_{313}	-0.00919 +/- 0.0003
H_{131}	0.165 +/- 0.003
H_{232}	0.149 +/- 0.002
H_{132}	0.111 +/- 0.002
H_{231}	0.109 +/- 0.001
H_{133}	0.0538 +/- 0.0005
H_{233}	0.0479 +/- 0.0003

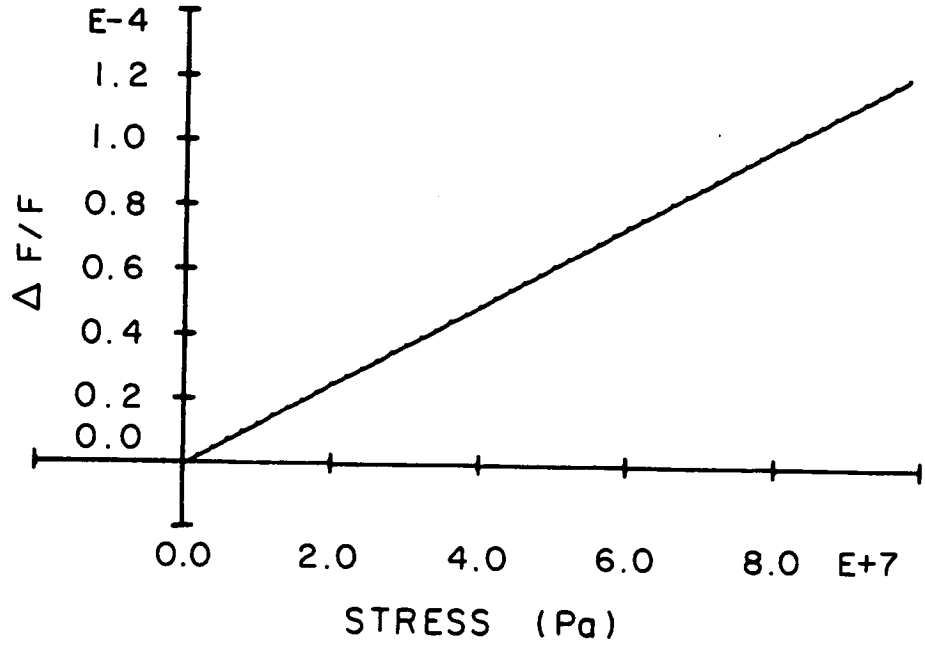

Figure 3.3 - Plot of normalized frequency change as a function of uniaxial stress for a longitudinal wave propagating along x_1 with stress applied along x_3.

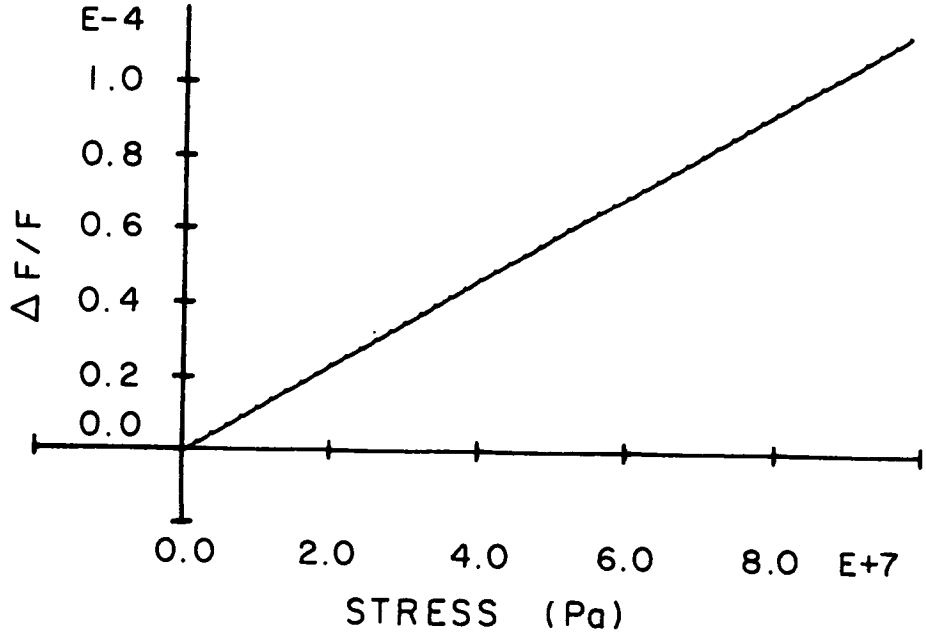

Figure 3.4 - Delta F/F versus stress for a longitudinal wave propagating along x_2 with stress applied along x_3.

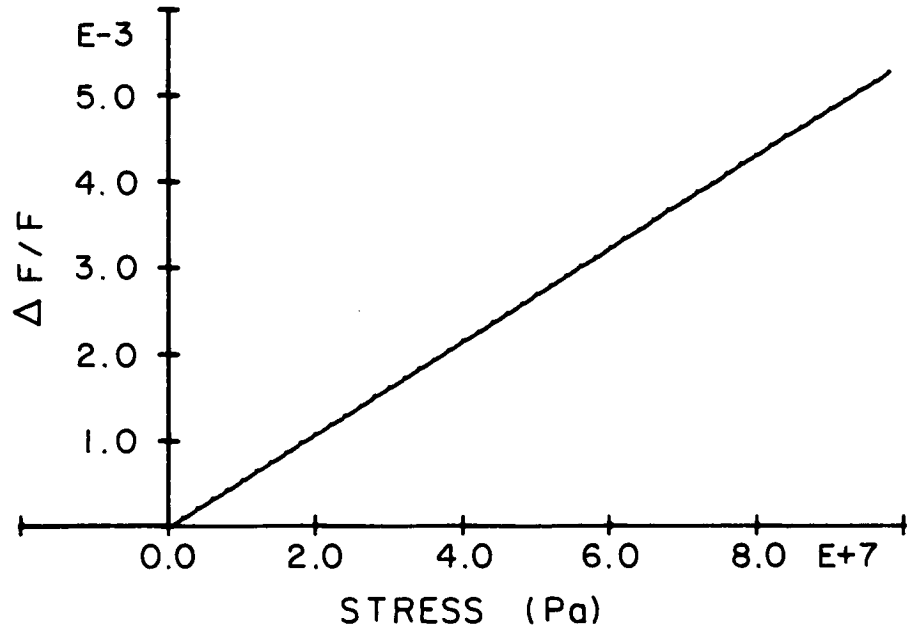

Figure 3.5 - Delta F/F versus stress for a longitudinal wave propagating along x_3 with stress applied along x_1.

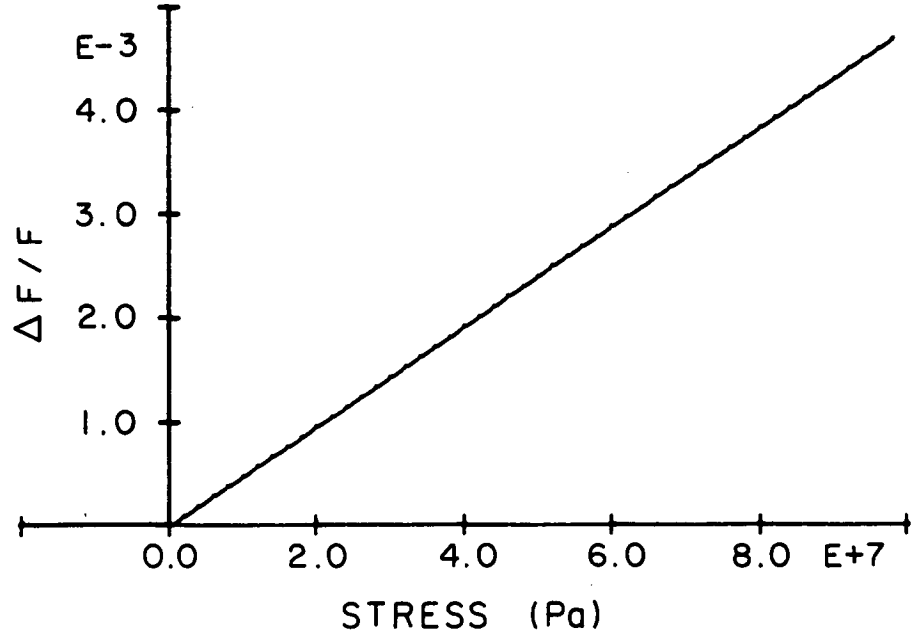

Figure 3.6 - Delta F/F versus stress for a longitudinal wave propagating along x_3 with stress applied along x_2.

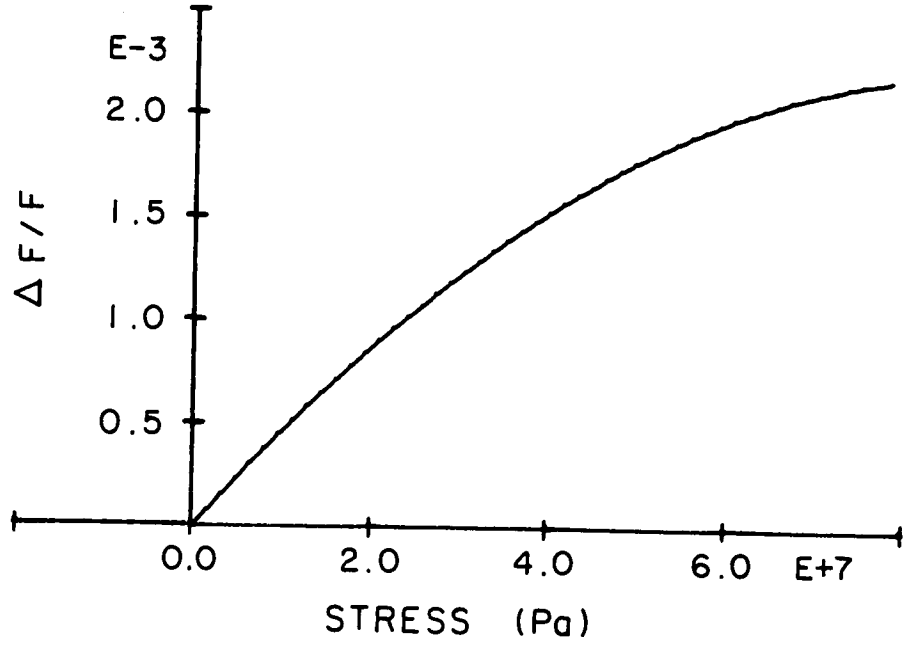

Figure 3.7 - Delta F/F versus stress for a longitudinal wave propagating along x_2 with stress applied along x_1.

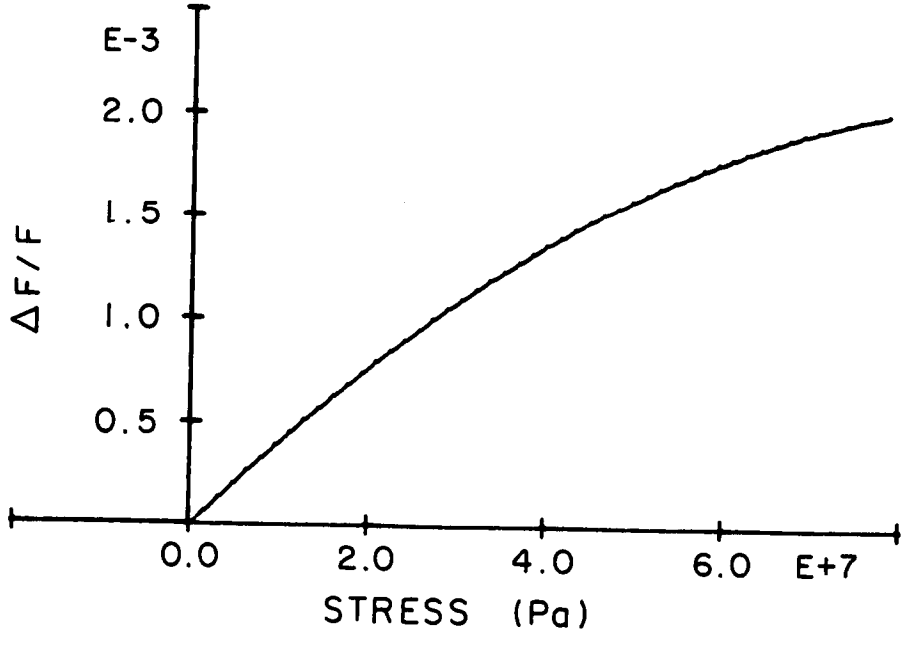

Figure 3.8 - Delta F/F versus stress for a longitudinal wave propagating along x_1 with stress applied along x_2.

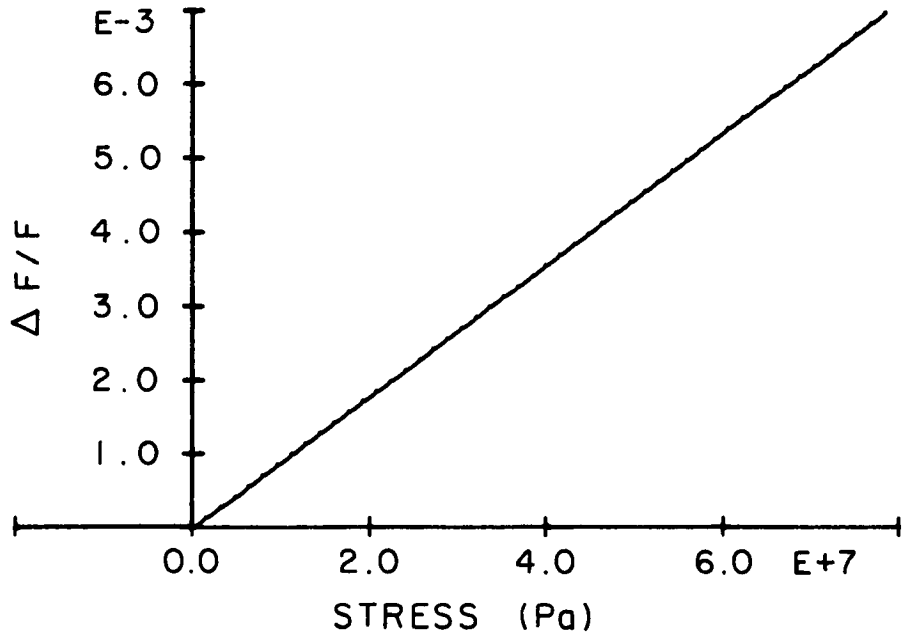

Figure 3.9 - Delta F/F versus stress for a shear wave propagating along x_2 polarized along x_1 with stress applied along x_1.

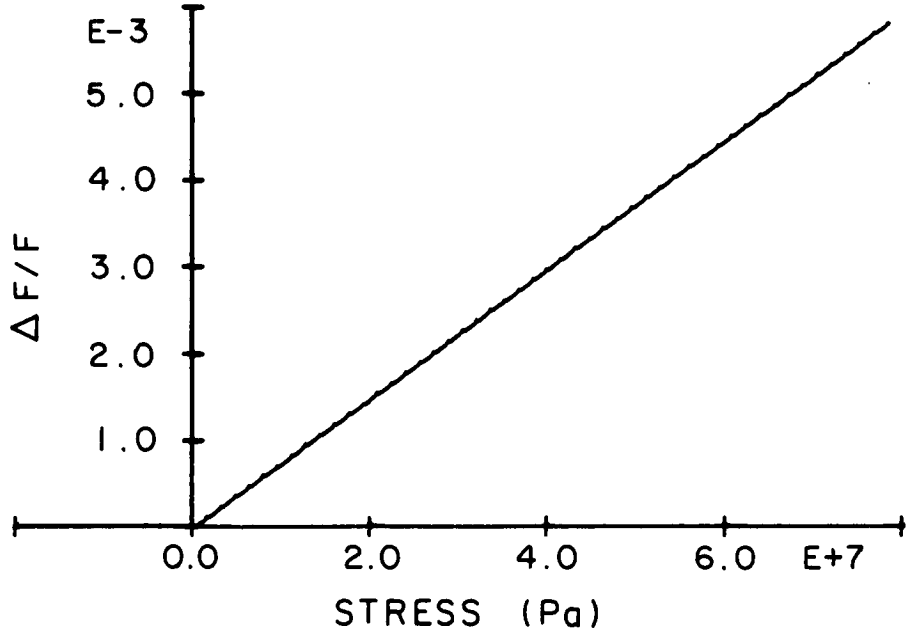

Figure 3.10 - Delta F/F versus stress for a shear wave propagating along x_1 polarized along x_2 with stress applied along x_2.

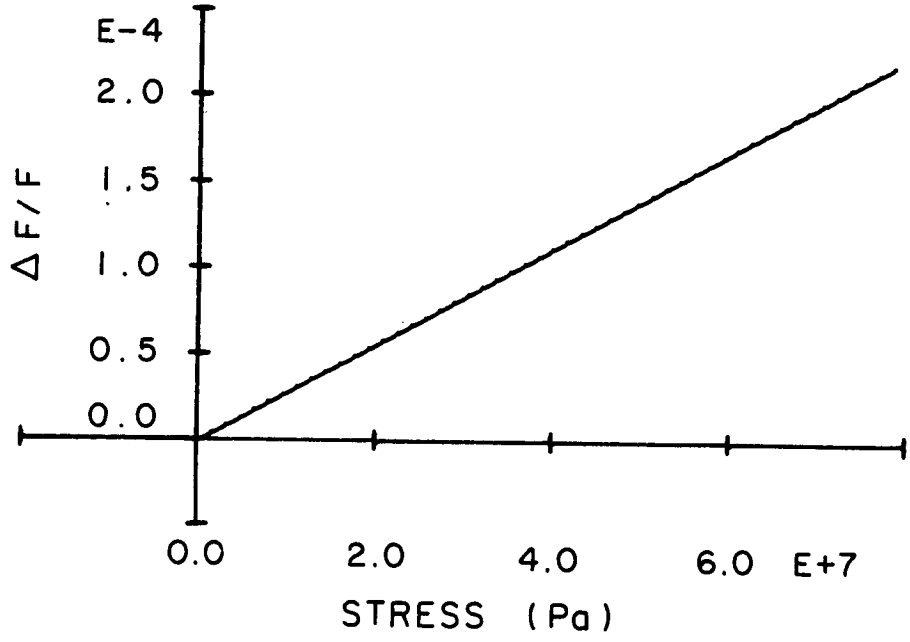

Figure 3.11 - Delta F/F versus stress for a shear wave propagating along x_1 polarized along x_2 with stress applied along x_3.

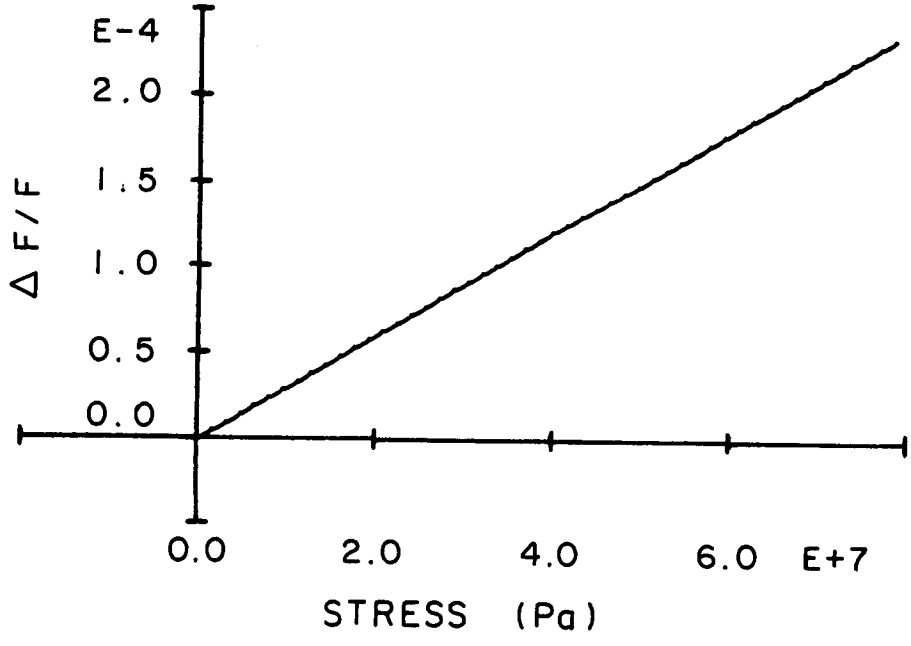

Figure 3.12 - Delta F/F versus stress for a shear wave propagating along x_2 polarized along x_1 with stress applied along x_3.

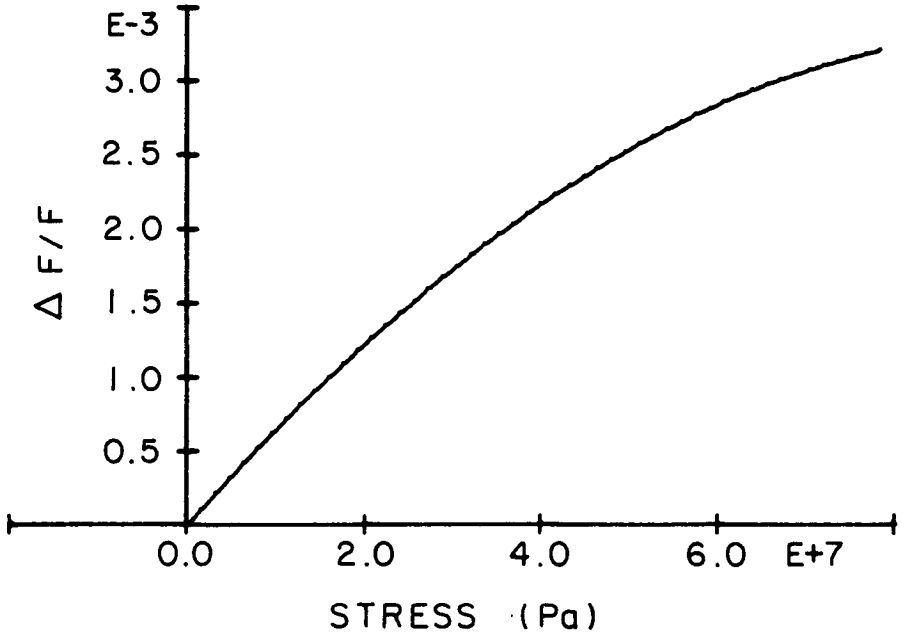

Figure 3.13 - Delta F/F versus stress for a shear wave propagating along x_2 polarized along x_3 with stress applied along x_1.

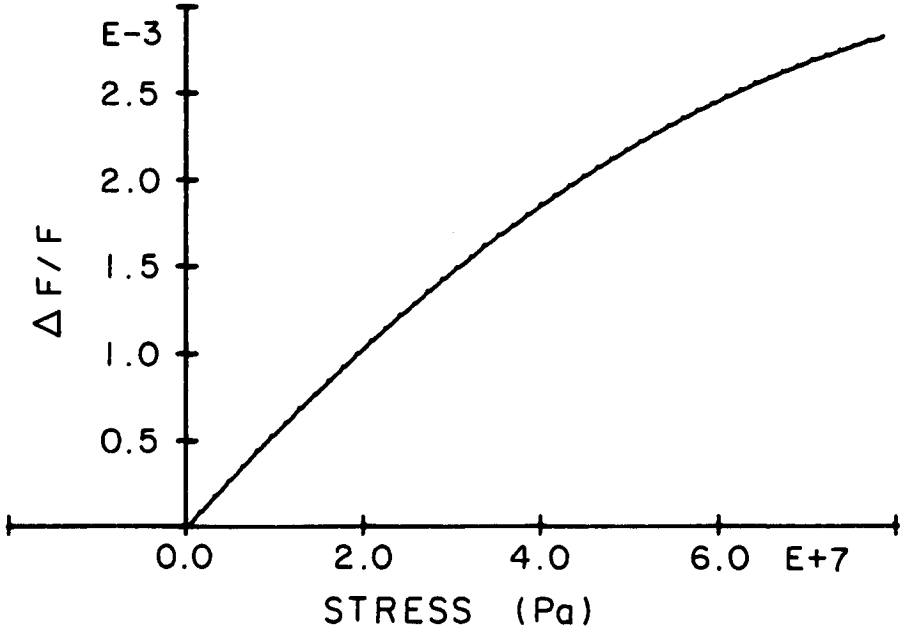

Figure 3.14 - Delta F/F versus stress for a shear wave propagating along x_1 polarized along x_3 with stress applied along x_2.

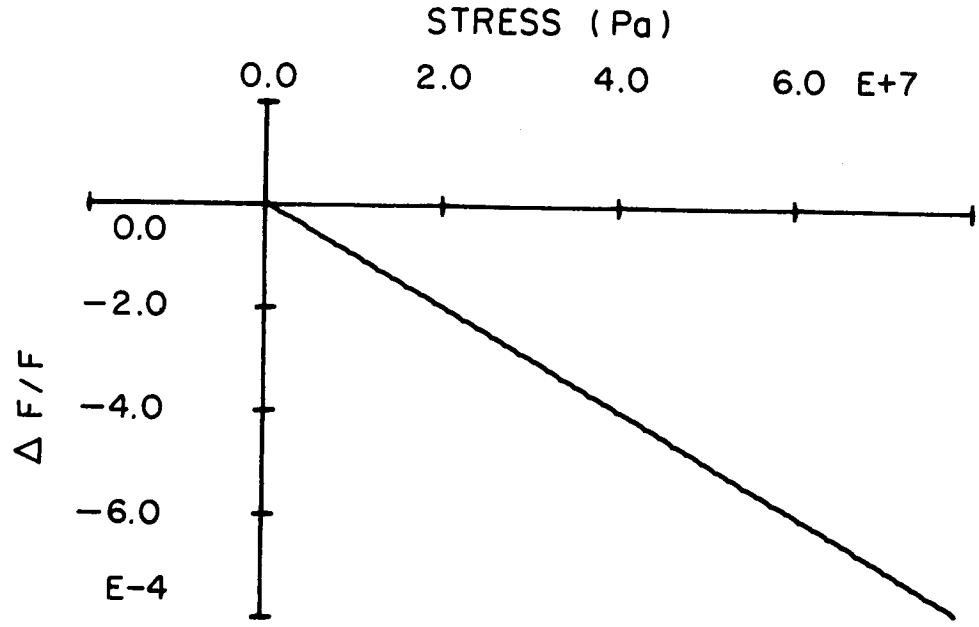

Figure 3.15 - Delta F/F versus stress for a shear wave propagating along x_2 polarized along x_3 with stress applied along x_3.

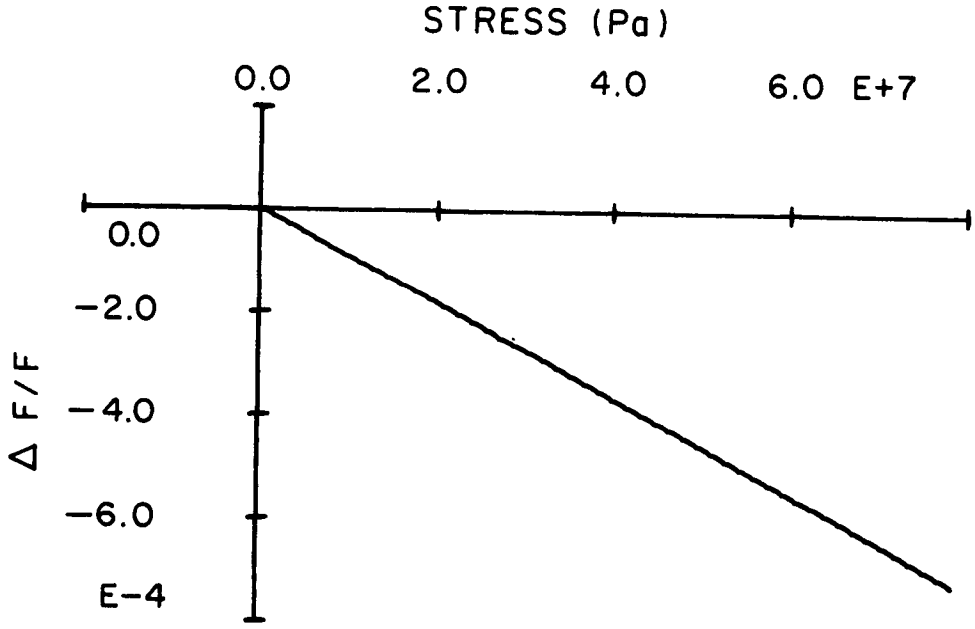

Figure 3.16 - Delta F/F versus stress for a shear wave propagating along x_1 polarized along x_3 with stress applied along x_1.

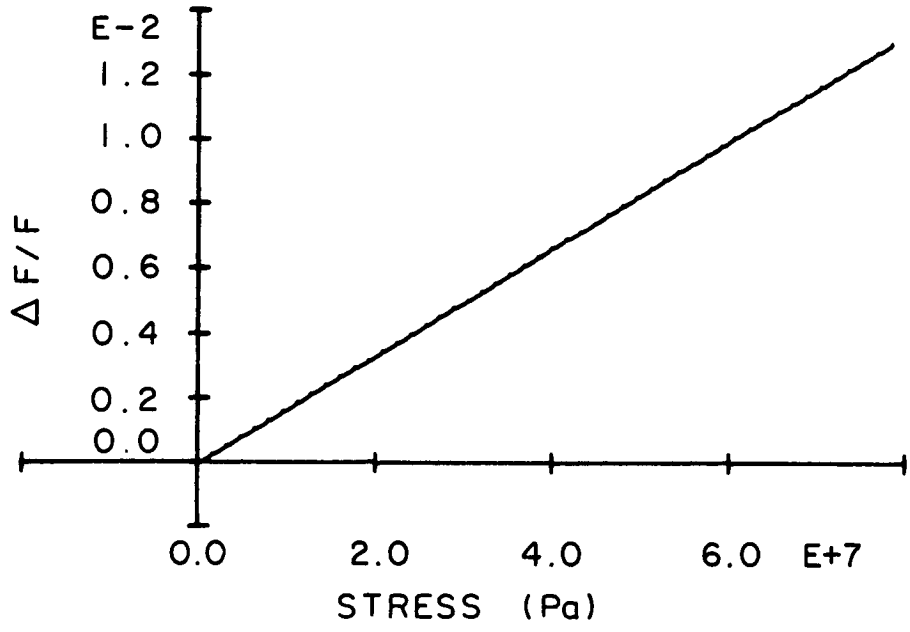

Figure 3.17 - Delta F/F versus stress for a shear wave propagating along x_3 polarized along x_1 with stress applied along x_1.

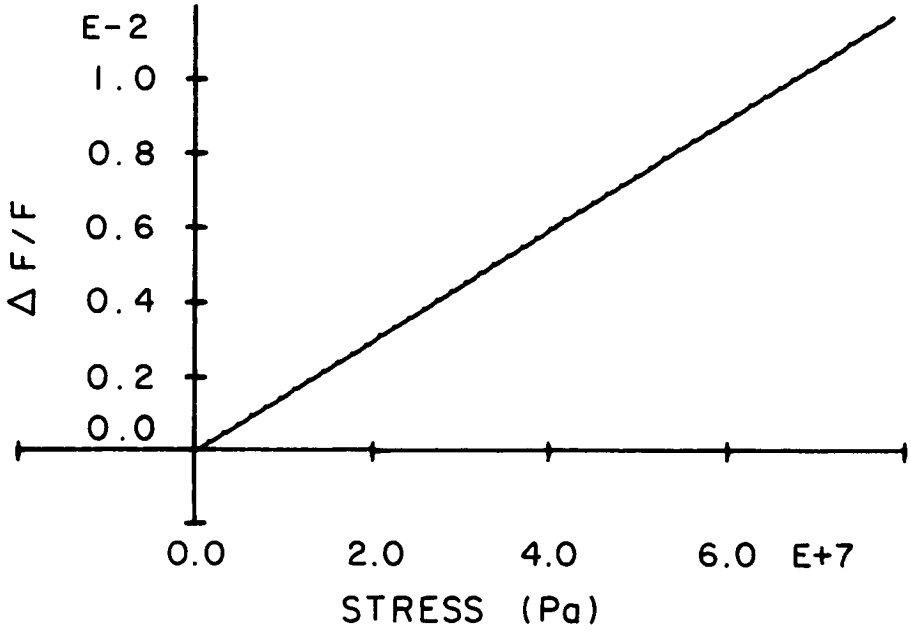

Figure 3.18 - Delta F/F versus stress for a shear wave propagating along x_3 polarized along x_2 with stress applied along x_2.

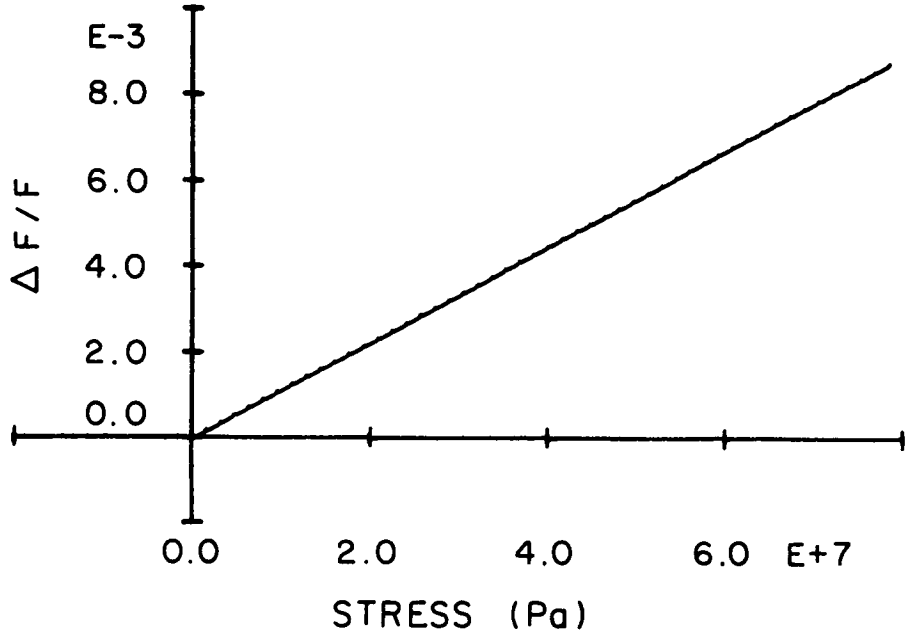

Figure 3.19 - Delta F/F versus stress for a shear wave propagating along x_3 polarized along x_2 with stress applied along x_1.

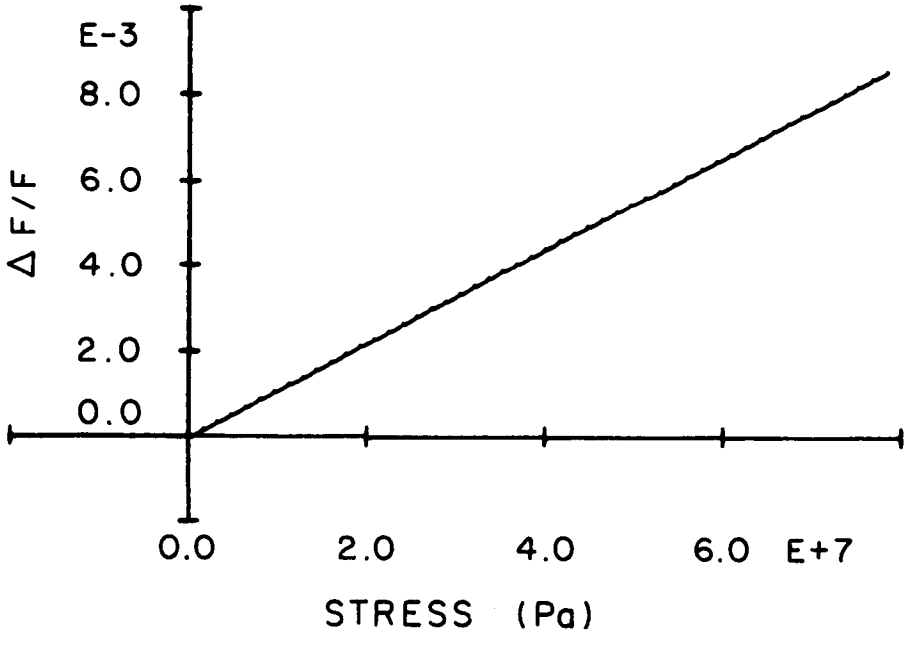

Figure 3.20 - Delta F/F versus stress for a shear wave propagating along x_3 polarized along x_1 with stress applied along x_2.

measurement as well as H_{131} and H_{232} . Thus, again measurable deviations from transverse isotropy were demonstrated. However, why this behavior is demonstrated only in some measurements and not in others is not clear.

The hydrostatic measurements were made in a similar fashion as those made under uniaxial compression. A block diagram of the set up is shown in Fig. 3.21. The change in "natural" velocity was again measured with the P2L2. Argon was used to increase the pressure within the pressure chamber. A H.P. 5316A universal counter monitored the frequency while a Tektronix 465B oscilloscope was used to view the ultrasonic, phase, and sample/hold signals. The Tektronix 4051 computer was used to read the frequency data. The pressure data was manually read from a Heise C-57488 pressure gauge and input into the computer.

There were several differences from the uniaxial measurements, however. While temperature variations during the uniaxial SAC measurements were insignificant, they were important in the hydrostatic measurements. Increasing the pressure 25 psi. suddenly, caused an increase in temperature of the gas and thus the sample of several tenths of a degree C. This temperature increase was significant. Therefore, the pressure had to be increased slowly and then time for thermal equilibrium to be obtained had to be given. Typically, there was a 20 to 30 minute delay between data points. Also, over this period of time the room temperature could vary significantly. This caused additional problems. To overcome this, heating elements were installed in the pressure chamber. A temperature controller was used with these heaters to maintain the temperature several degrees C above room temperature. This speeded the time required to attain thermal equilibrium and avoided the effect of room temperature variations provided it did not rise more than the several degree buffer. A Lake Shore Cryotronics Inc. model DRC84C temperature controller was used. This instrument had a reported ability to maintain the temperature within +/- 0.1 degree C. Although this instrument drastically improved the situation, these small variations in temperature

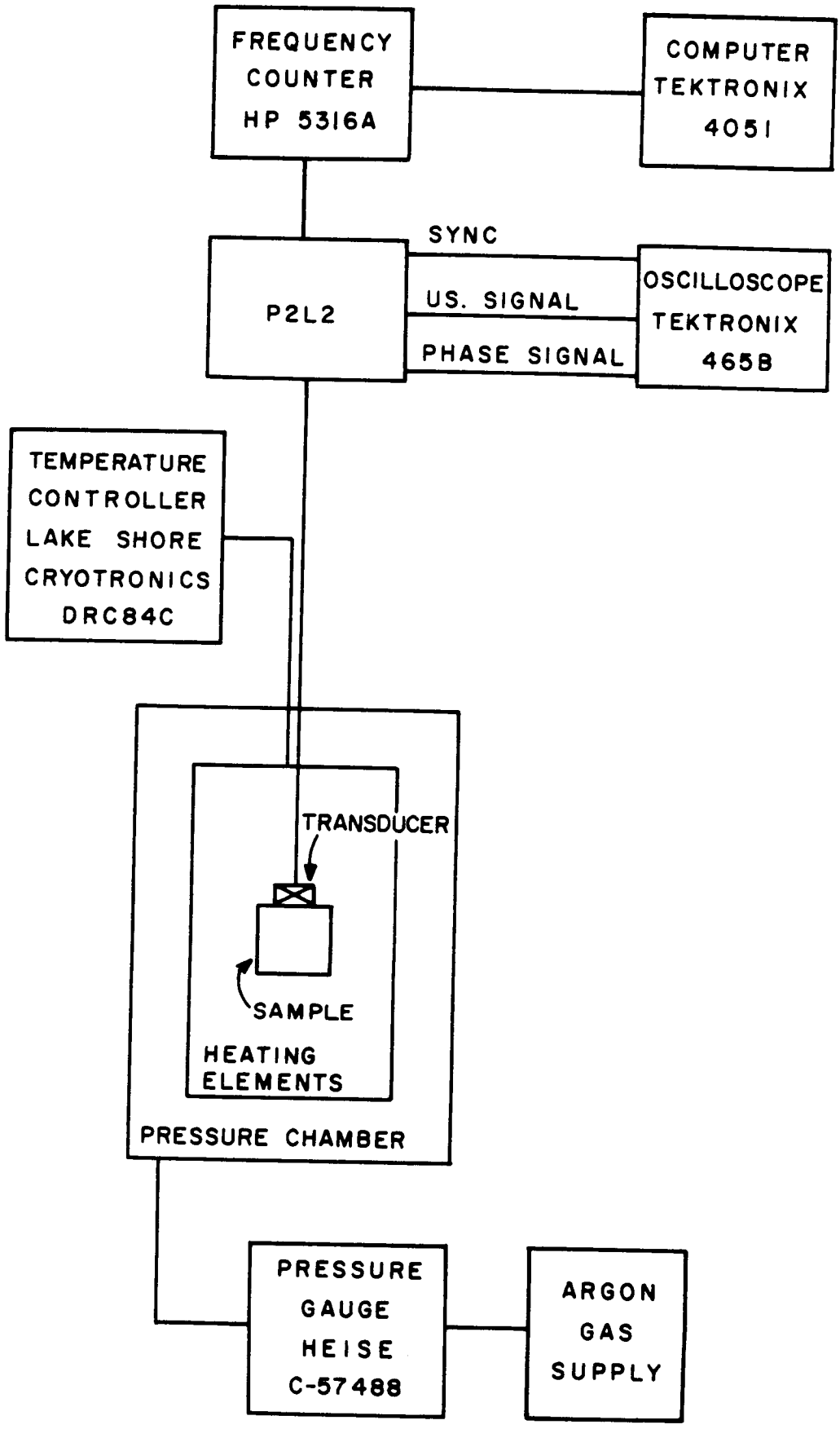

Figure 3.21 - Block diagram of apparatus used in the hydrostatic pressure stress acoustic constant measurements.

reduced the accuracy of the measurement significantly.

Another problem that increased the uncertainty in the hydrostatic measurements was the limitation in pressure. The upper limit of pressure in the chamber was set at only 250 psi. This was about a factor of 50 less than the maximum stress applied during the uniaxial measurements. Theoretically, the slope of the SAC should be evaluated at zero stress and thus this limitation in pressure should not be a problem. However, the low pressure produced much smaller velocity changes making them more uncertain. Also, the effect of temperature variations were much greater. Thus, the uncertainty of these measurements was much larger. It was on the order of ten percent of the measured SAC for most of the hydrostatic measurements. The limitation in maximum pressure also made the measurement of H_{033} impossible because the changes involved were to small to detect with the P2L2. The possibility of anomalous behavior at low pressures must also be considered. Therefore, although the hydrostatically measured SAC values were used with the uniaxial SAC measurements to determine the nonlinear moduli in this work, measurements at higher pressures are needed to determine the validity of these calculations.

Because of the tremendous amount of time involved in making a single hydrostatic SAC measurement (10 to 15 data points at 20 to 30 minutes per data point), only three measurements were used in the calculation of each hydrostatic SAC. This also contributed to the large uncertainty in these measurements. Measurements were again made for increasing and decreasing pressures with no observed differences.

The hydrostatic measurements were all made using undamped crystal transducers (PZT 5A) because of size limitations within the pressure chamber. This created the necessity of making corrections because of phase shifts at the transducer-specimen interface. These phase shifts are a function of frequency and can be calculated using the theory presented by McSkimmin [19]. The correction to the experimentally determined normalized frequency shift assuming zero bond thickness was given by

$$\frac{\Delta F}{F_{true}} = \frac{\Delta F}{F_{exp.}} - \frac{\Delta t}{t_{trans.}} \tag{3.32}$$

where $\frac{\Delta F}{F_{true}}$ was the true frequency change,

$\frac{\Delta F}{F_{exp.}}$ was the experimentally measured change,

and $\frac{\Delta t}{t_{trans.}}$ was the change in time of flight due to phase shifts.

The term $\frac{\Delta t}{t_{trans.}}$ was given by

$$\frac{\Delta t}{t_{trans.}} = \frac{\left[\frac{-\gamma_1}{F_1(360)} + \frac{\gamma_0}{F_0(360)}\right]}{t_0} \tag{3.33}$$

where F_0, F_1 were the measured frequencies of two data points,

t_0 was the time of flight in the unstressed specimen,

and γ_0, γ_1 were the phase angles of the two data points in degrees.

They were given by

$$\gamma_0 = \tan^{-1} \frac{2Z_s R_0}{R_0^2 - Z_s^2} \tag{3.34}$$

and

$$\gamma_1 = \tan^{-1} \frac{2Z_s R_1}{R_1^2 - Z_s^2} \tag{3.35}$$

where Z_s, Z_x were the mechanical impedances of the specimen and

transducer respectively,

and

$$R_0 = Z_x \tan\left(\frac{F_0}{F_R} \cdot 180\right), \tag{3.36}$$

and

$$R_1 = Z_x \tan\left(\frac{F_1}{F_R} \cdot 180\right), \tag{3.37}$$

where F_R was the resonant frequency of the transducer.

The effect of nonzero bond thickness on this correction term was also analyzed and found to be less than experimental uncertainty.

The original and corrected values for the hydrostatic SAC's are shown in Table 3.3. Typical curves are shown in Figs. 3.22 - 3.29. Comparisons of the data to check for transversely isotropic behavior show no measurable differences. This is most likely due to the large uncertainty of the measurements.

The effect of temperature on the "natural" velocity was also measured for small variations about room temperature. The apparatus used for these measurements was the same as that used in the hydrostatic measurements. The temperature was increased above room temperature several degrees C in 0.3 C steps using the heaters and the temperature controller. The frequency was measured at each point after thermal equilibrium was attained. Again corrections were applied to account for phase shifts at the transducer-specimen interface. Typical curves are shown in Figs. 3.30 - 3.38. The slopes of these curves were designated as the Thermal Acoustic Constants (H_{Tij}) and are given in Table 3.4 where the second and third subscripts give the directions of propagation and polarization respectively. The same samples used for the hydrostatic and uniaxial measurements were also used for these measurements.

The curves all demonstrated linear relationships between temperature change and normalized frequency shift for the limited range of the measurements. While these measurements were not used in the data reduction to determine the third order elastic coefficients, they were important in determining the effect of temperature changes on the SAC measurements.

Table 3.3 - Measured and corrected values for the Hydrostatic Stress Acoustic Constants.

Hydrostatic Stress Acoustic Constants $(GPa)^{-1}$		
SAC	Original Value	Corrected Value
H_{011}	0.46 +/- 0.02	0.39 +/- 0.02
H_{022}	0.44 +/- 0.02	0.37 +/- 0.02
H_{012}	0.301 +/- 0.007	0.257 +/- 0.007
H_{021}	0.305 +/- 0.006	0.261 +/- 0.006
H_{013}	0.32 +/- 0.03	0.27 +/- 0.03
H_{023}	0.32 +/- 0.02	0.27 +/- 0.02
H_{031}	0.33 +/- 0.02	0.28 +/- 0.02
H_{032}	0.30 +/- 0.02	0.25 +/- 0.02
H_{033}	Not Measured	

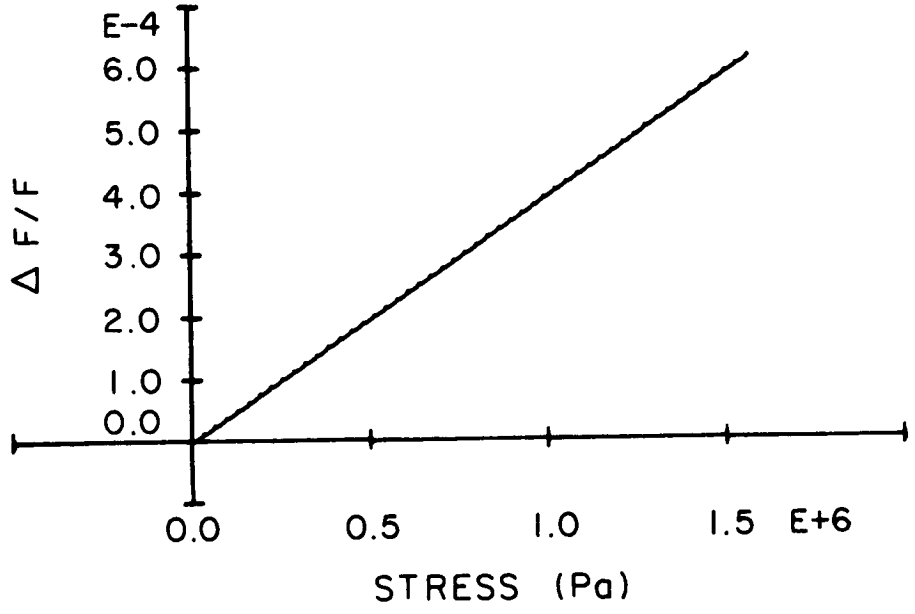

Figure 3.22 - Delta F/F versus pressure for a longitudinal wave propagating along x_1.

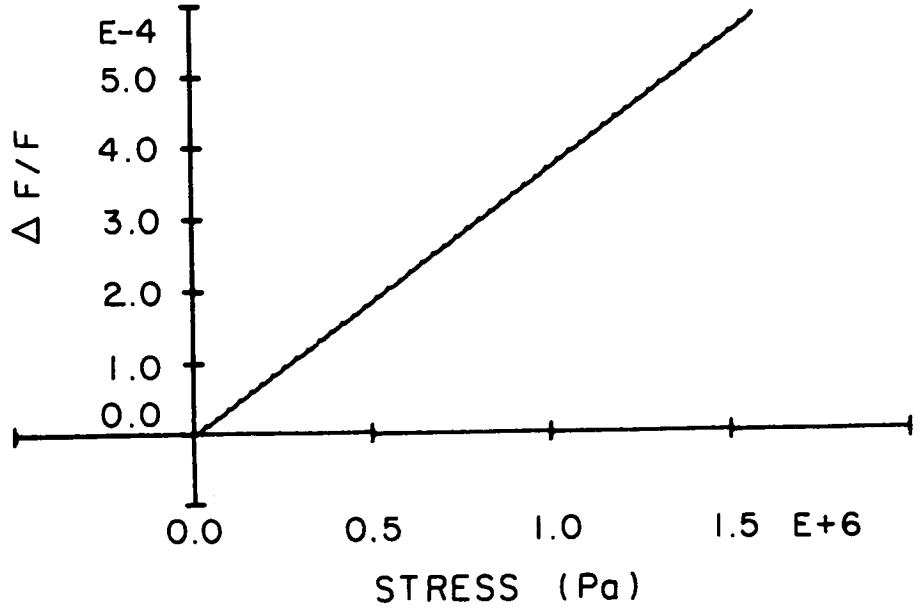

Figure 3.23 - Delta F/F versus pressure for a longitudinal wave propagating along x_2.

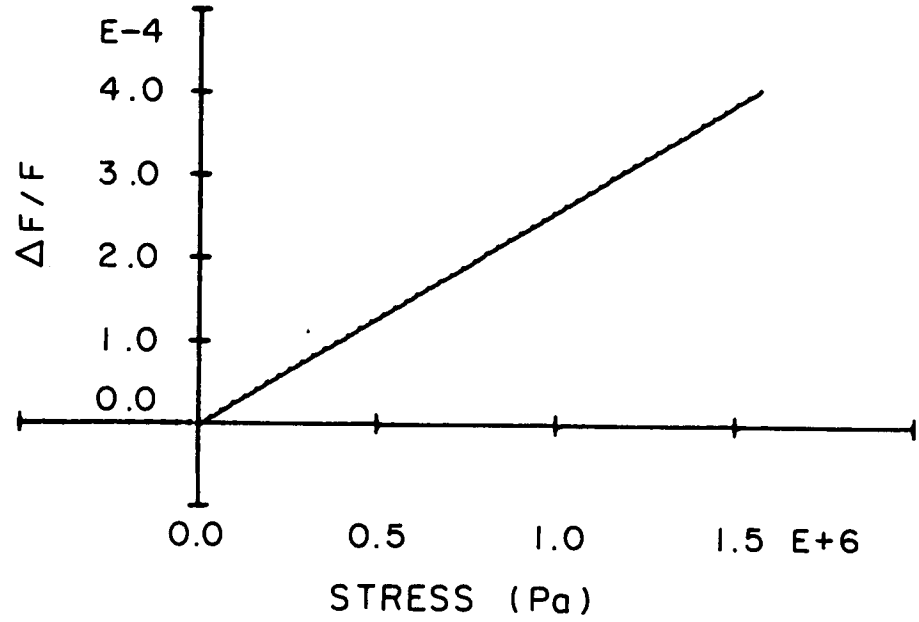

Figure 3.24 - Delta F/F versus pressure for a shear wave propagating along x_1 polarized along x_2.

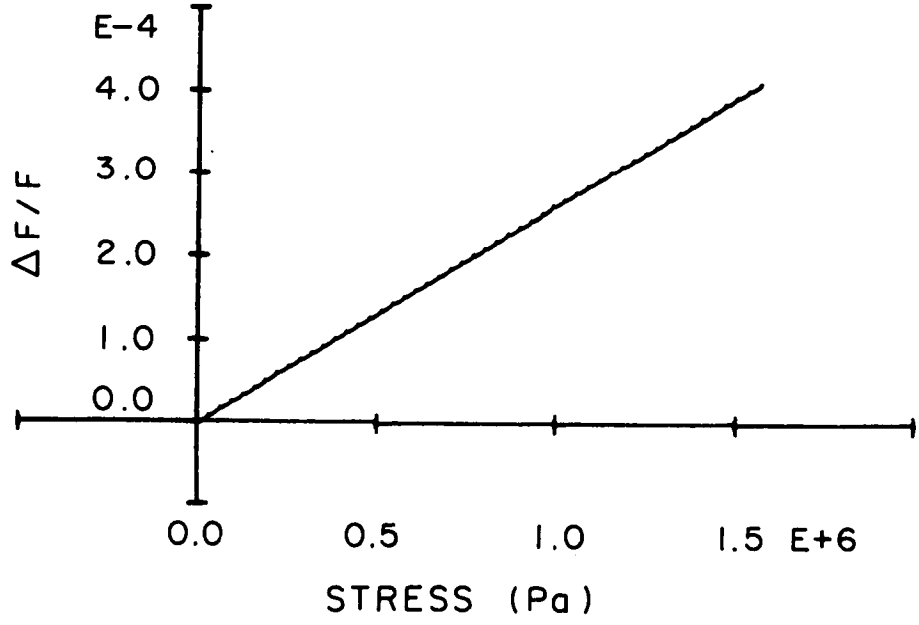

Figure 3.25 - Delta F/F versus pressure for a shear wave propagating along x_2 polarized along x_1.

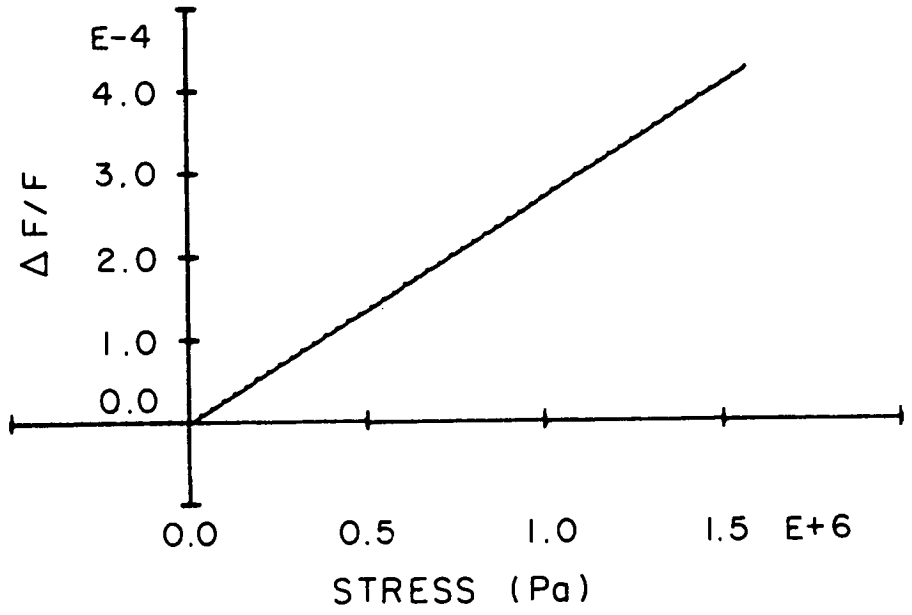

Figure 3.26 - Delta F/F versus pressure for a shear wave propagating along x_1 polarized along x_3.

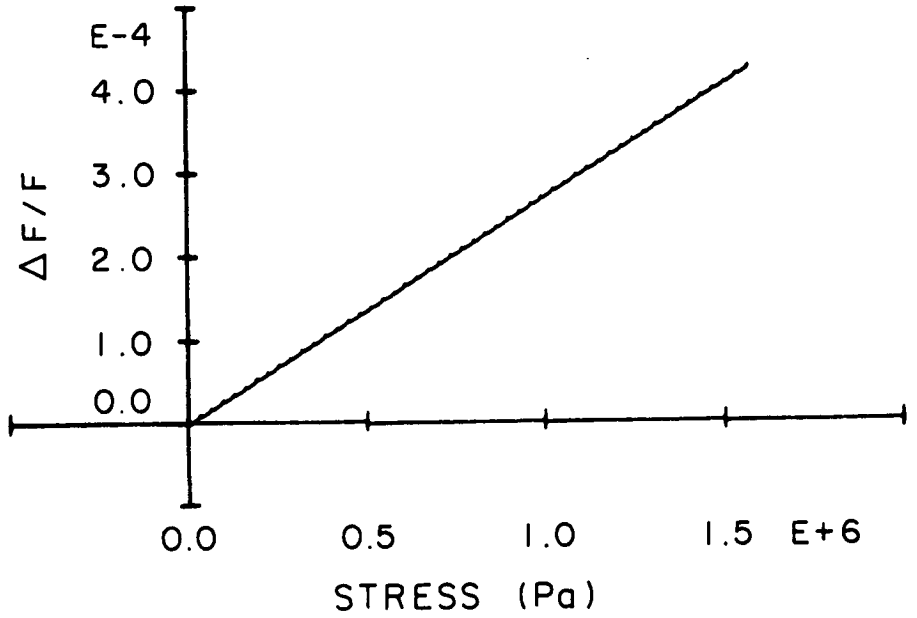

Figure 3.27 - Delta F/F versus pressure for a shear wave propagating along x_2 polarized along x_3.

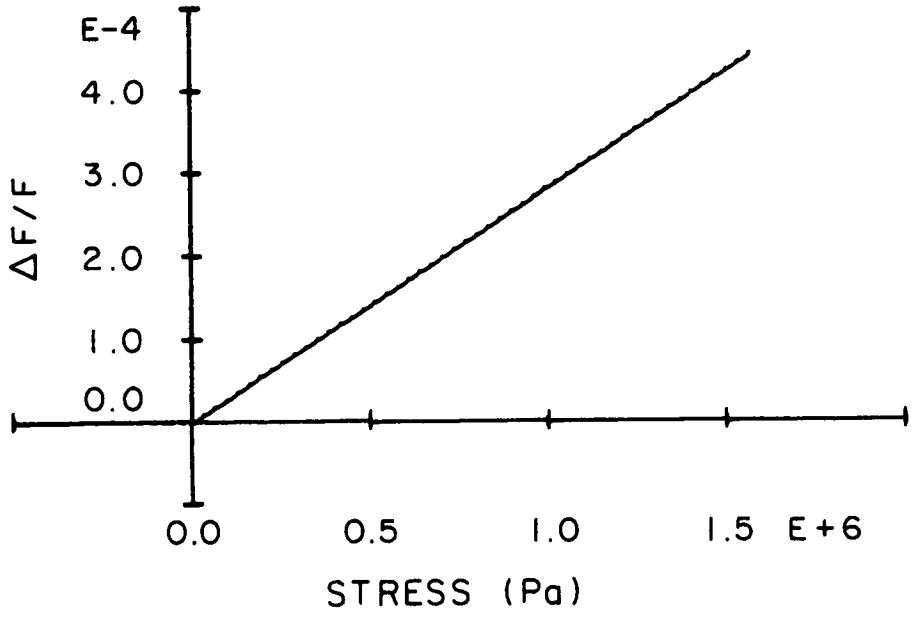

Figure 3.28 - Delta F/F versus pressure for a shear wave propagating along x_3 polarized along x_1.

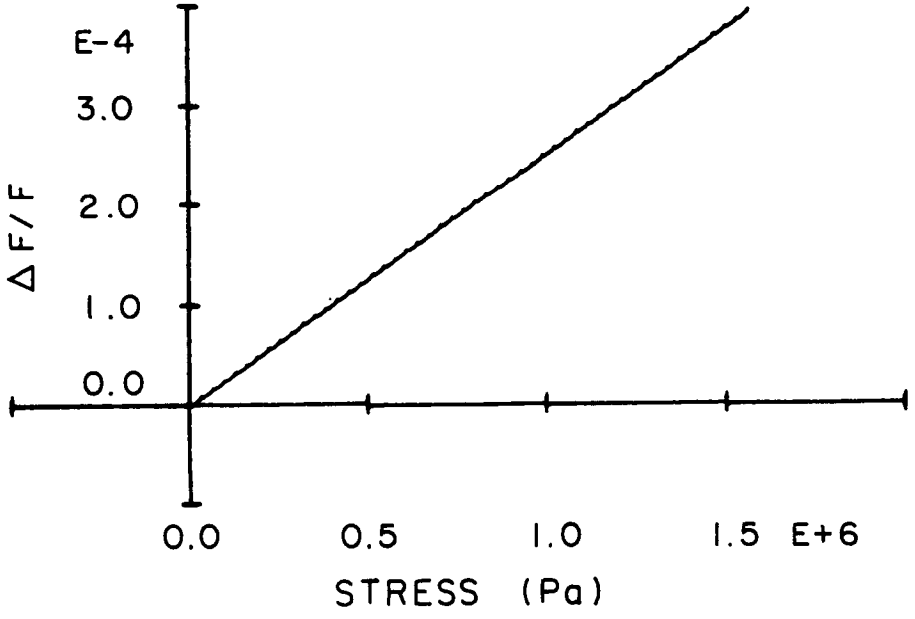

Figure 3.29 - Delta F/F versus pressure for a shear wave propagating along x_3 polarized along x_2.

Table 3.4 - Measured and corrected values for the Thermal Acoustic Constants.

Thermal Acoustic Constants (10^{-4} C^{-1})		
TAC	Original Value	Corrected Value
H_{T11}	-7.58 +/- 0.02	-6.36 +/- 0.02
H_{T22}	-7.55 +/- 0.03	-6.33 +/- 0.03
H_{T12}	-9.9 +/- 0.1	-8.5 +/- 0.1
H_{T21}	-9.9 +/- 0.1	-8.5 +/- 0.1
H_{T13}	-11.9 +/- 0.2	-10.2 +/- 0.2
H_{T23}	-11.8 +/- 0.2	-10.1 +/- 0.2
H_{T31}	-8.4 +/- 0.5	-7.1 +/- 0.5
H_{T32}	-9.0 +/- 0.7	-7.6 +/- 0.7
H_{T33}	-0.84 +/- 0.09	-0.72 +/- 0.09

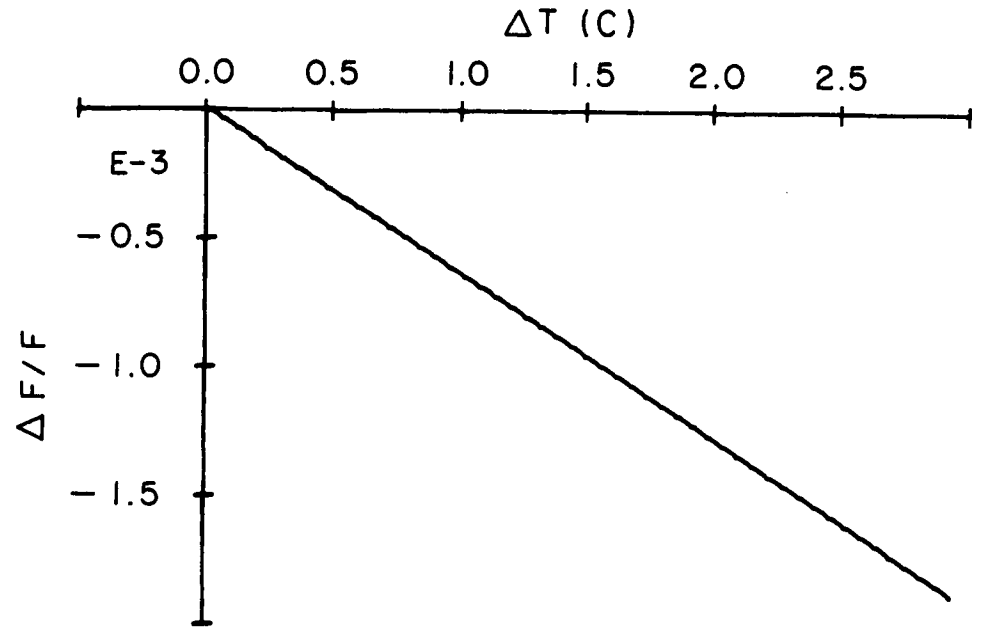

Figure 3.30 - Delta F/F versus temperature change for a longitudinal wave propagating along x_1.

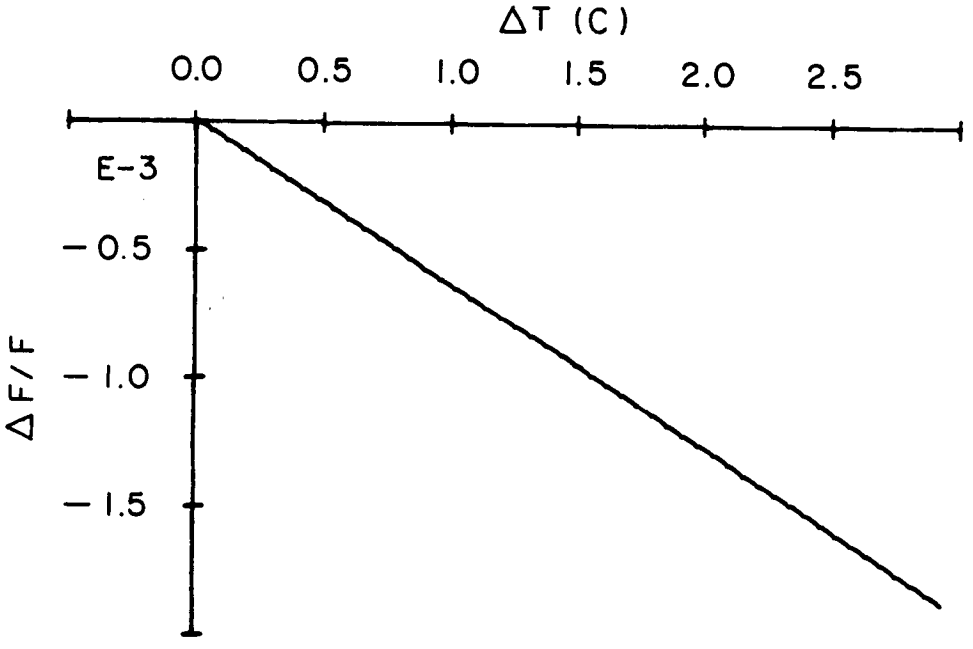

Figure 3.31 - Delta F/F versus temperature change for a longitudinal wave propagating along x_2.

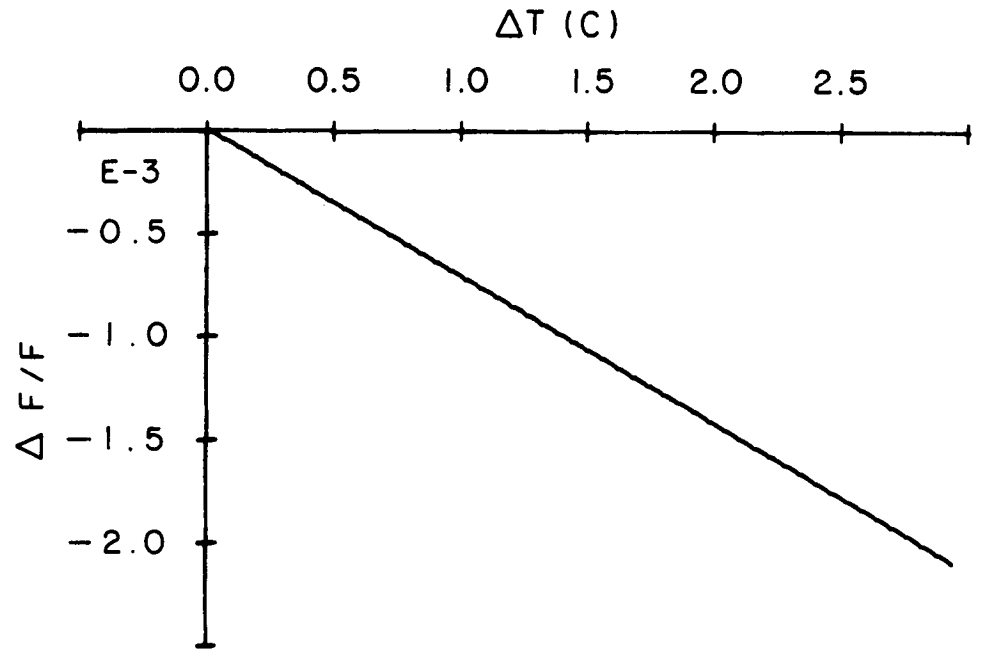

Figure 3.32 - Delta F/F versus temperature change for a shear wave propagating along x_3 polarized along x_1.

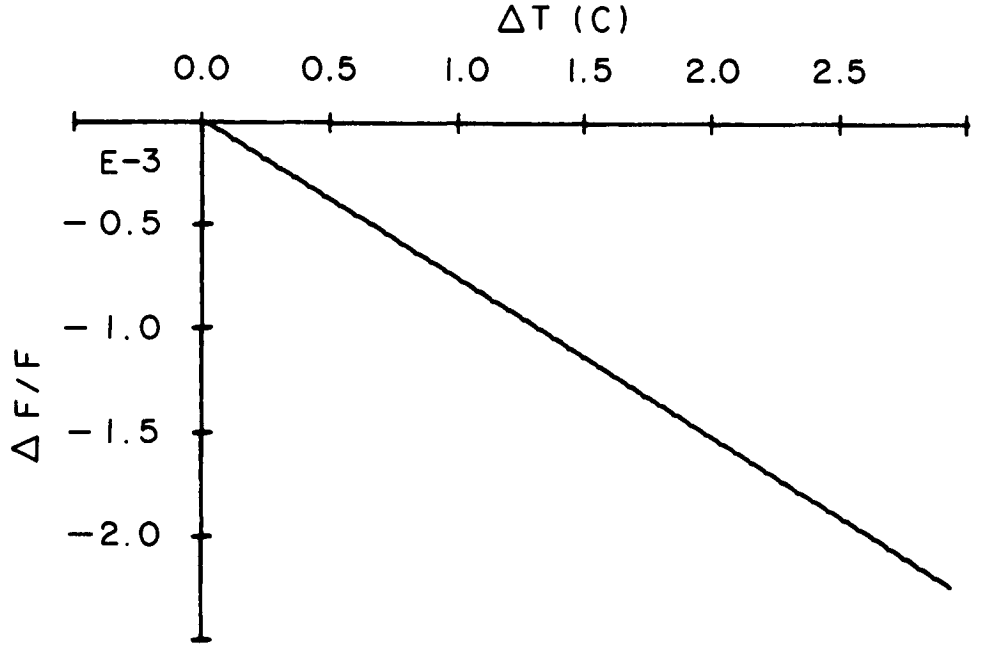

Figure 3.33 - Delta F/F versus temperature change for a shear wave propagating along x_3 polarized along x_2.

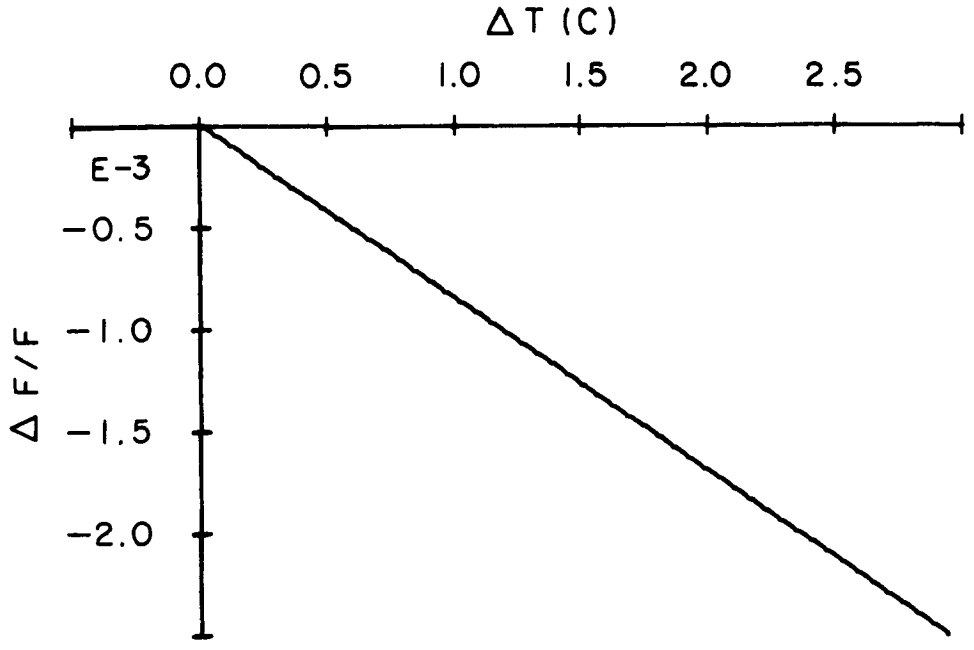

Figure 3.34 - Delta F/F versus temperature change for a shear wave propagating along x_1 polarized along x_2.

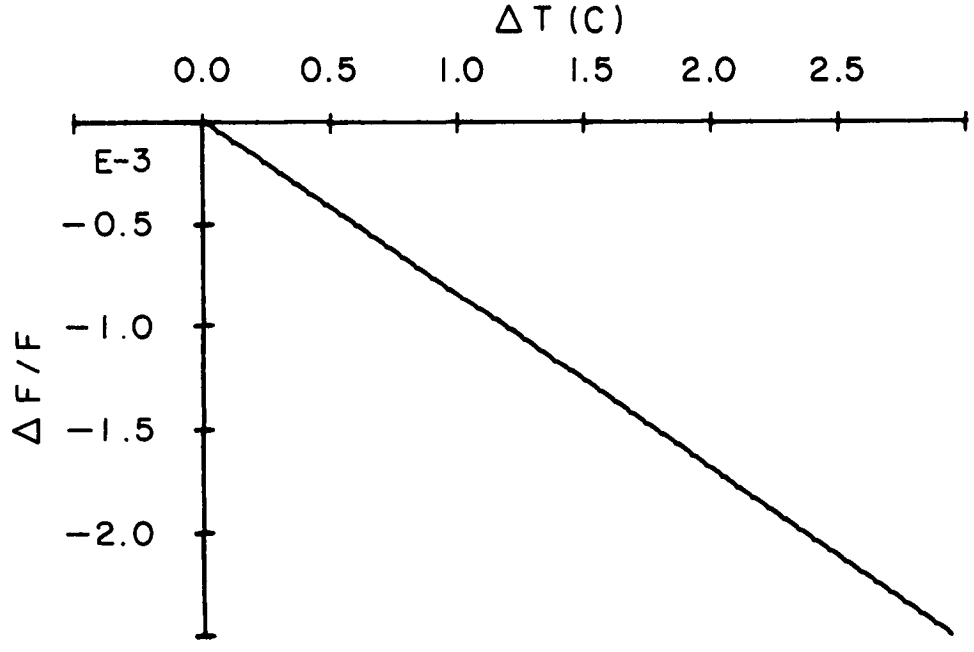

Figure 3.35 - Delta F/F versus temperature change for a shear wave propagating along x_2 polarized along x_1.

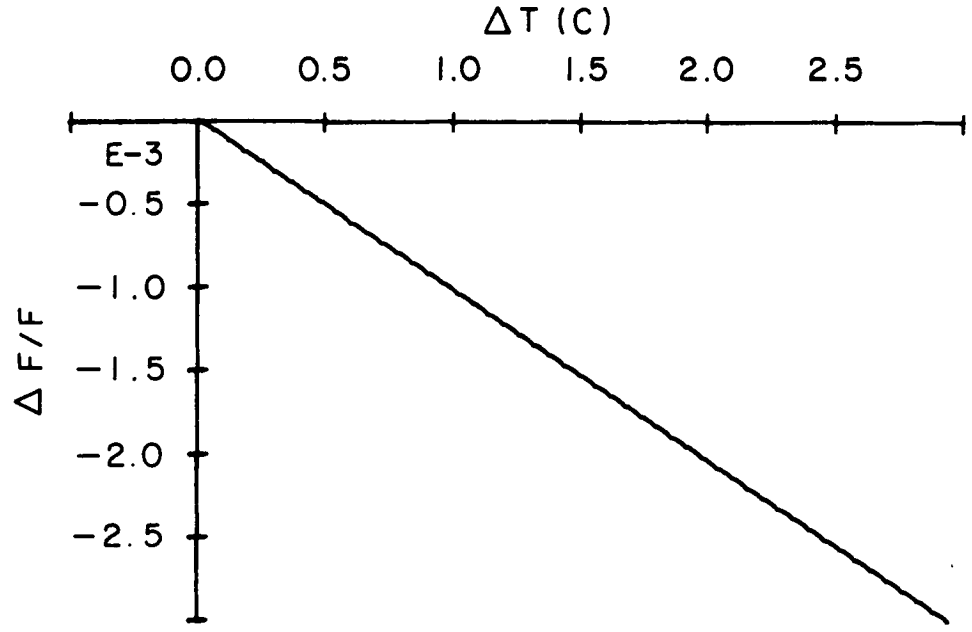

Figure 3.36 - Delta F/F versus temperature change for a shear wave propagating along x_1 polarized along x_3.

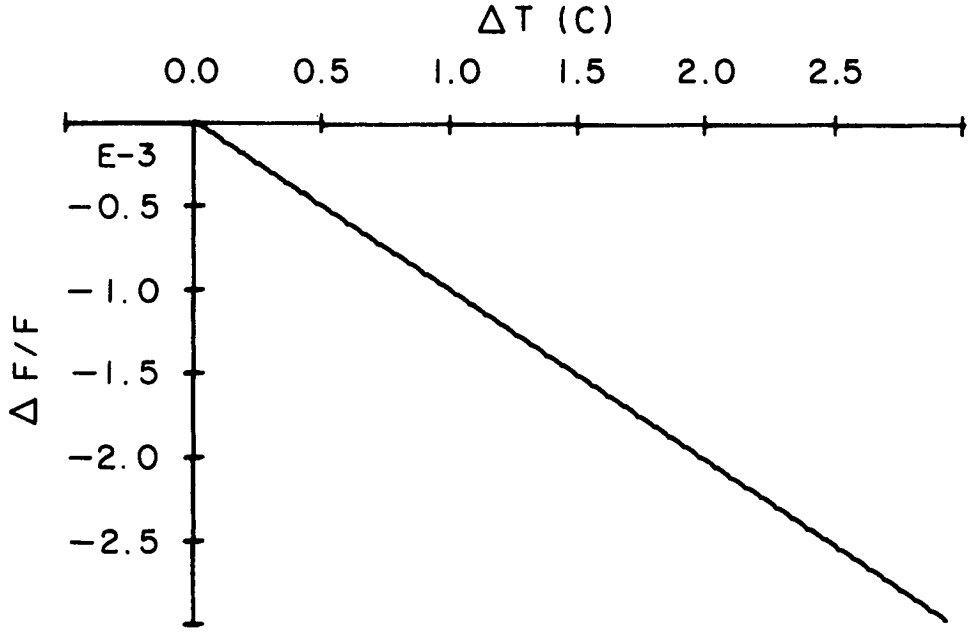

Figure 3.37 - Delta F/F versus temperature change for a shear wave propagating along x_2 polarized along x_3.

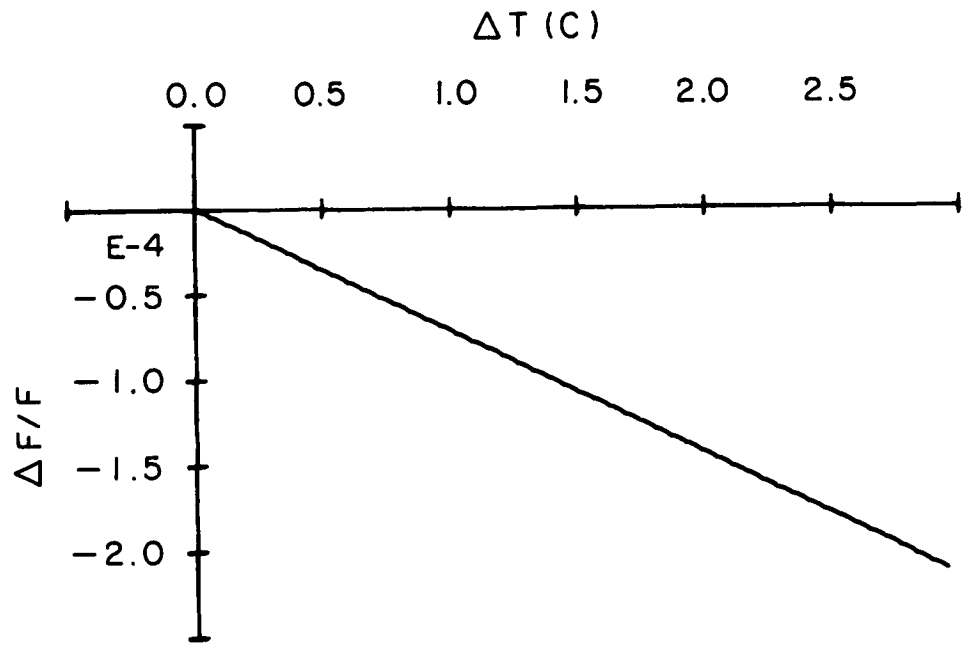

Figure 3.38 - Delta F/F versus temperature change for a longitudinal wave propagating along x_3.

III.D. Data Analysis

The SAC data, along with the linear moduli were used to determine some of the third order elastic moduli for this material. Since there were more equations and data than unknown moduli, the data was reduced by using a least squares fit to determine the best values for the moduli. The data was fit using both the transversely isotropic and orthotropic models. However, the lack of data for H_{033} prevented the calculation of the moduli c_{133} and c_{333} for the transversely isotropic model and the moduli c_{133}, c_{233}, c_{333}, c_{123}, and c_{456} for the orthotropic model.

The least squares procedure for the determination of third order moduli was outlined by Hankey and Schuele [40]. The formulation is as follows. The measured values for the SAC's are added to the constant terms in the equations of Table 3.1. These are designated M_i . The coefficients of the equations are designated A_{ij} and the moduli to be determined are D_j. Thus the equations of Table 3.1 are rewritten as

$$M_i = A_{ij}D_j \tag{3.38}$$

where i is summed over the number of data used and j is summed over the number of moduli to be determined. This can be rewritten as

$$A_{ik}M_i = (A_{ik}A_{ij})D_j \tag{3.39}$$

where k also runs from one to the number of coefficients to be determined. The best fit for the moduli D_j are then given by

$$D_j = (A_{ik}A_{ij})^{-1}A_{pk}M_p \tag{3.40}$$

where $(A_{ik}A_{ij})^{-1}$ is the inverse matrix element and p is summed over the number of measured values.

If it is assumed that the error in the measured values is much greater than the error in the coefficients, then the error in the coefficients can be dropped. The error in

the fitted values is then given by

$$\Delta D_j = \left|(A_{ik}A_{ij})^{-1}A_{pk}\right|\Delta M_p \tag{3.41}$$

where ΔD_j are the maximum limits of error,

and ΔM_p are the errors in the measured values.

The probable limit of error ($\Delta D_j'$) is given by

$$\Delta D_j' = \frac{\Delta D_j}{(N-1)^{1/2}} \tag{3.42}$$

where N is the number of measurements.

The above stated assumption was valid in these measurements as the errors in the measured SAC's ranged from one to ten percent while the errors in the linear coefficients were typically less (parts in 10^3)

Programs were written to perform the data reduction for the two symmetry models and are listed in Appendix H. The fitted values and their uncertainties are given in Table 3.5.

III.E. Conclusion

Using a pulsed phase locked loop interferometer, the normalized change in the ultrasonic "natural" phase velocity as a function of both stress and temperature have been measured. The stress measurements were made under conditions of hydrostatic and uniaxial stress. The measured curves were predominantly linear although several were nonlinear (quadratic) indicating higher than third order nonlinear elastic effects. Because of equipment limitations, the hydrostatic measurements were made at much lower pressures in comparison to the uniaxial measurements. Thus the uncertainties of the hydrostatic measurements were much larger making the validity of using them with the uniaxial measurements to calculate the third order moduli questionable. This

Table 3.5 - Calculated values of third order elastic stiffness moduli for transversely isotropic and orthotropic symmetries.

Third Order Elastic Moduli			
Transverse Isotropy			
Modulus	Value (GPa)	Max. Error	Probable Error
c_{111}	-214	17	4
c_{112}	-89	12	3
c_{113}	-4	110	23
c_{123}	65	109	23
c_{144}	-33.4	3	0.5
c_{155}	-49.1	4	0.8
c_{344}	-47	30	6
Orthotropy			
c_{111}	-196	15	3
c_{112}	-94	5	1
c_{113}	-63	63	13
c_{122}	-91	8	2

Table 3.5 - Continued

Orthotropic Nonlinear Moduli (Continued)			
Modulus	Value	Max. Error	Probable Error
c_{222}	-186	21	4
c_{223}	-60	93	19
c_{144}	-33.0	2.4	0.5
c_{244}	-47.8	3.3	0.7
c_{344}	-46	27	6
c_{155}	-50.1	3.9	0.8
c_{255}	-33.5	2.8	0.6
c_{355}	-49	32	7
c_{166}	-33.9	0.6	0.1
c_{266}	-33.1	0.6	0.1
c_{366}	-28.5	4.0	0.8

limitation in maximum hydrostatic pressure also prevented the measurement of H_{033} which prevented the calculation of several of the nonlinear moduli. The hydrostatic measurements need to be evaluated at higher pressures to reduce the uncertainties and to evaluate H_{033} . This would enable the determination of the remaining third order moduli.

The effect of temperature changes on "natural" velocity was also evaluated for nine combinations of propagation and polarization directions. These measurements were made over a narrow range of temperature change slightly above room temperature. The curves all demonstrated linear relationships between velocity and temperature. Although not directly used for the evaluation of third order moduli, these measurements were important in the evaluation of the effects of temperature variations during the SAC measurements.

The SAC values and the second order moduli were used to calculate some of the third order elastic moduli. A least squares fit was applied for both the transversely isotropic and the orthotropic models of elastic symmetry. The values for these moduli were all negative with the exception of the c_{123} . This is in agreement with the nonlinear behavior of conventional materials. Although the linear elastic moduli and the SAC data demonstrated small deviations from transverse isotropy, large uncertainties in the third order moduli masked any such deviations. The orthotropic moduli agree within experimental error to the conditions of transverse isotropy.

IV. SUMMARY AND CONCLUSIONS

The mechanical behavior of a unidirectional T300/5208 graphite/epoxy composite material has been evaluated in this research. In particular, the linear (second order) and nonlinear (third order) elastic properties have been measured. The linear moduli were measured by ultrasonic velocity measurements as well as by static loading strain gauge measurements. The nonlinear moduli were calculated from the linear moduli and measurements of the change in ultrasonic "natural" phase velocity as a function of stress.

The measured linear elastic properties of this material agreed well with previously reported values for a similar material except for the moduli c_{33} and s_{33} . These were the moduli that reveal the behavior of the composite under loading along the fiber direction. The low value for c_{33} and corresponding high value for s_{33} may have been a result of a lower fiber content or higher void content in this material. It could also have been the effect of misalignment of fibers in some of the laminae. However, the values of the ultrasonic and static measurements compared well with the exception of the off diagonal modulus c_{13} . This discrepancy was probably the result of either large uncertainties of the static measurements or error propagation in the inversion of the ultrasonic moduli. These measurements also pointed out measurable deviations from transversely isotropic elastic behavior which is usually assumed for unidirectional composites. The material more correctly possessed orthotropic symmetry although the deviations from transverse isotropy were small.

The change in ultrasonic "natural" velocity as a function of stress and temperature was measured with a pulsed phase locked loop ultrasonic interferometer for numerous wave modes. These measurements again demonstrated deviations from transversely isotropic behavior. Also, some of the stress-velocity curves were nonlinear (quadratic) which indicated higher than third order nonlinear effects. The

temperature-velocity curves were all linear over the small range of the measurements. Some of the third order elastic stiffness moduli were calculated from the stress dependence of velocity. These were all negative in agreement with nonlinear properties of conventional materials. The uncertainties of some of these moduli were large as a result of the large uncertainties of the hydrostatic pressure measurements propagating in the least squares data reduction. These large uncertainties masked any deviations from transverse isotropy that might have been present.

However, it should be noted here that the measured SAC's are probably more useful than the calculated nonlinear moduli. This is because they are more easily obtained with smaller experimental uncertainty and can be measured in an individual specimen instead of calculated from measurements made in several specimens. Also, the SAC's are the quantities that are more useful in experimental attempts to measure applied and residual stress and may be important in nondestructive evaluation of ultimate strength of materials.

It would be remiss to fail to point out several factors that could be improved to yield better measurements. First, the hydrostatic measurements should be carried out to higher pressures with improved temperature controller capabilities. This would reduce the uncertainties of these measurements and thus those of the nonlinear moduli. Also, the effect of sample to sample variations on both the linear and nonlinear properties needs to be evaluated further. These measurements were made on as few samples as possible to reduce this effect in the calculations. Future measurements should also evaluate the changes in velocity over wider temperature variations and with much higher stresses (i.e. near ultimate strength stresses) as well as evaluate the nonlinear properties by other techniques such as harmonic generation.

Although the primary goal of this investigation was a more thorough characterization of the mechanical properties of graphite/epoxy composites, these measurements serve as a basis for further study and potential applications in the area of

nondestructive testing of these materials. Also, the effects of fiber volume ratio and more complex lay up orientations on nonlinear properties of composites need to be evaluated. The relationships between nonlinear properties and important engineering properties such as strength, residual strength after impact and fatigue loading, and fiber-matrix interfacial strength need to be studied. These may lead to the development of needed nondestructive evaluation techniques for composite materials which will play an important role in the future of the aerospace industry.

The problem or residual strain in composites which arises because of the mismatch of coefficients of thermal expansion between fiber and matrix is another potential application for these measurements. When the composite material is cooled from the higher temperatures of polymerization during cure, large strains develop which may degrade the ultimate strength of the material. Although special curing cycles have been developed to reduce this effect, it still remains as an important problem in the field of composites. And as nonlinear ultrasonics have been used in attempts to nondestructively evaluate residual strains in conventional materials, they may well be useful in the measurement of residual stains in composites. Especially, since it may be possible to characterize the elastic symmetry of the composite better than in conventional materials because the symmetry of the material is determined by the lay up orientation. In conventional materials the problems associated with anisotropic textures of the material have limited the applicability of this technique.

APPENDIX A

The derivation of the independent linear (second order) elastic moduli for the symmetries of transverse isotropy and orthotropy are now presented. The case of orthotropic elastic symmetry is presented first. In an orthotropic material, there are three orthogonal planes of two fold symmetry. Therefore if the three coordinate axes are chosen such that they are the normals to these planes, then the independent elastic moduli can be determined by applying the two fold rotations about each of these axes on the strain energy function. The strain energy function is initially given by

$$\Phi = \frac{1}{2}(c_{11}\epsilon_1^2 + c_{22}\epsilon_2^2 + c_{33}\epsilon_3^2 + c_{44}\epsilon_4^2 + c_{55}\epsilon_5^2 + c_{66}\epsilon_6^2) + c_{12}\epsilon_1\epsilon_2$$

$$+ c_{13}\epsilon_1\epsilon_3 + c_{14}\epsilon_1\epsilon_4 + c_{15}\epsilon_1\epsilon_5 + c_{16}\epsilon_1\epsilon_6 + c_{23}\epsilon_2\epsilon_3 + c_{24}\epsilon_2\epsilon_4 + c_{25}\epsilon_2\epsilon_5$$

$$+ c_{26}\epsilon_2\epsilon_6 + c_{34}\epsilon_3\epsilon_4 + c_{35}\epsilon_3\epsilon_5 + c_{36}\epsilon_3\epsilon_6 + c_{45}\epsilon_4\epsilon_5 + c_{46}\epsilon_4\epsilon_6 + c_{56}\epsilon_5\epsilon_6. \quad \text{(A.1)}$$

The effect of a 180 degree rotation about the x_2 axis is now considered. The matrix of transformation is given by

$$[a_{ij}] = \begin{bmatrix} -1 & 0 & 0 \\ 0 & 1 & 0 \\ 0 & 0 & -1 \end{bmatrix}. \quad \text{(A.2)}$$

The effect on this rotation on the strains is given by

$$\epsilon'_{ij} = a_{im}a_{jn}\epsilon_{mn} \quad \text{(A.3)}$$

which yields the following relations between the rotated and original strains expressed in the Voigt reduced notation

$$\epsilon'_1 = \epsilon_1$$

$$\epsilon'_2 = \epsilon_2$$

$$\begin{aligned}
\epsilon_3' &= \epsilon_3 \\
\epsilon_4' &= -\epsilon_4 \\
\epsilon_5' &= \epsilon_5 \\
\epsilon_6' &= -\epsilon_6
\end{aligned} \qquad \text{(A.4)}$$

The strain energy function can be written for the rotated state and the above equations substituted to yield

$$\Phi' = \frac{1}{2}(c_{11}\epsilon_1^2 + c_{22}\epsilon_2^2 + c_{33}\epsilon_3^2 + c_{44}\epsilon_4^2 + c_{55}\epsilon_5^2 + c_{66}\epsilon_6^2) + c_{12}\epsilon_1\epsilon_2$$

$$+ c_{13}\epsilon_1\epsilon_3 - c_{14}\epsilon_1\epsilon_4 + c_{15}\epsilon_1\epsilon_5 - c_{16}\epsilon_1\epsilon_6 + c_{23}\epsilon_2\epsilon_3 - c_{24}\epsilon_2\epsilon_4 + c_{25}\epsilon_2\epsilon_5$$

$$- c_{26}\epsilon_2\epsilon_6 - c_{34}\epsilon_3\epsilon_4 + c_{35}\epsilon_3\epsilon_5 - c_{36}\epsilon_3\epsilon_6 - c_{45}\epsilon_4\epsilon_5 + c_{46}\epsilon_4\epsilon_6 - c_{56}\epsilon_5\epsilon_6. \qquad \text{(A.5)}$$

Equating Φ and Φ' term by term with respect to strain yields the following

$$\begin{aligned}
c_{14} &= -c_{14} \\
c_{16} &= -c_{16} \\
c_{24} &= -c_{24} \\
c_{26} &= -c_{26} \\
c_{34} &= -c_{34} \\
c_{36} &= -c_{36} \\
c_{45} &= -c_{45} \\
c_{56} &= -c_{56}
\end{aligned} \qquad \text{(A.6)}$$

For these relations to be true, then

$$c_{14} = c_{16} = c_{24} = c_{26} = c_{34} = c_{36} = c_{45} = c_{56} = 0. \qquad \text{(A.7)}$$

The matrix of elastic stiffness moduli is then given by

$$[c_{AB}] = \begin{bmatrix} c_{11} & c_{12} & c_{13} & 0 & c_{15} & 0 \\ c_{12} & c_{22} & c_{23} & 0 & c_{25} & 0 \\ c_{13} & c_{23} & c_{33} & 0 & c_{35} & 0 \\ 0 & 0 & 0 & c_{44} & 0 & c_{46} \\ c_{15} & c_{25} & c_{35} & 0 & c_{55} & 0 \\ 0 & 0 & 0 & c_{46} & 0 & c_{66} \end{bmatrix} \qquad \text{(A.7)}$$

The strain energy function is now given by

$$\Phi = \frac{1}{2}(c_{11}\epsilon_1^2 + c_{22}\epsilon_2^2 + c_{33} + \epsilon_3^2 + \epsilon_4^2 + c_{55}\epsilon_5^2 + \epsilon_6^2) + c_{12}\epsilon_1\epsilon_2$$

$$+ c_{13}\epsilon_1\epsilon_3 + c_{15}\epsilon_1\epsilon_5 + c_{23}\epsilon_2\epsilon_3 + c_{25}\epsilon_2\epsilon_5 + c_{35}\epsilon_3\epsilon_5 + c_{46}\epsilon_4\epsilon_6. \qquad \text{(A.8)}$$

The effect of a 180 degree rotation about the x_1 axis can now be considered. The transformation matrix is given by

$$[a_{ij}] = \begin{bmatrix} 1 & 0 & 0 \\ 0 & -1 & 0 \\ 0 & 0 & -1 \end{bmatrix} \qquad \text{(A.9)}$$

The rotated and original strains are related by

$$\begin{aligned} \epsilon_1' &= \epsilon_1 \\ \epsilon_2' &= \epsilon_2 \\ \epsilon_3' &= \epsilon_3 \\ \epsilon_4' &= \epsilon_4 \\ \epsilon_5' &= -\epsilon_5 \\ \epsilon_6' &= -\epsilon_6 \end{aligned} \qquad \text{(A.10)}$$

Again these are substituted into the equation for the strain energy function resulting in

$$\Phi' = \frac{1}{2}(c_{11}\epsilon_1^2 + c_{22}\epsilon_2^2 + c_{33}\epsilon_3^2 + c_{44}\epsilon_4^2 + c_{55}\epsilon_5^2 + c_{66}\epsilon_6^2) + c_{12}\epsilon_1\epsilon_2$$

$$+ c_{13}\epsilon_1\epsilon_3 - c_{15}\epsilon_1\epsilon_5 + c_{23}\epsilon_2\epsilon_3 - c_{25}\epsilon_2\epsilon_5 - c_{35}\epsilon_3\epsilon_5 - c_{46}\epsilon_4\epsilon_6. \tag{A.11}$$

Equating term by term yields

$$c_{15} = c_{25} = c_{35} = c_{46} = 0 \tag{A.12}$$

and reduces the elastic stiffness matrix to

$$[c_{AB}] = \begin{bmatrix} c_{11} & c_{12} & c_{13} & 0 & 0 & 0 \\ c_{12} & c_{22} & c_{23} & 0 & 0 & 0 \\ c_{13} & c_{23} & c_{33} & 0 & 0 & 0 \\ 0 & 0 & 0 & c_{44} & 0 & 0 \\ 0 & 0 & 0 & 0 & c_{55} & 0 \\ 0 & 0 & 0 & 0 & 0 & c_{66} \end{bmatrix}. \tag{A.13}$$

The third symmetry rotation about x_3 can be shown to have no further effect on the elastic stiffness tensor and thus the final form for an orthotropic body is given by equation A.13. There are nine independent moduli for an orthtropic material.

The reduction of moduli for a transversely isotropic material can be carried out beginning with the matrix form for orthotropy. This is because it possesses the same symmetry conditions as an orthotropic material in addition to having an isotropic plane perpendicular to x_3 . Thus the strain energy function can be written out with the orthotropic moduli and the effect of an arbitrary rotation around the x_3 axis can be considered. Φ is given by

$$\Phi = \frac{1}{2}(c_{11}\epsilon_1^2 + c_{22}\epsilon_2^2 + c_{33}\epsilon_3^2 + c_{44}\epsilon_4^2 + c_{55}\epsilon_5^2 + c_{66}\epsilon_6^2)$$

$$+ c_{12}\epsilon_1\epsilon_2 + c_{13}\epsilon_1\epsilon_3 + c_{23}\epsilon_2\epsilon_3. \tag{A.14}$$

The effect of an arbitrary rotation around x_3 by an angle θ on the strains is given by

$$\epsilon_1' = \cos^2\theta\epsilon_1 + \sin\theta\cos\theta\epsilon_6 + \sin^2\theta\epsilon_2$$

$$\epsilon_2' = \sin^2\theta\epsilon_1 + \sin\theta\cos\theta\epsilon_6 + \cos^2\theta\epsilon_2$$

$$\epsilon_3' = \epsilon_3$$

$$\epsilon_4' = -\sin\theta\epsilon_5 + \cos\theta\epsilon_4 \tag{A.15}$$

$$\epsilon_5' = \cos\theta\epsilon_5 - \sin\theta\epsilon_4$$

$$\epsilon_6' = -2\sin\theta\cos\theta\epsilon_1 + (\cos^2\theta - \sin^2\theta)\epsilon_6 + 2\sin\theta\cos\theta\epsilon_2.$$

These equations can be substituted into the strain energy function as before. Then comparing Φ and Φ' term by term will yield

$$\begin{aligned} c_{11} &= c_{22} \\ c_{13} &= c_{23} \\ c_{44} &= c_{55} \\ c_{66} &= \frac{1}{2}(c_{11} - c_{12}) \end{aligned} \tag{A.16}$$

which reduces the number of independent elastic moduli to five for a transversely isotropic body. The elastic stiffness matrix can be written out as

$$[c_{AB}] = \begin{bmatrix} c_{11} & c_{12} & c_{13} & 0 & 0 & 0 \\ c_{12} & c_{11} & c_{13} & 0 & 0 & 0 \\ c_{13} & c_{13} & c_{33} & 0 & 0 & 0 \\ 0 & 0 & 0 & c_{44} & 0 & 0 \\ 0 & 0 & 0 & 0 & c_{44} & 0 \\ 0 & 0 & 0 & 0 & 0 & \frac{1}{2}(c_{11} - c_{12}) \end{bmatrix}. \tag{A.17}$$

APPENDIX B

Using the equations derived for linear elastic wave propagation presented in Chapter II., the expressions for the velocities of ultrasonic waves in terms of elastic moduli and density are now derived. The expressions are derived for both transverse isotropy and orthotropy. The case of transversely isotropic elastic symmetry is considered first.

For the case of transverse isotropy, equation (2.84) can be used to show that there are several directions of propagation for pure mode elastic waves. Pure mode elastic waves may be propagated along the x_3 axis and along any direction perpendicular to the x_3 axis in the isotropic plane which of course includes the x_1 and x_2 axes. They may also be propagated in a direction which makes an angle Θ with the x_3 axis given by

$$\tan \Theta = \left[\frac{c_{13} + 2c_{44} - c_{33}}{c_{13} + 2c_{44} - c_{11}}\right]^{\frac{1}{2}}. \qquad \text{(B.1)}$$

However, for unidirectional graphite epoxy composites where the modulus c_{33} is usually about two orders of magnitude larger than the other moduli, this direction does not exist. Thus the pure mode directions to be considered are along each of the three coordinate axes.

The components of the matrix λ_{ik} for a transversely isotropic material are given by

$$\lambda_{11} = c_{11}l_1^2 + \frac{1}{2}(c_{11} - c_{12})l_2^2 + c_{44}l_3^2,$$

$$\lambda_{22} = \frac{1}{2}(c_{11} - c_{12})l_1^2 + c_{11}l_1^2 + c_{44}l_3^2,$$

$$\lambda_{33} = c_{44}l_1^2 + c_{44}l_2^2 + c_{33}l_3^2, \qquad \text{(B.2)}$$

$$\lambda_{12} = \lambda_{21} = \frac{1}{2}(c_{11} + c_{12})l_1l_2,$$

$$\lambda_{13} = \lambda_{31} = (c_{13} + c_{44})l_1l_3,$$

and

$$\lambda_{23} = \lambda_{32} = (c_{44} + c_{13})l_2l_3.$$

The solutions for the wave modes propagating along the x_1 axis are now derived. For waves propagating in this direction, the direction cosines of the wave normal are given by $l_1 = 1$, and $l_2 = l_3 = 0$. The components of the λ_{ij} matrix reduce to

$$\lambda_{11} = c_{11},$$

$$\lambda_{22} = \frac{1}{2}(c_{11} - c_{12}), \qquad \text{(B.3)}$$

$$\lambda_{33} = c_{44},$$

and all other $\lambda_{ij} = 0$. These are substituted into equation (2.55) to determine the solutions for the three modes of propagation in this direction by solving the equation

$$\text{DET}\begin{bmatrix} c_{11} - \rho_0 v^2 & 0 & 0 \\ 0 & \frac{1}{2}(c_{11} - c_{12}) - \rho_0 v^2 & 0 \\ 0 & 0 & c_{44} - \rho_0 v^2 \end{bmatrix} = 0. \qquad \text{(B.4)}$$

This can be expanded to

$$(c_{11} - \rho_0 v^2)(\frac{1}{2}(c_{11} - c_{12}) - \rho_0 v^2)(c_{44} - \rho_0 v^2) = 0. \qquad \text{(B.5)}$$

The solutions are then found to be

$$v_1 = \left(\frac{c_{11}}{\rho_0}\right)^{\frac{1}{2}},$$

$$v_2 = \left(\frac{c_{11} - c_{12}}{2\rho_0}\right)^{\frac{1}{2}}, \tag{B.6}$$

and

$$v_3 = \left(\frac{c_{44}}{\rho_0}\right)^{\frac{1}{2}}.$$

Solving for the eigenvectors for each of these eigenvalues yields the following particle displacements. For the first wave, the direction cosines of the particle displacements are $\alpha_2 = \alpha_3 = 0$ and $\alpha_1 = 1$. Therefore, since $\alpha_i = l_i$, the first wave is a pure mode longitudinal wave. For the second wave, the direction cosines are $\alpha_1 = \alpha_3 = 0$ and $\alpha_2 = 1$. Thus, since $\alpha_i l_i = 0$, it is a pure mode transverse wave. The particle displacement vector direction cosines for the third wave are found to be $\alpha_1 = \alpha_2 = 0$ and $\alpha_3 = 1$, which means it too is a pure mode shear wave. The energy flux equations can be used to show that there is no energy flux deviation for these waves.

The solutions for propagation along the x_2 axis are similar. The direction cosines of the wave normal are $l_1 = l_3 = 0$, and $l_2 = 1$. The λ_{ij} components are then

$$\lambda_{11} = \frac{1}{2}(c_{11} - c_{12}),$$

$$\lambda_{22} = c_{11}, \tag{B.6}$$

$$\lambda_{33} = c_{44},$$

and all other $\lambda_{ij} = 0$. The solutions for these wave modes are of course the same as for propagation along x_1 except the first and second waves are reversed. Waves propagating in any direction in the x_1, x_2 plane with $l_3 = 0$ can be shown to have similar solutions to the waves propagating along x_1 and x_2 .

Propagation along x_3 where $l_1 = l_2 = 0$, and $l_3 = 1$ is now considered. The components of λ_{ij} are now given by

$$\lambda_{11} = c_{44},$$

$$\lambda_{22} = c_{44}, \tag{B.7}$$

$$\lambda_{33} = c_{33},$$

and all other $\lambda_{ij} = 0$. Substitution into equation (2.55) yields

$$(c_{44} - \rho_0 v^2)^2 (c_{33} - \rho_0 v^2) = 0. \tag{B.8}$$

The solutions for this equation are given by

$$v_1 = v_2 = \left(\frac{c_{44}}{\rho_0} \right)^{\frac{1}{2}}, \tag{B.9}$$

and,

$$v_3 = \left(\frac{c_{33}}{\rho_0} \right)^{\frac{1}{2}}.$$

Solutions for the particle displacements for these wave modes show that for the first and second wave modes, $\alpha_3 = 0$ while α_1 and α_2 are arbitrary as long as $\alpha_1^2 + \alpha_2^2 = 1$. Thus these waves are pure mode shear waves with particle displacements in the x_1, x_2 plane. For the third wave, they are $\alpha_1 = \alpha_2 = 0$, and $\alpha_3 = 1$, which means it is a pure mode compressional wave. Again, it can be shown that these waves suffer no energy flux deviation.

Measurements of the velocities of the waves in these three directions can be used to determine four of the five independent elastic stiffness moduli. However, the modulus c_{13} can not be determined. To evaluate this modulus, an off axis non-pure mode wave must be used. The wave chosen for this purpose was a wave propagating in the x_1, x_3 plane 45 degrees between the two axes. Thus, $l_1 = l_3 = \frac{1}{\sqrt{2}}$, and $l_2 = 0$. The components of the λ_{ij} matrix are then

$$\lambda_{11} = \frac{1}{2}(c_{11} + c_{44}),$$

$$\lambda_{22} = \frac{1}{2}(c_{44} + \frac{1}{2}(c_{11} - c_{12})),$$

$$\lambda_{33} = \frac{1}{2}(c_{33} + c_{44}), \qquad \text{(B.10)}$$

$$\lambda_{13} = \frac{1}{2}(c_{13} + c_{44}),$$

and all other $\lambda_{ij} = 0$. These are substituted into the eigenvalue equation and the solutions are given by

$$\rho_0 v_1^2 = \frac{1}{4}\left[c_{11} + 2c_{44} + c_{33} + \sqrt{(c_{11} - c_{33})^2 + 4(c_{13} + c_{44})^2}\right],$$

$$\rho_0 v_2^2 = \frac{1}{2}\left[c_{44} + \frac{1}{2}(c_{11} - c_{12})\right], \qquad \text{(B.11)}$$

and

$$\rho_0 v_3^2 = \frac{1}{4}\left[c_{11} + 2c_{44} + c_{33} - \sqrt{(c_{11} - c_{33})^2 + 4(c_{13} + c_{44})^2}\right].$$

Solutions for the particle displacements of these waves show that the second wave is a pure mode shear wave. However, the first wave is a quasilongitudinal wave and the third wave is quasishear. Energy flux equations show that these wave modes also suffer energy flux deviation. Kriz and Stinchcomb [45] reported the energy flux deviation could be as high as 43.4 degrees for the quasilongitudinal wave and 28.7 degrees for the quasitransverse wave. The energy flux deviation was reported to be about 17.8 degrees for the pure mode transverse wave. Waves propagating in the x_2, x_3 plane 45 degrees between the axes with $l_1 = 0$ have the same solutions.

The solutions for the wave modes in an orthotropic medium will now be derived. The λ_{ij} matrix components are now given by

$$\lambda_{11} = c_{11}l_1^2 + c_{66}l_2^2 + c_{55}l_3^2,$$

$$\lambda_{22} = c_{66}l_1^2 + c_{22}l_2^2 + c_{44}l_3^2,$$

$$\lambda_{33} = c_{55}l_1^2 + c_{44}l_2^2 + c_{33}l_3^2,$$

$$\lambda_{12} = \lambda_{21} = (c_{12} + c_{66})l_1l_2, \tag{B.12}$$

$$\lambda_{13} = \lambda_{31} = (c_{55} + c_{13})l_1l_3,$$

and

$$\lambda_{23} = \lambda_{32} = (c_{44} + c_{23})l_2l_3.$$

For propagation along the x_1 axis, these equations reduce to

$$\lambda_{11} = c_{11},$$

$$\lambda_{22} = c_{66}, \tag{B.13}$$

$$\lambda_{33} = c_{55},$$

and all other components are zero. When these are substituted into equation (2.55), the wave solutions can be found to be

$$v_1 = \left(\frac{c_{11}}{\rho_0}\right)^{\frac{1}{2}},$$

$$v_2 = \left(\frac{c_{66}}{\rho_0}\right)^{\frac{1}{2}}, \tag{B.14}$$

and

$$v_3 = \left(\frac{c_{55}}{\rho_0}\right)^{\frac{1}{2}}.$$

with the first wave being a pure mode longitudinal wave. The second wave is a pure mode shear wave with particle displacements along the x_2 axis and the third wave is pure mode shear polarized along the x_3 axis. There is no energy flux deviation for these waves.

For propagation along x_2 , the components of λ_{ij} reduce to

$$\lambda_{11} = c_{66},$$

$$\lambda_{22} = c_{22}, \tag{B.15}$$

$$\lambda_{33} = c_{44},$$

and all other $\lambda_{ij} = 0$. When substituted, these yield the equation

$$(c_{66} - \rho_0 v^2)(c_{22} - \rho_0 v^2)(c_{44} - \rho_0 v^2) = 0 \tag{B.16}$$

which has the solutions

$$v_1 = \left(\frac{c_{66}}{\rho_0}\right)^{\frac{1}{2}},$$

$$v_2 = \left(\frac{c_{22}}{\rho_0}\right)^{\frac{1}{2}}, \tag{B.17}$$

and

$$v_3 = \left(\frac{c_{44}}{\rho_0}\right)^{\frac{1}{2}}.$$

In this case, the first and third waves turn out to be pure mode shear waves polarized along the x_1 and x_3 axes respectively while the second wave is a pure mode compressional wave. Again, there is no energy flux deviation for these waves.

Now the case of wave propagation along the x_3 axis in an orthotropic material is presented. With $l_1 = l_2 = 0$, and $l_3 = 1$, the components of λ_{ij} reduce to

$$\lambda_{11} = c_{55},$$

$$\lambda_{22} = c_{44}, \tag{B.18}$$

$$\lambda_{33} = c_{33},$$

and all other λ_{ij} components equal to zero. These yield the solutions for the three modes of propagation as

$$v_1 = \left(\frac{c_{55}}{\rho_0}\right)^{\frac{1}{2}},$$

$$v_2 = \left(\frac{c_{44}}{\rho_0}\right)^{\frac{1}{2}}, \tag{B.19}$$

and

$$v_3 = \left(\frac{c_{33}}{\rho_0}\right)^{\frac{1}{2}}.$$

In this case, the first and second waves are pure mode shear waves. The first wave is polarized along the x_1 axis. The particle displacements for the second wave are along the x_2 axis. The third wave is a pure mode compressional wave. There is no energy flux deviation for these waves.

As with the case of transverse isotropy, the pure mode waves do not yield sufficient data to determine all of the orthotropic moduli. Waves must be propagated off axis to determine the moduli c_{12}, c_{13}, and c_{23} . Waves propagating in the x_1, x_2 plane 45 degrees from each axis with $l_3 = 0$ are considered first. The direction cosines of the wave normal are given by $l_1 = l_2 = \frac{1}{\sqrt{2}}$, and $l_3 = 0$. Thus the λ_{ij} matrix components

are

$$\lambda_{11} = \frac{1}{2}(c_{11} + c_{66}),$$

$$\lambda_{22} = \frac{1}{2}(c_{66} + c_{22}),$$

$$\lambda_{33} = \frac{1}{2}(c_{55} + c_{44}), \tag{B.20}$$

$$\lambda_{12} = \lambda_{21} = \frac{1}{2}(c_{12} + c_{66}),$$

and all other $\lambda_{ij} = 0$. The solutions for the waves propagating along this direction can then be determined to be

$$\rho_0 v_1^2 = \frac{1}{4}\left[c_{11} + 2c_{66} + c_{22} + \sqrt{(c_{11} - c_{22})^2 + 4(c_{12} + c_{66})^2}\right],$$

$$\rho_0 v_2^2 = \frac{1}{2}(c_{44} + c_{55}), \tag{B.21}$$

and

$$\rho_0 v_3^2 = \frac{1}{4}\left[c_{11} + 2c_{66} + c_{22} - \sqrt{(c_{11} - c_{22})^2 + 4(c_{12} + c_{66})^2}\right].$$

The second wave is a pure mode shear wave while the first is quasilongitudinal and the third is a quasishear wave. The energy flux deviation for these waves is small because there is only a small deviation from isotropy in this plane.

The next off axis direction considered is that in the x_1, x_3 plane 45 degrees from either axis where the direction cosines for the wave normal are given by $l_1 = l_3 = \frac{1}{\sqrt{2}}$, and $l_3 = 0$. Therefore,

$$\lambda_{11} = \frac{1}{2}(c_{11} + c_{55}),$$

$$\lambda_{22} = \frac{1}{2}(c_{66} + c_{44}),$$

$$\lambda_{33} = \frac{1}{2}(c_{55} + c_{33}), \tag{B.22}$$

$$\lambda_{13} = \lambda_{31} = \frac{1}{2}(c_{13} + c_{55}),$$

and all other $\lambda_{ij} = 0$. The solutions for these waves are then found by solving the equation

$$(\lambda_{22} - \rho_0 v^2)[(\lambda_{11} - \rho_0 v^2)(\lambda_{33} - \rho_0 v^2) - \lambda_{13}^2] = 0. \tag{B.23}$$

The three roots of this equation are given by

$$\rho_0 v_1^2 = \frac{1}{4}\left[c_{11} + 2c_{55} + c_{33} + \sqrt{(c_{11} - c_{33})^2 + 4(c_{13} + c_{55})^2}\right],$$

$$\rho_0 v_2^2 = \frac{1}{2}(c_{44} + c_{66}), \tag{B.24}$$

and

$$\rho_0 v_3^2 = \frac{1}{4}\left[c_{11} + 2c_{55} + c_{33} - \sqrt{(c_{11} - c_{33})^2 + 4(c_{13} + c_{55})^2}\right].$$

The first and third waves are quasilongitudinal and quasishear mode waves respectively while the second is pure mode shear. The energy flux deviations are again large as was the case for the similar waves for transverse isotropy.

The final direction of propagation considered is that in the x_2, x_3 plane 45 degrees from either axis. This is similar to the previous case with the final solutions reducing to

$$\rho_0 v_1^2 = \frac{1}{4}\left[c_{22} + 2c_{44} + c_{33} + \sqrt{(c_{22} - c_{33})^2 + 4(c_{23} + c_{44})^2}\right],$$

$$\rho_0 v_2^2 = \frac{1}{2}(c_{55} + c_{66}), \tag{B.25}$$

and

$$\rho_0 v_3^2 = \frac{1}{4}\left[c_{22} + 2c_{44} + c_{33} - \sqrt{(c_{22} - c_{33})^2 + 4(c_{23} + c_{44})^2}\right].$$

Again, the second wave is pure mode shear while the first is quasilongitudinal and the third is quasishear. These equations reduce to those given for transverse isotropy if the appropriate substitutions are made. These equations allow the determination of all of the second order moduli for an orthotropic material.

APPENDIX C

The relationship between the measured time between echos (t) and the true time of flight (δ) was given by McSkimmin [19] as

$$t = p\delta - \left(\frac{p\gamma}{360F}\right) + \left(\frac{n}{F}\right) \qquad (C.1)$$

In this equation, p is an integer expressing the difference between the number of echos used for the overlap measurement. Since the first and second echos were used for these measurements, it was always true that $p = 1$. The variable n in this expression is an integer which gives the number of cycles of incorrect overlap between the two echos. If the echos are overlapped correctly, then $n = 0$. If the second echo is overlapped one cycle before the first then $n = -1$ and if the reverse is true then $n = 1$. γ is the phase angle (in degrees) accounting for phase shifts at the transducer-specimen interface. F is the frequency of the tone burst and not the repetition rate frequency.

Substituting the fact that $p = 1$ simplifies this equation to

$$t = \delta - \left(\frac{\gamma}{360F}\right) + \left(\frac{n}{F}\right) \qquad (C.2)$$

Thus both γ and n must be determined to evaluate the true round trip time. Therefore a second equation is introduced which is

$$\Delta t_{l} = \frac{1}{F_l}\left(n - \frac{\gamma_l}{360}\right) - \frac{1}{F_h}\left(n - \frac{\gamma_h}{360}\right) \qquad (C.3)$$

This equation expresses the change in measured time between echos as a function of a change in the frequency of the pulse from a higher frequency (F_h) to a lower frequency (F_l) . The phase shifts at these two frequencies are designated γ_h and γ_l . For these measurements F_h was chosen to be that of the resonant frequency of the transducer and F_l was chosen to be 0.9 times that value. Thus, this equation can be rewritten as

$$\Delta t = \frac{1}{0.9F_r}\left(n - \frac{\gamma_l}{360}\right) - \frac{1}{F_r}\left(n - \frac{\gamma_r}{360}\right) \qquad (C.4)$$

where F_r is the resonant frequency of the transducer.

The phase angles γ_l and γ_r can now be calculated from standard electrical transmission line theory. It is defined that Z_1, Z_2, and Z_3 are the mechanical impedances of the transducer, bond material, and sample respectively. Z_4 is the mechanical impedance of the transducer-bond composite resonator and it is defined that

$$r = \frac{Z_2}{Z_1}. \qquad (C.5)$$

Therefore,

$$Z_4 = iZ_2\left(\frac{r \tan k_2 l_2 + \tan k_1 l_1}{r - \tan k_1 l_1 \tan k_2 l_2}\right) \qquad (C.6)$$

where l_1, l_2 are the thicknesses of the transducer and bond respectively,

and k_1, k_2 are the wave numbers for the transducer and bond given by

$$k_i = \frac{\omega}{v_i} = \frac{2\pi}{\lambda_i} \qquad (C.7)$$

where v_i are the respective velocities of sound in the transducer and bond

and λ_i are the wavelengths of sound in the transducer and bond.

Now it is assumed that the bond thickness is zero, and thus equation (C.6) can be reduced to

$$Z_4 = iZ_1 \tan k_1 l_1. \qquad (C.8)$$

Since at the resonant frequency of the transducer,

$$F_r = \frac{c_1}{2l_1}, \qquad (C.9)$$

it is true that

$$k_1 l_1 = 180 \text{ degrees.} \tag{C.10}$$

At F_l,

$$k_1 l_1 = (0.9 \cdot 180) \text{ degrees.} \tag{C.11}$$

Therefore at F_r,

$$Z_4 = 0 \tag{C.12}$$

and at F_l,

$$Z_4 = iZ_1 \tan (0.9 \cdot 180) \tag{C.13}$$

For an elastic wave reflecting from the transducer-specimen interface, the ratio of the reflected pressure (P_r) to the incident pressure of the wave (P_i) is given by

$$\frac{P_r}{P_i} = \frac{Z_4 - Z_3}{Z_4 + Z_3} \tag{C.14}$$

and the phase angle is given by

$$\tan \gamma = \frac{\text{Im}\left(\frac{P_r}{P_i}\right)}{\text{Re}\left(\frac{P_r}{P_i}\right)}. \tag{C.15}$$

At $F = F_r$,

$$\frac{P_r}{P_i} = \frac{0 - Z_3}{0 + Z_3} = -1 \tag{C.16}$$

and therefore

$$\gamma_r = \tan^{-1} 0 = 0. \tag{C.17}$$

At $F = F_l$,

$$\frac{P_r}{P_i} = \frac{iR_4 - Z_3}{iR_4 + Z_3} \tag{C.18}$$

where $R_4 = Z_l \tan (0.9 \cdot 180)$.

Thus γ_l can be calculated to be

$$\gamma_l = \tan^{-1} \left(\frac{2Z_3R_4}{R_4^2 - Z_3^2} \right). \tag{C.18}$$

Therefore γ_l can be calculated from knowledge of the mechanical properties of the sample and the transducer.

Since $\gamma_r = 0$, the equation for the change in measured time of flight as a function of frequency can be reduced to

$$\Delta t^{(0)} = \frac{(0.111n - \gamma_l/324)}{F_r} \tag{C.19}$$

where the superscript (0) implies that this equation is true for zero bond thickness. If $n = 0$, this equation reduces to

$$\Delta t^{(0,0)} = -\frac{\gamma_l}{324F_r} \tag{C.20}$$

where the second superscript 0 implies that $n = 0$.

If measurements are made at F_r and F_l for a number of different overlap numbers (n) and the Δt's calculated for each n, the correct choice of $n = 0$ can be determined by comparing the experimental results with those predicted by the previous equation. The agreement will not be exact, but the one closest to the calculated value of $\Delta t^{(0,0)}$ and obeying the stipulation that

$$\Delta t_{measured} > \Delta t^{(0,0)} \tag{C.21}$$

which implies a positive bond thickness will be the correct choice for proper overlap. This theory can be extended to account for nonzero bond thickness. However, the

corrections were determined to be less than experimental error for these measurements.

APPENDIX D

```
100 REM    PROGRAM TO COLLECT AND ANALYZE DATA FROM PULSE ECHO
110 REM   OVERLAP ULTRASONIC TECHNIQUE.  WRITTEN BY PROSSER
120 REM                9/25/85.
150 REM
160 REM            variable list
170 REM
180 REM     variable     description          type
190 REM       f$         name of file       character (32)
200 REM       x$         transducer material    "     (32)
210 REM       b$         bond material          "     (32)
220 REM       s$         sample ID              "     (32)
230 REM       d$         date data taken        "     (20)
240 REM       m1         data pts/overlap   numeric
250 REM       m2         series format of m1    "
256 REM       T3         AVG. EXP. TRANSIT TIME "
257 REM       T2         AVG. EXP. DELTA T(0)   "
258 REM       E(I),F(I)  TRANSIT TIME, CORR. DELTA T  "
259 REM       F2         XDUCER RES. FREQ. IN HZ "
260 REM       j1         !QMAX!                 "
261 REM       F3         DATA FILE NO.           "
262 REM       Z          FILE LENGTH COUNTER     "
263 REM       C1         FREQ. DIVISION BY MATEC 110   "
264 REM       P(I),Q(I)  AVG. DELTA T AT RES.,LOW FREQ. "
265 REM       S(I),R(I)  ST. DEV. OF TIME AT RES.,LOW FREQ. "
266 REM       D(I)       DELTA T'S                          "
267 REM       U(I)       UNCERTAINTIES IN DELTA T           "
268 REM       W,X        SUM TOTALERS FOR AVG.'S            "
270 REM       t          sample temp.            "
280 REM       f1         xducer resonant freq.   "
290 REM       I,K        INTEGER LOOP COUNTERS   "
300 REM       l(i,k)     data at low freq. (.9f1) "
310 REM       h(i,k)     data at res. freq.      "
320 REM
330 REM     character variable dimensioning
340 REM
350 DIM F$(32),X$(32),B$(32),D$(20),S$(32)
360 REM
370 REM     file naming and variables
380 REM
390 REM
400 PRINT "what is the name of the file?"
410 INPUT F$
420 PRINT "what is the sample ID?"
430 INPUT S$
440 PRINT "what is the xducer material?"
450 INPUT X$
460 PRINT "what is the bond material?"
470 INPUT B$
480 PRINT "what was the date data was taken?"
490 INPUT D$
```

```
500 PRINT "what was the temp. of the sample in deg. C?"
510 INPUT T
520 PRINT "what was the xducer resonant freq. in MHz?"
530 INPUT F1
540 PRINT "what was !@MAX!?"
550 PRINT "= max. # of apparent echos in front of"
560 PRINT "or behind the reference burst"
570 PRINT "(ref. burst is taken to be the "
580 PRINT "larger amplitude burst)"
590 INPUT J1
600 PRINT "what is the # of data pts per overlap"
610 INPUT M1
620 PRINT "if series format of m1 was 1:2:3:4..."
630 PRINT "then input 1"
640 PRINT "if series format of m2 was 1:2:4:8..."
650 PRINT "then input 2"
660 INPUT M2
670 IF M2=1 THEN 710
680 IF M2=2 THEN 710
690 PRINT "expecting input of 1 or 2"
700 GO TO 620
710 REM
720 REM     description of echo-overlap data
730 REM     organization;  each data set has 2
740 REM     arrays (1 for res. freq. and 1 for .9*res freq.)
750 REM     each with (2*!@MAX!+1)*m1 datapoints.
760 REM     a final data set contains xducer material,
770 REM     bond material, temp., etc.
790 REM     dimensioning arrays
800 REM
810 LET I=2*(J1+1)-1
820 LET K=M1
830 DIM H(I,K),P(I),Q(I),F(I)
840 DIM L(I,K),R(I),S(I),D(I),U(I),E(I)
850 REM
860 REM     input data
870 FOR K=1 TO M1
880 PRINT "INPUT FREQ. DIVISION FACTOR FROM MATEC 110"
890 INPUT C1
900 FOR I=1 TO 2*(J1+1)-1
910 PRINT "freq. = resonant freq."
920 Z=I-(J1+1)
929 PRINT "PRESS RETURN TO"
930 PRINT "enter array member";Z,K
931 PRINT "INPUT YES TO CHANGE FREQ. DIVISION FACTOR FROM: ";C1
932 INPUT A$
933 IF A$<>"YES" THEN 940
934 PRINT "INPUT NEW FREQ. DIVISION FACTOR "
935 INPUT C1
940 INPUT @20:H(I,K)
941 H(I,K)=H(I,K)/10^C1
942 PRINT H(I,K)
943 PRINT " "
950 NEXT I
```

```
960 NEXT K
970 FOR K=1 TO M1
971 PRINT "INPUT FREQ. DIVISION FACTOR FROM MATEC 110"
972 INPUT C1
980 FOR I=1 TO 2*(J1+1)-1
990 PRINT "freq. = .9*res. freq."
1000 Z=I-(J1+1)
1009 PRINT "PRESS RETURN TO "
1010 PRINT "enter array member";Z,K
1011 PRINT "INPUT YES TO CHANGE FREQ. DIVISION FACTOR FROM: ";C1
1012 INPUT A$
1013 IF A$<>"YES" THEN 1020
1014 PRINT "INPUT NEW FREQ. DIVISION FACTOR"
1015 INPUT C1
1020 INPUT @20:L(I,K)
1021 L(I,K)=L(I,K)/10^C1
1022 PRINT L(I,K)
1023 PRINT " "
1030 NEXT I
1040 NEXT K
1050 REM    COMPUTE AVG.'S AND ST. DEV.'S
1060 REM
1070 FOR I=1 TO 2*(J1+1)-1
1080 W=0
1090 X=0
1100 FOR K=1 TO M1
1110 IF M2<>1 THEN 1140
1120 W=W+K/H(I,K)
1130 GO TO 1160
1140 Z=2^(K-1)
1150 W=W+Z/H(I,K)
1160 NEXT K
1170 P(I)=W/M1
1180 FOR K=1 TO M1
1190 IF M2<>1 THEN 1220
1200 X=X+(K/H(I,K)-P(I))^2
1210 GO TO 1240
1220 Z=2^(K-1)
1230 X=X+(Z/H(I,K)-P(I))^2
1240 NEXT K
1250 S(I)=(X/M1)^0.5
1260 NEXT I
1270 FOR I=1 TO 2*(J1+1)-1
1280 W=0
1290 X=0
1300 FOR K=1 TO M1
1310 IF M2<>1 THEN 1340
1320 W=W+K/L(I,K)
1330 GO TO 1360
1340 Z=2^(K-1)
1350 W=W+Z/L(I,K)
1360 NEXT K
```

```
1370 Q(I)=W/M1
1380 FOR K=1 TO M1
1390 IF M2<>1 THEN 1420
1400 X=X+(K/L(I,K)-Q(I))^2
1410 GO TO 1440
1420 Z=2^(K-1)
1430 X=X+(Z/L(I,K)-Q(I))^2
1440 NEXT K
1450 R(I)=(X/M1)^0.5
1460 NEXT I
1470 REM
1480 REM CALCULATES DELTA T AND UNCERTAINTIES IN DELTA T
1490 REM
1500 REM
1510 FOR I=1 TO 2*(J1+1)-1
1520 D(I)=Q(I)-P(I)
1530 U(I)=S(I)+R(I)
1540 NEXT I
1550 REM
1560 REM CALCULATES DELTA T(0)
1570 REM
1580 PRINT "WHAT IS THE IMPEDANCE (*1E5 MECH. OHMS) OF"
1590 PRINT "THE ";X$;" TRANSDUCER?"
1600 INPUT Z1
1610 PRINT "WHAT IS THE IMPEDANCE (*1E5 MECH. OHMS) OF SAMPLE ";S$
1620 INPUT Z3
1630 PRINT "WHAT IS THE IMPEDANCE (*1E5 MECH. OHMS) OF THE ";B$;" BOND"
1640 INPUT Z2
1650 Z4=Z1*TAN(0.9*PI)
1660 G=ATN(2*Z4*Z3/(Z4^2-Z3^2))
1661 IF G>0 THEN 1670
1662 G=G+PI
1670 F2=F1*1000000
1680 O1=-1/(2*PI*F2)*(G/0.9)
1690 REM
1700 REM IDENTIFY CORRECT N AND FIND DELTA T(0) FROM EXP. DATA
1710 REM
1720 REM
1730 PRINT "COMPARE THE CALCULATED DELTA T(0) = ";O1;" (SEC.)"
1740 PRINT "WITH THE FOLLOWING VALUES"
1750 PRINT ""
1760 FOR I=1 TO 2*(J1+1)-1
1770 PRINT "DELTA T (";I-(J1+1);") = ";D(I);" (SEC.)"
1780 PRINT ""
1790 NEXT I
1800 PRINT "ENTER THE # OF DELTA T THAT MOST CLOSELY MATCHES THE"
1810 PRINT "CALCULATED DELTA T(0)"
1820 INPUT B
1830 W=0
1840 REM
1850 REM CALCULATE EXPERIMENTAL DELTA T(0) AND AVG. TRANSIT TIME
1860 REM AND THEIR UNCERTAINTIES USING A WEIGHTED AVG.
1870 REM
```

```
1880 X1=0
1890 X2=0
1900 Y1=0
1910 Y2=0
1920 FOR I=1 TO 2*(J1+1)-1
1930 Z=I-(J1+1)
1931 N=Z-B
1940 E(I)=D(I)+N/F2*(1/0.9-1)
1950 F(I)=P(I)+N/F2
1960 X1=X1+E(I)*(1/U(I)^2)
1970 Y1=Y1+F(I)*(1/S(I)^2)
1980 X2=X2+1/U(I)^2
1990 Y2=Y2+1/S(I)^2
2000 NEXT I
2010 T2=X1/X2
2020 T3=Y1/Y2
2030 H1=X2^-0.5
2040 H2=Y2^-0.5
2080 GOSUB 3430
2090 REM STORE DATA
2100 REM
2110 TLIST
2120 PRINT ""
2130 PRINT "ENTER # OF (LAST) FILE TO STORE DATA ON"
2140 INPUT F3
2150 Z=30
2160 Z=Z+LEN(S$)+2+LEN(D$)+2+LEN(B$)+2+LEN(F$)+2
2170 Z=Z+LEN(X$)+2
2180 Z=Z+10*(9+2*(2*(J1+1)*M1))
2190 Z=Z+10*(6*2*(J1+1))
2200 FIND F3
2210 MARK 1,Z
2220 FIND F3
2230 WRITE F$,S$,B$,D$,X$,J1
2240 WRITE T,F1,F2,M1,M2,Z1,Z2
2250 WRITE Z3,Z4,G,O1,D,C6,C7
2260 FOR I=1 TO 2*(J1+1)-1
2270 WRITE P(I),Q(I),S(I),R(I),D(I),U(I)
2280 NEXT I
2290 FOR I=1 TO 2*(J1+1)-1
2300 FOR K=1 TO M1
2310 WRITE H(I,K),L(I,K)
2320 NEXT K
2330 NEXT I
2340 WRITE T2,T3,H1,H2
2350 CLOSE
2360 PRINT "DATA STORED"
2370 PRINT ""
2410 PRINT @2:"FILE NAME IS ";F$
2420 PRINT @2:"FILE # IS ";F3
2430 PRINT @2:"TRANSDUCER MATERIAL IS ";X$
2440 PRINT @2:"BOND MATERIAL IS ";B$
```

```
2450 PRINT @2:"SAMPLE ID IS ";S$
2460 PRINT @2:"DATE DATA WAS TAKEN IS ";D$
2461 PRINT @2:"SAMPLE TEMP WAS ";T;" C"
2470 PRINT @2:"DATA PTS/OVERLAP IS ";M1
2480 IF M2<>1 THEN 2520
2490 PRINT @2:"SERIES FORMAT OF M1 VALUES IS;"
2500 PRINT @2:"1:2:3:4..."
2510 GO TO 2540
2520 PRINT @2:"SERIES FORMAT OF M1 VALUES IS;"
2530 PRINT @2:"1:2:4:8..."
2540 PRINT @2:" "
2550 FOR Z=1 TO 2
2560 IF Z<>1 THEN 2590
2570 PRINT @2:"DATA AT RESONANT FREQ."
2580 GO TO 2610
2590 PRINT @2:" "
2600 PRINT @2:"DATA AT .9*RESONANT FREQ."
2610 PRINT @2:" "
2620 IMAGE 3A,1X,S
2630 IMAGE 2D,8X,S
2640 PRINT @2: USING 2620:"Q/M"
2650 FOR I=1 TO M1-1
2660 IF M2<>2 THEN 2690
2670 W=2^(I-1)
2680 GO TO 2700
2690 W=I
2700 PRINT @2: USING 2630:W
2710 NEXT I
2720 IMAGE 2D
2730 IF M2<>2 THEN 2760
2740 W=2^(M1-1)
2750 GO TO 2770
2760 W=M1
2770 PRINT @2: USING 2720:W
2780 FOR I=1 TO 2*(J1+1)-1
2790 IMAGE 2D,1X,S
2800 PRINT @2: USING 2790:I-(J1+1)
2810 FOR K=1 TO M1-1
2820 IF Z<>1 THEN 2860
2830 IMAGE 7D.2D,1X,S
2840 PRINT @2: USING 2830:H(I,K)
2850 GO TO 2870
2860 PRINT @2: USING 2830:L(I,K)
2870 NEXT K
2880 IF Z<>1 THEN 2920
2890 PRINT @2: USING 2900:H(I,M1)
2900 IMAGE 7D.2D
2910 GO TO 2930
2920 PRINT @2: USING 2900:L(I,M1)
2930 NEXT I
2940 NEXT Z
2950 PRINT @2:" "
2960 FOR Z=1 TO 2
```

```
2970 IF Z=2 THEN 3000
2980 PRINT @2:"DATA AT RESONANT FREQ."
2990 GO TO 3010
3000 PRINT @2:"DATA AT .9*RESONANT FREQ."
3010 PRINT @2:" "
3020 PRINT @2: USING 3030:"Q"
3030 IMAGE 2A,1X,S
3040 PRINT @2: USING 3050:"AVG. TIME (SEC.)"
3050 IMAGE 20A,1X,S
3060 PRINT @2: USING 3070:"STD. DEV. (SEC.)"
3070 IMAGE 20A
3080 PRINT @2:" "
3090 FOR I=1 TO 2*(J1+1)-1
3100 IF Z=2 THEN 3180
3110 PRINT @2: USING 3120:I-(J1+1)
3120 IMAGE 2D,1X,S
3130 PRINT @2: USING 3140:P(I)
3140 IMAGE 10E,10X,S
3150 PRINT @2: USING 3160:S(I)
3160 IMAGE 10E
3170 GO TO 3210
3180 PRINT @2: USING 3120:I-(J1+1)
3190 PRINT @2: USING 3140:Q(I)
3200 PRINT @2: USING 3160:R(I)
3210 PRINT @2:" "
3220 NEXT I
3230 PRINT @2:" "
3240 NEXT Z
3250 PRINT @2:" "
3260 PRINT @2:"IMPEDANCE OF XDUCER IS ";Z1;" (*1E5 MECH. OHMS)"
3270 PRINT @2:"IMPEDANCE OF SAMPLE IS ";Z3;" (*1E5 MECH. OHMS)"
3280 PRINT @2:"IMPEDANCE OF BOND IS ";Z2;" (*1E5 MECH. OHMS)"
3290 PRINT @2:"PHASE SHIFT AT LOW FREQ. IS ";G*360/(2*PI);" (DEG.)"
3300 PRINT @2:"CALCULATED DELTA T(0) IS ";O1;" (SEC.)"
3310 FOR I=1 TO 2*(J1+1)-1
3320 PRINT @2:" "
3330 PRINT @2:"DELTA T(";I-(J1+1);") IS ";D(I);" (SEC.)"
3340 PRINT @2:"UNCERTAINTY (";I-(J1+1);") IS ";U(I);"(SEC.)"
3350 NEXT I
3360 PRINT @2:" "
3370 PRINT @2:"CHOICE FOR CORRECT OVERLAP IS ";B
3380 PRINT @2:"AVG. EXPERIMENTAL DELTA T(N=0) IS ";T2;" (SEC.)"
3390 PRINT @2:"ST. DEV. IS ";H1;" (SEC.)"
3400 PRINT @2:" "
3410 PRINT @2:"AVG. TRANSIT TIME FROM EXP. DATA IS ";T3;" (SEC.)"
3420 PRINT @2:"ST. DEV. IS ";H2;" (SEC.)"
3421 PRINT @2:" "
3422 PRINT @2:"BOND ANGLE IS ";C6;" DEGREES"
3423 PRINT @2:"TIME CORRECTION FOR BOND IS ";C7;" SEC."
3424 GO TO 3740
3430 REM
3440 REM    BOND CORRECTION
```

```
3450 REM
3460 DIM V(30),C(30),O(30)
3470 FOR I=1 TO 30
3480 C1=(I-1)/2*(2*PI)/360
3490 Z5=Z2*(Z2/Z1*TAN(C1)+TAN(0.9*PI))/(Z2/Z1-TAN(0.9*PI)*TAN(C1))
3500 C2=-2*Z5*Z3
3510 C3=Z3*Z3-Z5*Z5
3520 C4=-2*Z2*TAN(C1)*Z3
3530 C5=Z3*Z3-Z2*TAN(C1)*(Z2*TAN(C1))
3540 V(I)=ATN(C4/C5)
3541 V(I)=V(I)*360/(2*PI)
3550 C(I)=ATN(C2/C3)
3551 IF C(I)>0 THEN 3555
3552 C(I)=C(I)+PI
3555 C(I)=C(I)*360/(2*PI)
3560 O(I)=V(I)/(360*F2)-C(I)/(360*0.9*F2)
3570 NEXT I
3580 PAGE
3581 VIEWPORT 10,120,10,90
3590 WINDOW 0,15,O(1)+5*O(1)/10,0
3591 MOVE 0,0
3592 FOR I=2 TO 16 STEP 2
3593 MOVE I-2,0
3594 PRINT "KH";I-2;
3595 NEXT I
3600 AXIS 2,O(1)/10,0,0
3610 MOVE 0,O(1)
3620 FOR I=1 TO 30
3630 DRAW (I-1)/2,O(I)
3640 NEXT I
3650 MOVE 0,T2
3660 DRAW 30,T2
3661 MOVE 0,T2+H1
3662 DRAW 15,T2+H1
3663 MOVE 0,T2-H1
3664 DRAW 15,T2-H1
3665 MOVE 0,8*O(1)/10
3670 PRINT "INPUT PHASE ANGLE OF INTERSECTION "
3680 INPUT C6
3681 HOME
3682 PAGE
3690 I=2*C6+1
3700 C7=V(I)/(360*F2)
3710 PRINT "BOND ANGLE IS ";C6;" DEGREES "
3720 PRINT "TIME CORRECTION FOR BOND IS ";C7;" SEC."
3730 RETURN
3740 END
```

APPENDIX E


```
100 REM   PROGRAM TO MEASURE STRESS VS. STRAIN
120 REM             WRITTEN BY PROSSER 7/15/86
130 REM
140 REM   VARIABLES                              NAME          TYPE
150 REM
160 REM SAMPLE ID.                               S$       CHARACTER(32)
170 REM DIRECTION OF STRAIN 1                    M$            "   (12)
180 REM DIRECTION OF STRAIN 2                    N$            "   (12)
200 REM    "      " LOADING                      L$            "   (12)
220 REM DATE                                     D$        CHARACTER(12)
270 REM CROSS SECTIONAL AREA OF SAMPLE (SQ. IN.)A1            "
280 REM EXCITATION VOLTAGE FOR STRAIN GAGE 1     A2
290 REM      "       "     "    "      " 2      A3
300 REM NUMBER OF DATA POINTS                    B1            "
330 REM VOLTAGE MEASUREMENTS FOR LOAD            F(I)       ARRAY
340 REM VOLTAGE MEASUREMENTS FOR STRAIN 1        V(I,1)        "
350 REM    "         "       " STRAIN 2         V(I,2)        "
400 REM STRAIN 1                                 L(I)       ARRAY
410 REM STRAIN 2                                 S(I)          "
460 REM STRESS                                   D(I)          "
520 REM MIN STRESS                               W1            "
530 REM MAX STRESS                               W2            "
540 REM MIN STRAIN 1                             W3            "
550 REM MAX STRAIN 1                             W4            "
560 REM MIN STRAIN 2                             W5            "
570 REM MAX STRAIN 2                             W6            "
571 REM SUM D(I)                                 X3            "
572 REM SUM (D(I))^2                             X4            "
573 REM SUM L(I)                                 X5            "
574 REM SUM (L(I))^2                             X6            "
575 REM SUM S(I)                                 X7            "
576 REM SUM (S(I))^2                             X8            "
577 REM SUM (D(I)*l(i)                           W7            "
578 REM SUM (D(I))*s(i))                         W8            "
590 REM DUMMY VARIABLE                           C$        CHARACTER(32)
600 REM    "     "                               A$            "
630 REM DUMMY VARIABLE                           A5            "
640 REM INTEGER COUNTERS                         I,J           "
650 REM DUMMY ARRAY FOR PLOTTING                 P(I)       ARRAY
660 REM  "    VARIABLES FOR PLOTTING             A8,A9      NUMERIC
670 REM PLOTTER #                                B2            "
680 REM REGRESSION COEF. FOR STRESS-STRAIN 1     R1            "
681 REM     "       "     " STRESS-STRAIN 2      R2
690 REM SLOPE FOR STRESS-STRAIN 1                C1            "
691 REM   "    " STRESS-STRAIN 2                 C2            "
692 REM Y-INTERCEPT FOR STRESS-STRAIN 1          E1            "
693 REM      "       " STRESS-STRAIN 2           E2            "
700 REM
710 REM    DIMENSION CHARACTER VARIABLES
720 REM
```

```
730 DIM S$(32),M$(12),N$(12),L$(12),D$(12)
740 DIM C$(32),A$(32)
750 REM
760 REM INPUT INITIAL VARIABLES
770 REM
780 PRINT "INPUT SAMPLE ID."
790 INPUT S$
800 PRINT "INPUT DIRECTION OF LOADING"
810 INPUT L$
820 PRINT "INPUT DIRECTION OF STRAIN 1"
830 INPUT M$
840 PRINT "INPUT DIRECTION OF STRAIN 2"
850 INPUT N$
860 PRINT "INPUT EXCITATION VOLTAGE FOR STRAIN GAGE 1       "
880 INPUT A2
890 PRINT "INPUT EXCITATION VOLTAGE FOR STRAIN GAGE 2       "
891 INPUT A3
900 PRINT "INPUT DATE"
910 INPUT D$
990 PRINT "INPUT CROSS SECTIONAL AREA OF SAMPLE (SQ. IN.)"
1000 INPUT A1
1300 REM
1310 REM DIMENSION VARIABLES  MAXIMUM 200 DATA PTS. TAKEN ABOUT EVERY
1320 REM ONE SECOND
1330 DIM F(200),V(200,2),L(200),S(200),D(200)
1350 REM
1360 REM SET UP INSTRON AND TAKE DATA
1370 REM
1380 PRINT "PRESS RETURN TO BEGIN TAKING DATA"
1390 PRINT "PRESS BREAK TO STOP TAKING DATA"
1391 PRINT "ENTER RUN 1510 TO RESUME PROGRAM"
1400 INPUT A$
1410 FOR I=1 TO 200
1420 INPUT @24:F(I)
1430 INPUT @12:V(I,1)
1440 INPUT @23:V(I,2)
1450 B1=I
1470 FOR J=1 TO 100
1480 B9=J
1490 NEXT J
1500 NEXT I
1510 REM CALCULATE STRESSES AND STRAINS
1520 REM
1540 FOR I=1 TO B1
1550 D(I)=(F(I)-F(1))/A1*1000*6895
1560 L(I)=-4*(V(I,1)-V(1,1))/(A2*2.075)
1570 S(I)=-4*(V(I,2)-V(1,2))/(A3*2.075)
1580 NEXT I
1890 REM
1900 REM CALCULATE MAX AND MIN STRESS, STRAINS
1910 W1=1
```

```
1920 W2=-1
1930 W3=1
1940 W4=-1
1950 W5=1
1960 W6=-1
1970 FOR I=1 TO B1
1980 IF L(I)>W3 THEN 2000
1990 W3=L(I)
2000 IF L(I)<W4 THEN 2020
2010 W4=L(I)
2020 IF D(I)>W1 THEN 2040
2030 W1=D(I)
2040 IF D(I)<W2 THEN 2060
2050 W2=D(I)
2060 IF S(I)>W5 THEN 2080
2070 W5=S(I)
2080 IF S(I)<W6 THEN 2100
2090 W6=S(I)
2100 NEXT I
2110 REM
2120 REM LINEAR REGRESSION
2130 REM
2140 GOSUB 7000
2150 REM PLOT STRESS AND STRAIN
2160 REM
2170 GOSUB 2190
2180 GO TO 3200
2190 B2=32
2200 FOR I=1 TO 2
2210 PAGE
2211 PRINT @B2:"DATE: ";D$;"   SAMPLE: ";S$;"   DIR. OF STRESS: ";L$
2212 PRINT @B2:"DIR. OF STRAIN 1: ";M$;"    DIR. OF STRAIN 2: ";N$
2220 VIEWPORT 20,120,30,90
2230 DIM P(8)
2240 P(1)=W1
2250 P(2)=W2
2260 P(3)=5
2270 IF I=1 THEN 2310
2280 P(5)=W5
2290 P(6)=W6
2300 GO TO 2330
2310 P(5)=W3
2320 P(6)=W4
2330 P(7)=5
2340 P5=3
2350 GOSUB 5000
2360 P5=7
2370 GOSUB 5000
2380 WINDOW P(1),P(2),P(5),P(6)
2390 AXIS @B2:P(3),P(7),0,0
2400 P5=4
2410 A$="HHH"
```

```
2420 GOSUB 6000
2430 P5=8
2440 A$=""
2450 GOSUB 6000
2460 IF I=2 THEN 2570
2470 MOVE @B2:D(1),L(1)
2480 FOR J=1 TO B1
2490 DRAW @B2:D(J),L(J)
2550 NEXT J
2560 GO TO 2660
2570 MOVE @B2:D(1),S(1)
2580 FOR J=1 TO B1
2590 DRAW @B2:D(J),S(J)
2650 NEXT J
2660 IF I=2 THEN 2700
2670 A8=W3
2680 A9=W4
2690 GO TO 2720
2700 A8=W5
2710 A9=W6
2720 MOVE @B2:W1,A9
2730 PRINT @B2:"HHHHHJJ";
2740 GO TO 2810
2750 FOR J=1 TO LEN(C$)
2760 A$=SEG(C$,J,1)
2770 PRINT @B2:A$;"HJ";
2780 NEXT J
2790 MOVE @B2:W1,A8
2800 PRINT @B2:"JJJ ";
2801 GO TO 2842
2810 IF I=2 THEN 2840
2820 C$="STRAIN 2"
2830 GO TO 2750
2840 C$="STRAIN 1"
2841 GO TO 2750
2842 C$="STRESS (Pa)"
2843 PRINT @B2:C$
2850 IF B2<>32 THEN 2880
2860 Z9=30
2870 GO TO 2890
2880 Z9=2
2890 HOME
2900 FOR Z8=1 TO Z9
2910 PRINT @B2:" "
2920 NEXT Z8
2930 PRINT @B2:"MIN. STRESS: ";W1;" Pa   MAX. STRESS: ";W2;" Pa"
2960 IF I=2 THEN 2990
2970 PRINT @B2:"MIN. STRAIN 1: ";W3;"    MAX. STRAIN 1: ";W4
2980 GO TO 3020
2990 PRINT @B2:"MIN. STRAIN 2: ";W5;"    MAX. STRAIN 2: ";W6
3020 IF I=2 THEN 3050
3030 PRINT @B2:"SLOPE IS: ";C1;" (Pa^-1)"
```

```
3040 GO TO 3080
3050 PRINT @B2:"SLOPE IS: ";C2;" (Pa^-1)"
3080 IF I=2 THEN 3110
3090 PRINT @B2:"Y-INTERCEPT: ";E1
3100 GO TO 3130
3110 PRINT @B2:"Y-INTERCEPT: ";E2
3130 IF I=2 THEN 3160
3140 PRINT @B2:"REGRESSION COEF.: ";R1
3150 GO TO 3170
3160 PRINT @B2:"REGRESSION COEF.: ";R2
3170 INPUT A$
3180 NEXT I
3190 RETURN
3200 HOME
3201 PAGE
3210 PRINT "HARD COPY OF PLOTS? YES=1 NO=2"
3220 INPUT A5
3230 IF A5<>1 THEN 3270
3240 PRINT "INPUT PLOTTER NUMBER"
3241 INPUT B2
3250 GOSUB 2200
3260 GO TO 3300
3270 IF A5=2 THEN 3300
3280 PRINT "BAD CHOICE, TRY AGAIN"
3290 GO TO 3210
3300 PRINT "STORE DATA? YES =1 NO=2"
3310 INPUT A5
3320 IF A5<>1 THEN 3350
3330 GOSUB 8000
3340 GO TO 3380
3350 IF A5=2 THEN 3380
3360 PRINT "BAD CHOICE, TRY AGAIN"
3370 GO TO 3300
3380 REM
3460 PRINT "ANOTHER RUN? YES=1 NO=2"
3470 INPUT A5
3480 IF A5<>1 THEN 3500
3490 GO TO 1370
3500 IF A5=2 THEN 3530
3510 PRINT "BAD CHOICE, TRY AGAIN"
3520 GO TO 3460
3530 END
5000 REM SUBROUTINE FOR PLOTTING
5001 REM P(P5)=MINIMUM # OF TICS
5010 P1=(P(P5-1)-P(P5-2))/P(P5)
5020 P2=10^INT(LGT(P1))
5030 P1=P1/P2
5040 IF P1>2 THEN 5080
5050 IF P1=1 THEN 5120
5060 P2=2*P2
5070 GO TO 5120
5080 IF P1>5 THEN 5110
```

```
5090 P2=5*P2
5100 GO TO 5120
5110 P2=10*P2
5120 REM ADJUST DATA MINIMUM
5130 P1=INT(P(P5-2)/P2)
5140 P3=P2*(P1+2)
5150 IF P3<P(P5-2) THEN 5180
5160 P3=P3-P2
5170 GO TO 5150
5180 P(P5-2)=P3
5190 REM ADJUST DATA MAXIMUM
5200 P1=INT(P(P5-1)/P2)
5210 P3=P2*(P1-2)
5220 IF P(P5-1)<P3 THEN 5250
5230 P3=P3+P2
5240 GO TO 5220
5250 P(P5-1)=P3
5260 REM P(P5)=ADJUSTED TIC INTERVAL
5270 P(P5)=P2
5280 RETURN
6000 REM LABLE AXIS
6010 P4=P(P5-1)
6020 P(4)=P(1)
6030 P(8)=P(5)
6040 P3=ABS(P(P5-3)+P4) MAX ABS(P(P5-2)-P4)
6050 P3=INT(LGT(P3)+1.0E-8)
6060 P2=10^-P3
6070 P1=P(P5-2)-P4/2
6080 P(P5)=P(P5)+P4
6090 IF P(P5)>P1 THEN 6140
6100 MOVE @B2:P(4),P(8)
6110 PRINT A$;
6120 PRINT @B2: USING "-D.2D,S":P(P5)*P2
6130 GO TO 6080
6140 IF P3=0 THEN 6180
6150 P(P5)=P1
6160 MOVE @B2:P(4),P(8)
6170 PRINT @B2: USING "2A,+FD,S":" E";P3
6180 RETURN
7000 REM
7010 REM SUBROUTINE TO DO LINEAR REGRESSION ON DATA
7020 REM
7030 X3=0
7040 X4=0
7050 X5=0
7060 X6=0
7070 X7=0
7080 X8=0
7090 W7=0
7100 W8=0
7110 FOR I=1 TO B1
```

```
7120 X3=X3+D(I)
7130 X4=X4+D(I)^2
7140 X5=X5+L(I)
7150 X6=X6+L(I)^2
7160 X7=X7+S(I)
7170 X8=X8+S(I)^2
7180 W7=W7+D(I)*L(I)
7190 W8=W8+D(I)*S(I)
7200 NEXT I
7210 C1=(B1*W7-X3*X5)/(B1*X4-X3^2)
7220 C2=(B1*W8-X3*X7)/(B1*X4-X3^2)
7230 E1=(X4*X5-X3*W7)/(B1*X4-X3^2)
7240 E2=(X4*X7-X3*W8)/(B1*X4-X3^2)
7250 R1=(B1*W7-X3*X5)/((B1*X4-X3^2)*(B1*X6-X5^2))^0.5
7260 R2=(B1*W8-X3*X7)/((B1*X4-X3^2)*(B1*X8-X7^2))^0.5
7270 RETURN
8000 REM
8010 REM SUBROUTINE TO STORE DATA
8020 PRINT "INPUT TITLE FOR STESS-STRAIN 1 FILE (MAX 64 LETTERS)"
8030 DIM B$(64),K$(64)
8040 INPUT B$
8050 PRINT "INPUT TITLE FOR STRESS-STRAIN 2 FILE (MAX 64 LETTERS)"
8060 INPUT K$
8070 A5=0
8071 A5=A5+LEN(B$)+LEN(K$)+10*(B1*2)+10
8080 TLIST
8090 PRINT ""
8100 PRINT "INPUT # OF (LAST) FILE TO STORE DATA FOR STESS STRAIN 1"
8110 INPUT M3
8120 FIND M3
8130 MARK 1,A5
8140 FIND M3
8150 WRITE B$
8160 WRITE B1
8170 FOR I=1 TO B1
8180 WRITE D(I),L(I)
8190 NEXT I
8200 CLOSE
8210 FIND M3+1
8220 MARK 1,A5
8230 FIND M3+1
8240 WRITE K$
8250 WRITE B1
8260 FOR I=1 TO B1
8270 WRITE D(I),S(I)
8280 NEXT I
8290 CLOSE
8300 PRINT "DATA FOR STRESS-STRAIN 1 STORED ON FILE ";M3
8310 PRINT "DATA FOR STRESS-STRAIN 2 STORED ON FILE ";M3+1
8320 RETURN
```

APPENDIX F

In this appendix, the derivations of the independent third order elastic moduli for the symmetries of transverse isotropy and orthotropy are considered. After considerations of the symmetry of the stress and strain tensors and the existence of a strain energy function, the number of independent third order moduli for the most general anisotropic solid is reduced to 56. The number of independent third order elastic coefficients can be reduced further if the effect of the elastic symmetry of the material is considered. As with the case of the linear elastic moduli, the effect of symmetry rotations on the strain energy function which is extended to include terms up to third order can be used to determine the independent moduli for the different symmetries. Since only third order terms are being considered, only the portion of the strain energy with third order terms (Φ_3) need be considered. It is given by

$$\Phi_3 = \frac{1}{6}\sum_{A} c_{AAA}\eta_A^3 + \frac{1}{2}\sum_{A\neq B} c_{AAB}\eta_A^2\eta_B + \sum_{A<B<D} c_{ABD}\eta_A\eta_B\eta_D. \qquad (F.1)$$

The process is exactly the same as was the case of reduction of the second order moduli. The strain energy function is written out. Then the effect of a specified rotation on the strain tensor components is determined and then substituted into the strain energy function. Then the rotated and original strain energy functions are equated term by term to determine the relationships between the moduli. However, it would be both too time consuming and space consuming to write out the necessary equations for each symmetry rotation. Thus, in this appendix only the effects on the moduli for each rotation will be given. These are determined by simple algebraic manipulations.

The orthotropic moduli are determined first by considering the effects of two fold rotations about each of the three axes. For a 180 degree rotation about the x_2 axis which has a transformation matrix given by

$$[a_{ij}] = \begin{bmatrix} -1 & 0 & 0 \\ 0 & 1 & 0 \\ 0 & 0 & -1 \end{bmatrix}, \qquad \text{(F.2)}$$

24 of the moduli drop out leaving 32 independent moduli. The moduli which drop out are c_{114}, c_{116}, c_{124}, c_{126}, c_{134}, c_{136}, c_{145}, c_{156}, c_{224}, c_{226}, c_{234}, c_{236}, c_{245}, c_{256}, c_{334}, c_{336}, c_{345}, c_{356}, c_{444}, c_{446}, c_{455}, c_{466}, c_{556}, and c_{666}. These can all be shown to equal zero.

The effect of a two fold rotation about the x_1 axis is to reduce the number of independent moduli to twenty. The moduli c_{555}, c_{115}, c_{225}, c_{335}, c_{445}, c_{146}, c_{125}, c_{135}, c_{235}, c_{346}, and c_{566} all become equal to zero. This leaves the remaining independent moduli as c_{111}, c_{112}, c_{113}, c_{122}, c_{123}, c_{133}, c_{144}, c_{155}, c_{166}, c_{222}, c_{223}, c_{233}, c_{244}, c_{255}, c_{266}, c_{333}, c_{344}, c_{355}, c_{366}, and c_{456}. As with the case of the second order moduli, the third symmetry rotation about the x_3 axis does not reduce the number of independent moduli further. Thus the 20 independent moduli for an orthotropic material are those listed above with all other $c_{ABD} = 0$.

Again, the transversely isotropic moduli can be determined by further reducing the orthotropic moduli by applying the additional symmetry condition that the material be isotropic in the x_1, x_2 plane. This means that the material can be rotated by any angle around the x_3 axis and be in an elastically equivalent position. This reduces the number of independent moduli to nine. They are c_{111}, c_{112}, c_{113}, c_{123}, c_{133}, c_{144}, c_{155}, c_{333}, and c_{344}. The following relations hold for the remaining nonzero moduli

$$c_{222} = c_{111}, \quad c_{355} = c_{344}$$

$$c_{223} = c_{113}, \quad c_{166} = c_{266} = \frac{1}{4}(c_{111} - c_{112})$$

$$c_{255} = c_{144}, \quad c_{223} = c_{133} \qquad \text{(F.3)}$$

$$c_{244} = c_{155}, \quad c_{366} = \frac{1}{2}(c_{113} - c_{123})$$

$$c_{122} = c_{112}, \quad c_{456} = \frac{1}{2}(c_{155} - c_{144}).$$

APPENDIX G

```
100 REM   PROGRAM TO MEASURE P2L2 FREQUENCY
110 REM CHANGES AS A FUNCTION OF APPLIED LOAD AND PLOT AND
120 REM STORE DATA.  WRITTEN BY PROSSER 2/25/86
130 REM
140 REM   VARIABLES                              NAME          TYPE
150 REM
160 REM SAMPLE ID.                               S$       CHARACTER(32)
170 REM MODE OF WAVE                             M$            "   (12)
180 REM DIRECTION OF PROPAGATION                 N$            "   (12)
190 REM  "  "      "  POLARIZATION               P$            "   (12)
200 REM   "      "  LOADING                      L$            "   (12)
220 REM DATE                                     D$       CHARACTER(12)
270 REM CROSS SECTIONAL AREA OF SAMPLE (SQ. IN.)A1            "
300 REM NUMBER OF DATA POINTS                    B1            "
330 REM FREQUENCY MEASUREMENTS   (Hz)            F(I)       ARRAY
340 REM VOLTAGE MEASUREMENTS FOR LOAD  (VOLTS)   V(I)         "
400 REM STRESS              (Pa)                 L(I)       ARRAY
460 REM DELTA F/F AT EACH POINT                  D(I)          "
520 REM MINIMUM DELTA F/F                        W1            "
530 REM MAXIMUM DELTA F/F                        W2            "
540 REM MINIMUM STRESS          (Pa)             W3            "
550 REM MAXIMUM STRESS           "               W4            "
571 REM SUM D(I)                                 X3            "
572 REM SUM (D(I))^2                             X4            "
573 REM SUM L(I)                                 X5            "
574 REM SUM (L(I))^2                             X6            "
577 REM SUM (D(I)*L(i)                           W7            "
590 REM DUMMY VARIABLE                           C$       CHARACTER(32)
600 REM    "     "                               A$            "
630 REM DUMMY VARIABLE                           A5            "
640 REM INTEGER COUNTERS                         I,J           "
650 REM DUMMY ARRAY FOR PLOTTING                 P(I)       ARRAY
660 REM  "    VARIABLES FOR PLOTTING             A8,A9      NUMERIC
670 REM PLOTTER #                                B2            "
680 REM REGRESSION COEF. FOR STRESS-DELTA F/F    R1            "
690 REM SLOPE FOR STRESS-DELTA F/F               C1            "
692 REM Y-INTERCEPT FOR STRESS-DELTA F/F         E1            "
700 REM
710 REM    DIMENSION CHARACTER VARIABLES
720 REM
730 DIM S$(32),M$(12),N$(12),P$(12),L$(12),D$(12)
740 DIM C$(32),A$(32)
750 REM
760 REM INPUT INITIAL VARIABLES
770 REM
780 PRINT "INPUT SAMPLE ID."
790 INPUT S$
800 PRINT "INPUT MODE OF WAVE"
810 INPUT M$
820 PRINT "INPUT DIRECTION OF POLARIZATION"
```

```
830 INPUT P$
840 PRINT "INPUT DIRECTION OF PROPAGATION"
850 INPUT N$
860 PRINT "INPUT DIRECTION OF LOADING"
870 INPUT L$
900 PRINT "INPUT DATE"
910 INPUT D$
990 PRINT "INPUT CROSS SECTIONAL AREA OF SAMPLE (SQ. IN.)"
1000 INPUT A1
1300 REM
1310 REM DIMENSION VARIABLES  MAXIMUM 200 DATA PTS. TAKEN ABOUT EVERY
1320 REM ONE SECOND
1330 DIM F(200),V(200),L(200),D(200)
1350 REM
1360 REM SET UP INSTRON AND TAKE DATA
1370 REM
1380 PRINT "PRESS RETURN TO START TAKING DATA"
1390 PRINT "PRESS BREAK TO QUIT TAKING DATA"
1391 PRINT "THEN ENTER RUN 1510"
1400 INPUT A$
1410 FOR I=1 TO 200
1420 INPUT @3:F(I)
1430 INPUT @24:V(I)
1450 B1=I
1470 FOR J=1 TO 85
1480 B9=J
1490 NEXT J
1500 NEXT I
1510 REM CALCULATE STRESSES            AND DELTA F/F
1520 REM
1540 FOR I=1 TO B1
1550 L(I)=(V(I)-V(1))/A1*6895*1000*-1
1570 D(I)=(F(I)-F(1))/F(1)
1580 NEXT I
1890 REM
1900 REM CALCULATE MAX AND MIN STRESS        AND DELTA F/F
1910 W1=1
1920 W2=-1
1930 W3=1
1940 W4=-1
1970 FOR I=1 TO B1
1980 IF L(I)>W3 THEN 2000
1990 W3=L(I)
2000 IF L(I)<W4 THEN 2020
2010 W4=L(I)
2020 IF D(I)>W1 THEN 2040
2030 W1=D(I)
2040 IF D(I)<W2 THEN 2100
2050 W2=D(I)
2100 NEXT I
2110 REM
2120 REM LINEAR REGRESSION
2130 REM
```

```
2140 GOSUB 7000
2150 REM PLOT STRESS           VS. DELTA F/F
2160 REM
2170 GOSUB 2190
2180 GO TO 3200
2190 B2=32
2210 PAGE
2211 PRINT @B2:"DATE: ";D$;"   SAMPLE: ";S$;"   WAVE MODE: ";M$
2212 PRINT @B2:"DIR. OF PROPAGATION: ";N$;"   DIR. OF STRESS: ";L$
2213 PRINT @B2:"DIR. OF POLARIZATION: ";P$
2220 VIEWPORT 20,120,30,90
2230 DIM P(8)
2240 P(5)=W1
2250 P(6)=W2
2260 P(3)=5
2310 P(1)=W3
2320 P(2)=W4
2330 P(7)=5
2340 P5=3
2350 GOSUB 5000
2360 P5=7
2370 GOSUB 5000
2380 WINDOW P(1),P(2),P(5),P(6)
2390 AXIS @B2:P(3),P(7),0,0
2400 P5=4
2410 A$="HHH"
2420 GOSUB 6000
2430 P5=8
2440 A$=""
2450 GOSUB 6000
2470 MOVE @B2:L(1),D(1)
2480 FOR J=1 TO B1
2490 DRAW @B2:L(J),D(J)
2550 NEXT J
2670 A8=W3
2680 A9=W4
2720 MOVE @B2:A8,W2
2730 PRINT @B2:"HHHHHJJ";
2740 C$="DELTA F/F"
2750 FOR J=1 TO LEN(C$)
2760 A$=SEG(C$,J,1)
2770 PRINT @B2:A$;"HJ";
2780 NEXT J
2790 MOVE @B2:A8,W1
2800 PRINT @B2:"JJJ ";
2820 C$="STRESS (Pa)"
2841 PRINT @B2:C$
2850 IF B2<>32 THEN 2880
2860 Z9=30
2870 GO TO 2890
2880 Z9=2
```

```
2890 HOME
2900 FOR Z8=1 TO Z9
2910 PRINT @B2:" "
2920 NEXT Z8
2930 PRINT @B2:"MIN. DELTA F/F: ";W1;"   MAX. DELTA F/F: ";W2
2970 PRINT @B2:"MIN. STRESS: ";W3;" (Pa)";"   MAX. STRESS: ";W4;" (Pa)"
3030 PRINT @B2:"SLOPE IS: ";C1;" (Pa^-1)"
3090 PRINT @B2:"Y-INTERCEPT: ";E1;" (Pa^-1)"
3140 PRINT @B2:"REGRESSION COEF.: ";R1
3170 INPUT A$
3190 RETURN
3200 HOME
3201 PAGE
3210 PRINT "HARD COPY OF PLOTS? YES=1 NO=2"
3220 INPUT A5
3230 IF A5<>1 THEN 3270
3240 PRINT "INPUT PLOTTER NUMBER"
3241 INPUT B2
3250 GOSUB 2210
3260 GO TO 3300
3270 IF A5=2 THEN 3300
3280 PRINT "BAD CHOICE, TRY AGAIN"
3290 GO TO 3210
3300 PRINT "STORE DATA? YES =1 NO=2"
3310 INPUT A5
3320 IF A5<>1 THEN 3350
3330 GOSUB 8000
3340 GO TO 3380
3350 IF A5=2 THEN 3380
3360 PRINT "BAD CHOICE, TRY AGAIN"
3370 GO TO 3300
3380 REM
3460 PRINT "ANOTHER RUN? YES=1 NO=2"
3470 INPUT A5
3480 IF A5<>1 THEN 3500
3490 GO TO 1370
3500 IF A5=2 THEN 3530
3510 PRINT "BAD CHOICE, TRY AGAIN"
3520 GO TO 3460
3530 END
5000 REM SUBROUTINE FOR PLOTTING
5001 REM P(P5)=MINIMUM # OF TICS
5010 P1=(P(P5-1)-P(P5-2))/P(P5)
5020 P2=10^INT(LGT(P1))
5030 P1=P1/P2
5040 IF P1>2 THEN 5080
5050 IF P1=1 THEN 5120
5060 P2=2*P2
5070 GO TO 5120
5080 IF P1>5 THEN 5110
5090 P2=5*P2
```

```
5100 GO TO 5120
5110 P2=10*P2
5120 REM ADJUST DATA MINIMUM
5130 P1=INT(P(P5-2)/P2)
5140 P3=P2*(P1+2)
5150 IF P3<P(P5-2) THEN 5180
5160 P3=P3-P2
5170 GO TO 5150
5180 P(P5-2)=P3
5190 REM ADJUST DATA MAXIMUM
5200 P1=INT(P(P5-1)/P2)
5210 P3=P2*(P1-2)
5220 IF P(P5-1)<P3 THEN 5250
5230 P3=P3+P2
5240 GO TO 5220
5250 P(P5-1)=P3
5260 REM P(P5)=ADJUSTED TIC INTERVAL
5270 P(P5)=P2
5280 RETURN
6000 REM LABLE AXIS
6010 P4=P(P5-1)
6020 P(4)=P(1)
6030 P(8)=P(5)
6040 P3=ABS(P(P5-3)+P4) MAX ABS(P(P5-2)-P4)
6050 P3=INT(LGT(P3)+1.0E-8)
6060 P2=10^-P3
6070 P1=P(P5-2)-P4/2
6080 P(P5)=P(P5)+P4
6090 IF P(P5)>P1 THEN 6140
6100 MOVE @B2:P(4),P(8)
6110 PRINT A$;
6120 PRINT @B2: USING "-D.2D,S":P(P5)*P2
6130 GO TO 6080
6140 IF P3=0 THEN 6180
6150 P(P5)=P1
6160 MOVE @B2:P(4),P(8)
6170 PRINT @B2: USING "2A,+FD,S":" E";P3
6180 RETURN
7000 REM
7010 REM SUBROUTINE TO DO LINEAR REGRESSION ON DATA
7020 REM
7030 X3=0
7040 X4=0
7050 X5=0
7060 X6=0
7090 W7=0
7110 FOR I=1 TO B1
7120 X3=X3+D(I)
7130 X4=X4+D(I)^2
7140 X5=X5+L(I)
7150 X6=X6+L(I)^2
```

```
7180 W7=W7+D(I)*L(I)
7200 NEXT I
7210 C1=(B1*W7-X3*X5)/(B1*X6-X5^2)
7230 E1=(X6*X3-X5*W7)/(B1*X6-X5^2)
7250 R1=(B1*W7-X3*X5)/((B1*X4-X3^2)*(B1*X6-X5^2))^0.5
7270 RETURN
8000 REM
```

APPENDIX H


```
100 REM NONLINEAR DATA ANALYSIS PROGRAM (TRANSVERSE ISOTROPY)
110 REM DETERMINE 7 OF 9 NONLINEAR COEF. BY LEAST SQUARES FIT
120 REM USING 24 SAC MEASUREMENTS
130 REM WRITTEN BY PROSSER 11-10-86
140 REM
150 REM VARIABLES
160 REM LINEAR ELASTIC STIFFNESSES                    K(I)
170 REM    "     "     COMPLIANCES                    S(I)
180 REM SAC MEASUREMENTS                              H(I,1)
190 REM UNCERTAINTIES IN SAC'S                        H(I,2)
200 REM NONLINEAR COEF'S                              C(I,1)
210 REM MAX. UNCERTAINTY IN NONLINEAR COEF'S          C(I,2)
220 REM PROB.   "       "    "       "                C(I,3)
230 REM RECALCULATED SAC'S                            H(I,3)
240 REM MAX. UNCERTAINTY IN RECALCULATED SAC'S        H(I,4)
250 REM PROB.    "       "     "       "              H(I,5)
260 REM COEFICIENTS OF EQ'S (24 EQ., 7 UNKNOWNS)      A(I,J)
270 REM A(I,J)*A(I,M)                                 E(I,J)
280 REM INVERSE OF E(I,J)                             F(I,J)
290 REM PRODUCT OF E AND F                            F1(I,J)
300 REM PRODUCT OF F AND E                            F2(I,J)
310 REM CONDITION NUMBER OF E                         Z3
320 REM H(I,1)+CONSTANT TERMS                         Y(I)
330 REM INTEGER COUNTERS                              I,J,L,M
340 REM PERCENT DIFFERENCE BETWEEN MEASURED AND CALC SAC'S  V(I)
350 REM   "     UNCERTAINTY IN CALCULATED SAC'S       T(I,2)
1000 REM INPUT DATA
1001 DIM K(3),S(4),H(24,5),A(24,7),C(7,3)
1010 PAGE
1020 PRINT "INPUT LINEAR ELASTIC STIFFNESS MODULI (GPa)"
1030 PRINT "11-1,12-2,44-3"
1040 FOR I=1 TO 3
1050 PRINT "INPUT C";I
1060 INPUT K(I)
1070 NEXT I
1080 PAGE
1090 PRINT "INPUT LINEAR ELASTIC COMPLIANCE MODULI (GPA)^-1"
1100 PRINT "11-1,12-2,13-3,33-4"
1110 FOR I=1 TO 4
1120 PRINT "INPUT S";I
1130 INPUT S(I)
1140 NEXT I
1150 PAGE
1160 PRINT "INPUT SAC'S AND UNCERTAINTIES (GPa)^-1"
1170 PRINT "122-1,211-2,322-3,311-4,121-5,212-6,312-7,321-8"
1180 FOR I=1 TO 8
1190 PRINT "INPUT SAC ";I
1200 INPUT H(I,1)
1210 PRINT "INPUT UNCERTAINTY"
1220 INPUT H(I,2)
1230 NEXT I
```

```
1240 PAGE
1250 PRINT "SAC'S CONT'D."
1260 PRINT "123-9,213-10,323-11,313-12,131-13,232-14,132-15,231-16"
1270 FOR I=9 TO 16
1280 PRINT "INPUT SAC ";I
1290 INPUT H(I,1)
1300 PRINT "INPUT UNCERTAINTY"
1310 INPUT H(I,2)
1320 NEXT I
1330 PAGE
1340 PRINT "SAC'S CON'T."
1350 PRINT "011-17,022-18,012-19,021-20,013-21,023-22,031-23,032-24"
1360 FOR I=17 TO 24
1370 PRINT "INPUT SAC ";I
1380 INPUT H(I,1)
1390 PRINT "INPUT UNCERTAINTY"
1400 INPUT H(I,2)
1410 NEXT I
1420 REM CALCULATE COEF'S OF EQ.S
1430 A=0
1440 A(1,1)=S(2)/(2*K(1))
1450 A(1,2)=S(1)/(2*K(1))
1460 A(1,3)=S(3)/(2*K(1))
1470 A(3,1)=A(1,3)
1480 A(3,2)=A(1,3)
1490 A(3,3)=S(4)/(2*K(1))
1500 A(5,1)=(S(1)+S(2))*0.25/(K(1)-K(2))
1510 A(5,2)=-A(5,1)
1520 A(5,3)=0.5*S(3)/(K(1)-K(2))
1530 A(5,4)=-A(5,3)
1531 A(7,1)=A(5,3)
1532 A(7,2)=A(5,4)
1540 A(7,3)=0.5*S(4)/(K(1)-K(2))
1550 A(7,4)=-A(7,3)
1560 A(9,5)=S(1)/(2*K(3))
1570 A(9,6)=S(2)/(2*K(3))
1580 A(9,7)=S(3)/(2*K(3))
1590 A(11,5)=A(9,7)
1600 A(11,6)=A(9,7)
1610 A(11,7)=S(4)/(2*K(3))
1620 A(13,5)=A(9,6)
1630 A(13,6)=A(9,5)
1640 A(13,7)=A(9,7)
1650 A(15,5)=A(9,5)
1660 A(15,6)=A(9,6)
1670 A(15,7)=A(9,7)
1680 B=S(1)+S(2)+S(3)
1690 D=2*S(3)+S(4)
1700 A(17,1)=B/(2*K(1))
1710 A(17,2)=A(17,1)
1720 A(17,3)=D/(2*K(1))
1730 A(19,1)=0.5*B/(K(1)-K(2))
1740 A(19,2)=-A(19,1)
```

```
1750 A(19,3)=D/(K(1)-K(2))*0.5
1760 A(19,4)=-A(19,3)
1770 A(21,5)=B/(2*K(3))
1780 A(21,6)=A(21,5)
1790 A(21,7)=D/(2*K(3))
1800 A(23,5)=A(21,5)
1810 A(23,6)=A(21,5)
1820 A(23,7)=A(21,7)
1830 FOR J=1 TO 12
1840 FOR I=1 TO 7
1850 A(2*J,I)=A(2*J-1,I)
1860 NEXT I
1870 NEXT J
1880 REM ADD CONSTANT TERMS TO SAC`S
1890 DIM Y(24)
1900 Y(1)=-(H(1,1)+S(2))
1910 Y(2)=-(H(2,1)+S(2))
1920 Y(3)=-(H(3,1)+S(3))
1930 Y(4)=-(H(4,1)+S(3))
1940 Y(5)=-(H(5,1)+S(1))
1950 Y(6)=-(H(6,1)+S(1))
1960 Y(7)=-(H(7,1)+S(3))
1970 Y(8)=-(H(8,1)+S(3))
1980 Y(9)=-(H(9,1)+S(3))
1990 Y(10)=-(H(10,1)+S(3))
2000 Y(11)=-(H(11,1)+S(4))
2010 Y(12)=-(H(12,1)+S(4))
2020 Y(13)=-(H(13,1)+S(1))
2030 Y(14)=-(H(14,1)+S(1))
2040 Y(15)=-(H(15,1)+S(2))
2050 Y(16)=-(H(16,1)+S(2))
2060 Y(17)=-(H(17,1)+B+1/(2*K(1)))
2070 Y(18)=-(H(18,1)+B+1/(2*K(1)))
2080 Y(19)=-(H(19,1)+B+1/(K(1)-K(2)))
2090 Y(20)=-(H(20,1)+B+1/(K(1)-K(2)))
2100 Y(21)=-(H(21,1)+D+1/(2*K(3)))
2110 Y(22)=-(H(22,1)+D+1/(2*K(3)))
2120 Y(23)=-(H(23,1)+B+1/(2*K(3)))
2130 Y(24)=-(H(24,1)+B+1/(2*K(3)))
2140 REM COMPUTE A(I,M)*A(I,J)
2150 DIM E(7,7)
2160 FOR M=1 TO 7
2170 FOR J=1 TO 7
2180 E(M,J)=0
2190 FOR I=1 TO 24
2200 E(M,J)=E(M,J)+A(I,M)*A(I,J)
2210 NEXT I
2220 NEXT J
2230 NEXT M
2240 REM COMPUTE INVERSE OF E(M,J)
2250 DIM F(7,7),F1(7,7),F2(7,7)
2260 F=INV(E)
2270 REM COMPUTE CONDITION NUMBER
```

```
2280 Z1=-1.0E+100
2290 Z2=-1.0E+100
2300 FOR I=1 TO 7
2310 FOR J=1 TO 7
2320 IF E(I,J)<Z1 THEN 2340
2330 Z1=E(I,J)
2340 IF F(I,J)<Z2 THEN 2360
2350 Z2=F(I,J)
2360 NEXT J
2370 NEXT I
2380 Z3=ABS(Z2*Z1)
2390 F1=E MPY F
2400 F2=F MPY E
2440 REM COMPUTE NONLINEAR COEF'S
2450 FOR I=1 TO 7
2460 C(I,1)=0
2470 C(I,2)=0
2480 C(I,3)=0
2490 FOR J=1 TO 24
2500 FOR L=1 TO 7
2510 C(I,1)=C(I,1)+F(L,I)*A(J,L)*Y(J)
2520 C(I,2)=C(I,2)+ABS(F(L,I)*A(J,L))*H(J,2)
2530 NEXT L
2540 NEXT J
2550 C(I,3)=C(I,2)/23^0.5
2560 NEXT I
2570 REM RECALCULATE SAC VALUES USING DERIVED VALUES
2580 H(1,3)=-(2*K(1)*S(2)+S(1)*C(2,1)+S(2)*C(1,1)+S(3)*C(3,1))
2590 H(1,3)=H(1,3)/(2*K(1))
2600 H(3,3)=-(2*K(1)*S(3)+S(3)*(C(1,1)+C(2,1))+S(4)*C(3,1))
2610 H(3,3)=H(3,3)/(2*K(1))
2620 H(5,3)=(K(1)-K(2))*S(1)+0.25*(S(1)+S(2))*(C(1,1)-C(2,1))
2630 H(5,3)=H(5,3)+0.5*S(3)*(C(3,1)-C(4,1))
2640 H(5,3)=-H(5,3)/(K(1)-K(2))
2650 H(7,3)=(K(1)-K(2))*S(3)+0.5*S(3)*(C(1,1)-C(2,1))
2660 H(7,3)=H(7,3)+0.5*S(4)*(C(3,1)-C(4,1))
2670 H(7,3)=-H(7,3)/(K(1)-K(2))
2680 H(9,3)=-(2*K(3)*S(3)+S(1)*C(5,1)+S(2)*C(6,1)+S(3)*C(7,1))/(2*K(3))
2690 H(11,3)=-(2*K(3)*S(4)+S(3)*(C(5,1)+C(6,1))+S(3)*C(7,1))/(2*K(3))
2700 H(13,3)=-(2*K(3)*S(1)+S(1)*C(6,1)+S(2)*C(5,1)+S(3)*C(7,1))/(2*K(3))
2710 H(15,3)=-(2*K(3)*S(2)+S(1)*C(5,1)+S(2)*C(6,1)+S(3)*C(7,1))/(2*K(3))
2720 H(17,3)=-(1+2*K(1)*B+B*(C(1,1)+C(2,1))+D*C(3,1))/(2*K(1))
2730 H(19,3)=1+(K(1)-K(2))*B
2740 H(19,3)=H(19,3)+0.5*(B*(C(1,1)-C(2,1))+D*(C(3,1)-C(4,1)))
2750 H(19,3)=-H(19,3)/(K(1)-K(2))
2760 H(21,3)=-(1+2*K(3)*D+B*(C(5,1)+C(6,1))+D*C(7,1))/(2*K(3))
2770 H(23,3)=-(1+2*K(3)*B+B*(C(5,1)+C(6,1))+D*C(7,1))/(2*K(3))
2780 FOR I=1 TO 12
2790 H(2*I,3)=H(2*I-1,3)
2800 NEXT I
2810 DIM W(7,2)
2820 FOR I=1 TO 2
2830 FOR J=1 TO 7
```

```
2840 W(J,I)=ABS(C(J,I+1)/C(J,1))
2850 NEXT J
2860 NEXT I
2870 FOR I=1 TO 2
2880 FOR J=1 TO 4
2890 H(J,I+3)=(W(1,I)+W(2,I)+W(3,I))*H(J,3)
2900 NEXT J
2910 FOR J=5 TO 8
2920 H(J,I+3)=(W(1,I)+W(2,I)+W(3,I)+W(4,I))*H(J,3)
2930 NEXT J
2940 FOR J=9 TO 16
2950 H(J,I+3)=(W(5,I)+W(6,I)+W(7,I))*H(J,3)
2960 NEXT J
2970 FOR J=17 TO 18
2980 H(J,I+3)=(W(1,I)+W(2,I)+W(3,I))*H(J,3)
2990 NEXT J
3000 FOR J=19 TO 20
3010 H(J,I+3)=(W(1,I)+W(2,I)+W(3,I)+W(4,I))*H(J,3)
3020 NEXT J
3030 FOR J=21 TO 24
3040 H(J,I+3)=(W(5,I)+W(6,I)+W(7,I))*H(J,3)
3050 NEXT J
3060 NEXT I
3070 FOR I=4 TO 5
3080 FOR J=1 TO 24
3090 H(J,I)=ABS(H(J,I))
3100 NEXT J
3110 NEXT I
3120 DIM V(24)
3130 FOR I=1 TO 24
3140 V(I)=ABS((H(I,1)-H(I,3))/H(I,1))
3150 V(I)=V(I)*100
3160 NEXT I
3170 DIM T(24,2)
3180 FOR I=1 TO 2
3190 FOR J=1 TO 24
3200 T(J,I)=H(J,I+3)/H(J,3)*100
3201 T(J,I)=ABS(T(J,I))
3210 NEXT J
3220 NEXT I
3230 REM PRINT OUT DATA
3240 REM
3250 N=32
3260 PAGE
3270 GOSUB 3380
3280 PRINT "PRINTED COPY? YES =1 NO =2 "
3290 INPUT Z5
3300 IF Z5=1 THEN 3340
3310 IF Z5=2 THEN 4010
3320 PRINT "BAD CHOICE"
3330 GO TO 3280
3340 PRINT "INPUT PRINTER #"
3350 INPUT N
```

```
3360 GOSUB 3380
3370 GO TO 4010
3380 PRINT @N:"NONLINEAR DATA ANALYSIS FOR TRANSVERSE ISOTROPY MODEL"
3390 PRINT @N:" "
3400 PRINT @N:"                INPUT DATA"
3410 PRINT @N:"  "
3420 PRINT @N:"LINEAR ELASTIC MODULI"
3430 PRINT @N:"  "
3440 PRINT @N:"C11 = ";K(1);" (GPa)    S11 = ";S(1);" (GPa)^-1"
3450 PRINT @N:"C12 = ";K(2);" (GPa)    S12 = ";S(2);" (GPa)^-1"
3460 PRINT @N:"C44 = ";K(3);" (GPa)    S13 = ";S(3);" (GPa)^-1"
3470 PRINT @N:"                    S33 = ";S(4);" (GPa)^-1"
3480 PRINT @N:" "
3490 PRINT @N:"VELOCITY DERIVATIVE DATA (GPa)^-1"
3500 PRINT @N:"  "
3510 PRINT @N:"1.  H122 = ";H(1,1);" +/- ";H(1,2)
3520 PRINT @N:"2.  H211 = ";H(2,1);" +/- ";H(2,2)
3530 PRINT @N:"3.  H322 = ";H(3,1);" +/- ";H(3,2)
3540 PRINT @N:"4.  H311 = ";H(4,1);" +/- ";H(4,2)
3550 PRINT @N:"5.  H121 = ";H(5,1);" +/- ";H(5,2)
3560 PRINT @N:"6.  H212 = ";H(6,1);" +/- ";H(6,2)
3570 PRINT @N:"7.  H312 = ";H(7,1);" +/- ";H(7,2)
3580 PRINT @N:"8.  H321 = ";H(8,1);" +/- ";H(8,2)
3590 PRINT @N:"9.  H123 = ";H(9,1);" +/- ";H(9,2)
3600 PRINT @N:"10. H213 = ";H(10,1);" +/- ";H(10,2)
3610 PRINT @N:"11. H323 = ";H(11,1);" +/- ";H(11,2)
3620 PRINT @N:"12. H313 = ";H(12,1);" +/- ";H(12,2)
3630 PRINT @N:"13. H131 = ";H(13,1);" +/- ";H(13,2)
3640 PRINT @N:"14. H232 = ";H(14,1);" +/- ";H(14,2)
3650 PRINT @N:"15. H132 = ";H(15,1);" +/- ";H(15,2)
3660 PRINT @N:"16. H231 = ";H(16,1);" +/- ";H(16,2)
3670 PRINT @N:"17. H011 = ";H(17,1);" +/- ";H(17,2)
3680 PRINT @N:"18. H022 = ";H(18,1);" +/- ";H(18,2)
3690 PRINT @N:"19. H012 = ";H(19,1);" +/- ";H(19,2)
3700 PRINT @N:"20. H021 = ";H(20,1);" +/- ";H(20,2)
3710 PRINT @N:"21. H013 = ";H(21,1);" +/- ";H(21,2)
3720 PRINT @N:"22. H023 = ";H(22,1);" +/- ";H(22,2)
3730 PRINT @N:"23. H031 = ";H(23,1);" +/- ";H(23,2)
3740 PRINT @N:"24. H032 = ";H(24,1);" +/- ";H(24,2)
3750 PRINT @N:" "
3760 PRINT @N:"THIRD ORDER ELASTIC CONSTANTS DERIVED FROM LEAST"
3770 PRINT @N:"SQUARES FIT AND MAX. ERROR AND PROB. ERROR (GPa)"
3780 PRINT @N:"  "
3790 PRINT @N:"C111 = ";C(1,1);" +/- ";C(1,2);" +/- ";C(1,3)
3800 PRINT @N:"C112 = ";C(2,1);" +/- ";C(2,2);" +/- ";C(2,3)
3810 PRINT @N:"C113 = ";C(3,1);" +/- ";C(3,2);" +/- ";C(3,3)
3820 PRINT @N:"C123 = ";C(4,1);" +/- ";C(4,2);" +/- ";C(4,3)
3830 PRINT @N:"C144 = ";C(5,1);" +/- ";C(5,2);" +/- ";C(5,3)
3840 PRINT @N:"C155 = ";C(6,1);" +/- ";C(6,2);" +/- ";C(6,3)
3850 PRINT @N:"C344 = ";C(7,1);" +/- ";C(7,2);" +/- ";C(7,3)
3860 PRINT @N:"C133,C333 UNDETERMINED DUE TO LACK OF DATA"
3870 PRINT @N:" "
3880 PRINT @N:"RECALCULATED VELOCITY DERIVATIVES USING FITTED TOEC'S"
```

```
3890 PRINT @N:"AND MAX. AND PROB. ERRORS IN SAME ORDER AS BEFORE"
3900 PRINT @N:"  "
3910 FOR I=1 TO 24
3920 PRINT @N:I;". ";H(I,3);" +/- ";H(I,4);" +/- ";H(I,5)
3930 NEXT I
3940 PRINT @N:"  "
3950 PRINT @N:"PERCENT DIFFERENCES, MAX. AND PROB. UNCERTAINTIES"
3960 PRINT @N:" "
3970 FOR I=1 TO 24
3980 PRINT @N:I;". ";V(I);T(I,1);T(I,2)
3990 NEXT I
3991 PRINT @N:"  "
3992 PRINT @N:"CONDITION # FOR INVERTING MATRIX IS: ";Z3
4000 RETURN
4010 END
```


ORIGINAL PAGE IS
OF POOR QUALITY

```
100 REM NONLINEAR DATA ANALYSIS PROGRAM (ORTHOTROPIC MODEL)
110 REM DETERMINE 15 OF 20 NONLINEAR COEF. BY LEAST SQUARES FIT
120 REM USING 24 SAC MEASUREMENTS
130 REM WRITTEN BY PROSSER 11-13-86
140 REM
150 REM VARIABLES
160 REM LINEAR ELASTIC STIFFNESSES                    K(I)
170 REM    "     "     COMPLIANCES                    S(I)
180 REM SAC MEASUREMENTS                              H(I,1)
190 REM UNCERTAINTIES IN SAC'S                        H(I,2)
200 REM NONLINEAR COEF'S                              C(I,1)
210 REM MAX. UNCERTAINTY IN NONLINEAR COEF'S          C(I,2)
220 REM PROB.   "         "    "      "              C(I,3)
230 REM RECALCULATED SAC'S                            H(I,3)
240 REM MAX. UNCERTAINTY IN RECALCULATED SAC'S        H(I,4)
250 REM PROB.    "        "    "        "            H(I,5)
260 REM COEFICIENTS OF EQ'S (24 EQ.,15 UNKNOWNS)      A(I,J)
270 REM A(I,J)*A(I,M)                                 E(I,J)
280 REM INVERSE OF E(I,J)                             F(I,J)
290 REM PRODUCT OF E AND F                            F1(I,J)
300 REM PRODUCT OF F AND E                            F2(I,J)
310 REM CONDITION NUMBER OF E                         Z3
320 REM H(I,1)+CONSTANT TERMS                         Y(I)
330 REM INTEGER COUNTERS                              I,J,L,M
340 REM PERCENT DIFFERENCE BETWEEN MEASURED AND CALC SAC'S  V(I)
350 REM   "     UNCERTAINTY IN CALCULATED SAC'S       T(I,2)
1000 REM INPUT DATA
1001 DIM K(6),S(6),H(24,5),A(24,15),C(15,3)
1010 PAGE
1020 PRINT "INPUT LINEAR ELASTIC STIFFNESS MODULI (GPa)"
1030 PRINT "11-1,22-2,33-3,44-4,55-5,66-6"
1040 FOR I=1 TO 6
1050 PRINT "INPUT C";I
1060 INPUT K(I)
1070 NEXT I
1080 PAGE
1090 PRINT "INPUT LINEAR ELASTIC COMPLIANCE MODULI (GPA)^-1"
1100 PRINT "11-1,22-2,33-3,23-4,13-5,12-6"
1110 FOR I=1 TO 6
1120 PRINT "INPUT S";I
1130 INPUT S(I)
1140 NEXT I
1150 PAGE
1160 PRINT "INPUT SAC'S AND UNCERTAINTIES (GPa)^-1"
1170 PRINT "122-1,211-2,322-3,311-4,121-5,212-6,312-7,321-8"
1180 FOR I=1 TO 8
1190 PRINT "INPUT SAC ";I
1200 INPUT H(I,1)
1210 PRINT "INPUT UNCERTAINTY"
1220 INPUT H(I,2)
1230 NEXT I
```

```
1240 PAGE
1250 PRINT "SAC'S CONT'D."
1260 PRINT "123-9,213-10,323-11,313-12,131-13,232-14,132-15,231-16"
1270 FOR I=9 TO 16
1280 PRINT "INPUT SAC ";I
1290 INPUT H(I,1)
1300 PRINT "INPUT UNCERTAINTY"
1310 INPUT H(I,2)
1320 NEXT I
1330 PAGE
1340 PRINT "SAC'S CON'T."
1350 PRINT "011-17,022-18,012-19,021-20,013-21,023-22,031-23,032-24"
1360 FOR I=17 TO 24
1370 PRINT "INPUT SAC ";I
1380 INPUT H(I,1)
1390 PRINT "INPUT UNCERTAINTY"
1400 INPUT H(I,2)
1410 NEXT I
1420 REM CALCULATE COEF'S OF EQ.S
1430 A=0
1440 A(1,4)=S(1)/(2*K(2))
1441 A(1,5)=S(6)/(2*K(2))
1442 A(1,6)=S(5)/(2*K(2))
1443 A(2,1)=S(6)/(2*K(1))
1444 A(2,2)=S(2)/(2*K(1))
1445 A(2,3)=S(4)/(2*K(1))
1446 A(3,4)=S(5)/(2*K(2))
1447 A(3,5)=S(4)/(2*K(2))
1448 A(3,6)=S(3)/(2*K(2))
1449 A(4,1)=S(5)/(2*K(1))
1450 A(4,2)=S(4)/(2*K(1))
1451 A(4,3)=S(3)/(2*K(1))
1452 A(5,13)=S(1)/(2*K(6))
1453 A(5,14)=S(6)/(2*K(6))
1454 A(5,15)=S(5)/(2*K(6))
1455 A(6,13)=S(6)/(2*K(6))
1456 A(6,14)=S(2)/(2*K(6))
1457 A(6,15)=S(4)/(2*K(6))
1458 A(7,13)=S(5)/(2*K(6))
1459 A(7,14)=S(4)/(2*K(6))
1460 A(7,15)=S(3)/(2*K(6))
1461 A(8,13)=A(7,13)
1462 A(8,14)=A(7,14)
1463 A(8,15)=A(7,15)
1464 A(9,7)=S(1)/(2*K(4))
1465 A(9,8)=S(6)/(2*K(4))
1466 A(9,9)=S(5)/(2*K(4))
1467 A(10,10)=S(6)/(2*K(5))
1468 A(10,11)=S(2)/(2*K(5))
1469 A(10,12)=S(4)/(2*K(5))
1470 A(11,7)=S(5)/(2*K(4))
1471 A(11,8)=S(4)/(2*K(4))
1472 A(11,9)=S(3)/(2*K(4))
```

```
1473 A(12,10)=S(5)/(2*K(5))
1474 A(12,11)=S(4)/(2*K(5))
1475 A(12,12)=S(3)/(2*K(5))
1476 A(13,10)=S(1)/(2*K(5))
1477 A(13,11)=S(6)/(2*K(5))
1478 A(13,12)=S(5)/(2*K(5))
1479 A(14,7)=S(6)/(2*K(4))
1480 A(14,8)=S(2)/(2*K(4))
1481 A(14,9)=S(4)/(2*K(4))
1490 A(15,7)=A(9,7)
1500 A(15,8)=A(9,8)
1510 A(15,9)=A(9,9)
1520 A(16,10)=A(10,10)
1530 A(16,11)=A(10,11)
1540 A(16,12)=A(10,12)
1550 B1=S(1)+S(6)+S(5)
1560 B2=S(6)+S(2)+S(4)
1570 B3=S(5)+S(4)+S(3)
1580 A(17,1)=B1/(2*K(1))
1590 A(17,2)=B2/(2*K(1))
1600 A(17,3)=B3/(2*K(1))
1610 A(18,4)=B1/(2*K(2))
1620 A(18,5)=B2/(2*K(2))
1630 A(18,6)=B3/(2*K(2))
1640 A(19,13)=B1/(2*K(6))
1650 A(19,14)=B2/(2*K(6))
1660 A(19,15)=B3/(2*K(6))
1670 A(20,13)=A(19,13)
1680 A(20,14)=A(19,14)
1690 A(20,15)=A(19,15)
1700 A(21,10)=B1/(2*K(5))
1710 A(21,11)=B2/(2*K(5))
1720 A(21,12)=B3/(2*K(5))
1730 A(22,7)=B1/(2*K(4))
1740 A(22,8)=B2/(2*K(4))
1750 A(22,9)=B3/(2*K(4))
1760 A(23,10)=A(21,10)
1770 A(23,11)=A(21,11)
1780 A(23,12)=A(21,12)
1790 A(24,7)=A(22,7)
1800 A(24,8)=A(22,8)
1810 A(24,9)=A(22,9)
1880 REM ADD CONSTANT TERMS TO SAC'S
1890 DIM Y(24)
1900 Y(1)=-(H(1,1)+S(6))
1910 Y(2)=-(H(2,1)+S(6))
1920 Y(3)=-(H(3,1)+S(4))
1930 Y(4)=-(H(4,1)+S(5))
1940 Y(5)=-(H(5,1)+S(1))
1950 Y(6)=-(H(6,1)+S(2))
1960 Y(7)=-(H(7,1)+S(4))
1970 Y(8)=-(H(8,1)+S(5))
```

```
1980 Y(9)=-(H(9,1)+S(5))
1990 Y(10)=-(H(10,1)+S(4))
2000 Y(11)=-(H(11,1)+S(3))
2010 Y(12)=-(H(12,1)+S(3))
2020 Y(13)=-(H(13,1)+S(1))
2030 Y(14)=-(H(14,1)+S(2))
2040 Y(15)=-(H(15,1)+S(6))
2050 Y(16)=-(H(16,1)+S(6))
2060 Y(17)=-(H(17,1)+B1+1/(2*K(1)))
2070 Y(18)=-(H(18,1)+B2+1/(2*K(2)))
2080 Y(19)=-(H(19,1)+B2+1/(2*K(6)))
2090 Y(20)=-(H(20,1)+B1+1/(2*K(6)))
2100 Y(21)=-(H(21,1)+B3+1/(2*K(5)))
2110 Y(22)=-(H(22,1)+B3+1/(2*K(4)))
2120 Y(23)=-(H(23,1)+B1+1/(2*K(5)))
2130 Y(24)=-(H(24,1)+B2+1/(2*K(4)))
2140 REM COMPUTE A(I,M)*A(I,J)
2150 DIM E(15,15)
2160 FOR M=1 TO 15
2170 FOR J=1 TO 15
2180 E(M,J)=0
2190 FOR I=1 TO 24
2200 E(M,J)=E(M,J)+A(I,M)*A(I,J)
2210 NEXT I
2220 NEXT J
2230 NEXT M
2240 REM COMPUTE INVERSE OF E(M,J)
2250 DIM F(15,15)
2260 F=INV(E)
2270 REM COMPUTE CONDITION NUMBER
2280 Z1=-1.0E+100
2290 Z2=-1.0E+100
2300 FOR I=1 TO 15
2310 FOR J=1 TO 15
2320 IF E(I,J)<Z1 THEN 2340
2330 Z1=E(I,J)
2340 IF F(I,J)<Z2 THEN 2360
2350 Z2=F(I,J)
2360 NEXT J
2370 NEXT I
2380 Z3=ABS(Z2*Z1)
2440 REM COMPUTE NONLINEAR COEF'S
2450 FOR I=1 TO 15
2460 C(I,1)=0
2470 C(I,2)=0
2480 C(I,3)=0
2490 FOR J=1 TO 24
2500 FOR L=1 TO 15
2510 C(I,1)=C(I,1)+F(L,I)*A(J,L)*Y(J)
2520 C(I,2)=C(I,2)+ABS(F(L,I)*A(J,L))*H(J,2)
2530 NEXT L
2540 NEXT J
2550 C(I,3)=C(I,2)/23^0.5
```

```
2560 NEXT I
2570 REM RECALCULATE SAC VALUES USING DERIVED VALUES
2580 H(1,3)=-(2*K(2)*S(6)+S(1)*C(4,1)+S(6)*C(5,1)+S(5)*C(6,1))
2581 H(1,3)=H(1,3)/(2*K(2))
2582 H(2,3)=-(2*K(1)*S(6)+S(6)*C(1,1)+S(2)*C(2,1)+S(4)*C(3,1))
2583 H(2,3)=H(2,3)/(2*K(1))
2584 H(3,3)=-(2*K(2)*S(4)+S(5)*C(4,1)+S(4)*C(5,1)+S(3)*C(6,1))
2585 H(3,3)=H(3,3)/(2*K(2))
2586 H(4,3)=-(2*K(1)*S(5)+S(5)*C(1,1)+S(4)*C(2,1)+S(3)*C(3,1))
2587 H(4,3)=H(4,3)/(2*K(1))
2588 H(5,3)=-(2*K(6)*S(1)+S(1)*C(13,1)+S(6)*C(14,1)+S(5)*C(15,1))
2589 H(5,3)=H(5,3)/(2*K(6))
2590 H(6,3)=-(2*K(6)*S(2)+S(6)*C(13,1)+S(2)*C(14,1)+S(4)*C(15,1))
2591 H(6,3)=H(6,3)/(2*K(6))
2592 H(7,3)=-(2*K(6)*S(4)+S(5)*C(13,1)+S(4)*C(14,1)+S(3)*C(15,1))
2593 H(7,3)=H(7,3)/(2*K(6))
2594 H(8,3)=-(2*K(6)*S(5)+S(5)*C(13,1)+S(4)*C(14,1)+S(3)*C(15,1))
2595 H(8,3)=H(8,3)/(2*K(6))
2596 H(9,3)=-(2*K(4)*S(5)+S(1)*C(7,1)+S(6)*C(8,1)+S(5)*C(9,1))
2597 H(9,3)=H(9,3)/(2*K(4))
2598 H(10,3)=-(2*K(5)*S(4)+S(6)*C(10,1)+S(2)*C(11,1)+S(4)*C(12,1))
2599 H(10,3)=H(10,3)/(2*K(5))
2600 H(11,3)=-(2*K(4)*S(3)+S(5)*C(7,1)+S(4)*C(8,1)+S(3)*C(9,1))
2601 H(11,3)=H(11,3)/(2*K(4))
2602 H(12,3)=-(2*K(5)*S(3)+S(5)*C(10,1)+S(4)*C(11,1)+S(3)*C(12,1))
2603 H(12,3)=H(12,3)/(2*K(5))
2604 H(13,3)=-(2*K(5)*S(1)+S(1)*C(10,1)+S(6)*C(11,1)+S(5)*C(12,1))
2605 H(13,3)=H(13,3)/(2*K(5))
2606 H(14,3)=-(2*K(4)*S(2)+S(6)*C(7,1)+S(2)*C(8,1)+S(4)*C(9,1))
2607 H(14,3)=H(14,3)/(2*K(4))
2608 H(15,3)=-(2*K(4)*S(6)+S(1)*C(7,1)+S(6)*C(8,1)+S(5)*C(9,1))
2609 H(15,3)=H(15,3)/(2*K(4))
2610 H(16,3)=-(2*K(5)*S(6)+S(6)*C(10,1)+S(2)*C(11,1)+S(4)*C(12,1))
2611 H(16,3)=H(16,3)/(2*K(5))
2620 H(17,3)=-(1+2*B1*K(1)+B1*C(1,1)+B2*C(2,1)+B3*C(3,1))
2630 H(17,3)=H(17,3)/(2*K(1))
2640 H(18,3)=-(1+2*K(2)*B2+B1*C(4,1)+B2*C(5,1)+B3*C(6,1))
2650 H(18,3)=H(18,3)/(2*K(2))
2660 H(19,3)=-(1+2*K(6)*B2+B1*C(13,1)+B2*C(14,1)+B3*C(15,1))
2670 H(19,3)=H(19,3)/(2*K(6))
2680 H(20,3)=-(1+2*K(6)*B1+B1*C(13,1)+B2*C(14,1)+B3*C(15,1))
2690 H(20,3)=H(20,3)/(2*K(6))
2700 H(21,3)=-(1+2*K(5)*B3+B1*C(10,1)+B2*C(11,1)+B3*C(12,1))
2710 H(21,3)=H(21,3)/(2*K(5))
2720 H(22,3)=-(1+2*K(4)*B3+B1*C(7,1)+B2*C(8,1)+B3*C(9,1))
2730 H(22,3)=H(22,3)/(2*K(4))
2740 H(23,3)=-(1+2*K(5)*B1+B1*C(10,1)+B2*C(11,1)+B3*C(12,1))
2750 H(23,3)=H(23,3)/(2*K(5))
2760 H(24,3)=-(1+2*K(4)*B2+B1*C(7,1)+B2*C(8,1)+B3*C(9,1))
2770 H(24,3)=H(24,3)/(2*K(4))
2810 DIM W(15,2)
2820 FOR I=1 TO 2
```

```
2830 FOR J=1 TO 15
2840 W(J,I)=ABS(C(J,I+1)/C(J,1))
2850 NEXT J
2860 NEXT I
2870 FOR I=1 TO 2
2880 H(1,I+3)=(W(4,I)+W(5,I)+W(6,I))*H(1,3)
2881 H(2,I+3)=(W(1,I)+W(2,I)+W(3,I))*H(2,3)
2882 H(3,I+3)=(W(4,I)+W(5,I)+W(6,I))*H(3,3)
2883 H(4,I+3)=(W(1,I)+W(2,I)+W(3,I))*H(4,3)
2884 H(5,I+3)=(W(13,I)+W(14,I)+W(15,I))*H(5,3)
2885 H(6,I+3)=(W(13,I)+W(14,I)+W(15,I))*H(6,3)
2886 H(7,I+3)=(W(13,I)+W(14,I)+W(15,I))*H(7,3)
2887 H(8,I+3)=(W(13,I)+W(14,I)+W(15,I))*H(8,3)
2888 H(9,I+3)=(W(7,I)+W(8,I)+W(9,I))*H(9,3)
2889 H(10,I+3)=(W(10,I)+W(11,I)+W(12,I))*H(10,3)
2890 H(11,I+3)=(W(7,I)+W(8,I)+W(9,I))*H(11,3)
2891 H(12,I+3)=(W(10,I)+W(11,I)+W(12,I))*H(12,3)
2892 H(13,I+3)=(W(10,I)+W(11,I)+W(12,I))*H(13,3)
2893 H(14,I+3)=(W(7,I)+W(8,I)+W(9,I))*H(14,3)
2894 H(15,I+3)=(W(7,I)+W(8,I)+W(9,I))*H(15,3)
2895 H(16,I+3)=(W(10,I)+W(11,I)+W(12,I))*H(16,3)
2896 H(17,I+3)=(W(1,I)+W(2,I)+W(3,I))*H(17,3)
2897 H(18,I+3)=(W(4,I)+W(5,I)+W(6,I))*H(18,3)
2898 H(19,I+3)=(W(13,I)+W(14,I)+W(15,I))*H(19,3)
2899 H(20,I+3)=(W(13,I)+W(14,I)+W(15,I))*H(20,3)
2900 H(21,I+3)=(W(10,I)+W(11,I)+W(12,I))*H(21,3)
2901 H(22,I+3)=(W(7,I)+W(8,I)+W(9,I))*H(22,3)
2902 H(23,I+3)=(W(10,I)+W(11,I)+W(12,I))*H(23,3)
2903 H(24,I+3)=(W(7,I)+W(8,I)+W(9,I))*H(24,3)
3060 NEXT I
3070 FOR I=4 TO 5
3080 FOR J=1 TO 24
3090 H(J,I)=ABS(H(J,I))
3100 NEXT J
3110 NEXT I
3120 DIM V(24)
3130 FOR I=1 TO 24
3140 V(I)=ABS((H(I,1)-H(I,3))/H(I,1))
3150 V(I)=V(I)*100
3160 NEXT I
3170 DIM T(24,2)
3180 FOR I=1 TO 2
3190 FOR J=1 TO 24
3200 T(J,I)=H(J,I+3)/H(J,3)+100
3201 T(J,I)=ABS(T(J,I))
3210 NEXT J
3220 NEXT I
3230 REM PRINT OUT DATA
3240 REM
3250 N=32
3260 PAGE
3270 GOSUB 3390
3280 PRINT "PRINTED COPY? YES =1 NO =2 "
```

```
3290 INPUT Z5
3300 IF Z5=1 THEN 3340
3310 IF Z5=2 THEN 4010
3320 PRINT "BAD CHOICE"
3330 GO TO 3280
3340 PRINT "INPUT PRINTER #"
3350 INPUT N
3360 GOSUB 3380
3370 GO TO 4010
3380 PRINT @N:"NONLINEAR DATA ANALYSIS FOR ORTHOTROPIC MODEL  "
3390 PRINT @N:" "
3400 PRINT @N:"                INPUT DATA"
3410 PRINT @N:"  "
3420 PRINT @N:"LINEAR ELASTIC MODULI"
3430 PRINT @N:"  "
3440 PRINT @N:"C11 = ";K(1);" (GPa)    S11 = ";S(1);" (GPa)^-1"
3450 PRINT @N:"C22 = ";K(2);" (GPa)    S22 = ";S(2);" (GPa)^-1"
3460 PRINT @N:"C33 = ";K(3);" (GPa)    S33 = ";S(3);" (GPa)^-1"
3470 PRINT @N:"C44 = ";K(4);" (GPa)    S23 = ";S(4);" (GPa)^-1"
3471 PRINT @N:"C55 = ";K(5);" (GPa)    S13 = ";S(5);" (GPa)^-1"
3472 PRINT @N:"C66 = ";K(6);" (GPa)    S12 = ";S(6);" (GPa)^-1"
3480 PRINT @N:" "
3490 PRINT @N:"VELOCITY DERIVATIVE DATA (GPa)^-1"
3500 PRINT @N:"  "
3510 PRINT @N:"1.  H122 = ";H(1,1);" +/- ";H(1,2)
3520 PRINT @N:"2.  H211 = ";H(2,1);" +/- ";H(2,2)
3530 PRINT @N:"3.  H322 = ";H(3,1);" +/- ";H(3,2)
3540 PRINT @N:"4.  H311 = ";H(4,1);" +/- ";H(4,2)
3550 PRINT @N:"5.  H121 = ";H(5,1);" +/- ";H(5,2)
3560 PRINT @N:"6.  H212 = ";H(6,1);" +/- ";H(6,2)
3570 PRINT @N:"7.  H312 = ";H(7,1);" +/- ";H(7,2)
3580 PRINT @N:"8.  H321 = ";H(8,1);" +/- ";H(8,2)
3590 PRINT @N:"9.  H123 = ";H(9,1);" +/- ";H(9,2)
3600 PRINT @N:"10. H213 = ";H(10,1);" +/- ";H(10,2)
3610 PRINT @N:"11. H323 = ";H(11,1);" +/- ";H(11,2)
3620 PRINT @N:"12. H313 = ";H(12,1);" +/- ";H(12,2)
3630 PRINT @N:"13. H131 = ";H(13,1);" +/- ";H(13,2)
3640 PRINT @N:"14. H232 = ";H(14,1);" +/- ";H(14,2)
3650 PRINT @N:"15. H132 = ";H(15,1);" +/- ";H(15,2)
3660 PRINT @N:"16. H231 = ";H(16,1);" +/- ";H(16,2)
3670 PRINT @N:"17. H011 = ";H(17,1);" +/- ";H(17,2)
3680 PRINT @N:"18. H022 = ";H(18,1);" +/- ";H(18,2)
3690 PRINT @N:"19. H012 = ";H(19,1);" +/- ";H(19,2)
3700 PRINT @N:"20. H021 = ";H(20,1);" +/- ";H(20,2)
3710 PRINT @N:"21. H013 = ";H(21,1);" +/- ";H(21,2)
3720 PRINT @N:"22. H023 = ";H(22,1);" +/- ";H(22,2)
3730 PRINT @N:"23. H031 = ";H(23,1);" +/- ";H(23,2)
3740 PRINT @N:"24. H032 = ";H(24,1);" +/- ";H(24,2)
3750 PRINT @N:" "
3760 PRINT @N:"THIRD ORDER ELASTIC CONSTANTS DERIVED FROM LEAST"
3770 PRINT @N:"SQUARES FIT AND MAX. ERROR AND PROB. ERROR (GPa)"
3780 PRINT @N:"  "
```

```
3790 PRINT @N:"C111 = ";C(1,1);" +/- ";C(1,2);" +/- ";C(1,3)
3800 PRINT @N:"C112 = ";C(2,1);" +/- ";C(2,2);" +/- ";C(2,3)
3810 PRINT @N:"C113 = ";C(3,1);" +/- ";C(3,2);" +/- ";C(3,3)
3820 PRINT @N:"C122 = ";C(4,1);" +/- ";C(4,2);" +/- ";C(4,3)
3830 PRINT @N:"C222 = ";C(5,1);" +/- ";C(5,2);" +/- ";C(5,3)
3840 PRINT @N:"C223 = ";C(6,1);" +/- ";C(6,2);" +/- ";C(6,3)
3850 PRINT @N:"C144 = ";C(7,1);" +/- ";C(7,2);" +/- ";C(7,3)
3851 PRINT @N:"C244 = ";C(8,1);" +/- ";C(8,2);" +/- ";C(8,3)
3852 PRINT @N:"C344 = ";C(9,1);" +/- ";C(9,2);" +/- ";C(9,3)
3853 PRINT @N:"C155 = ";C(10,1);" +/- ";C(10,2);" +/- ";C(10,3)
3854 PRINT @N:"C255 = ";C(11,1);" +/- ";C(11,2);" +/- ";C(11,3)
3855 PRINT @N:"C355 = ";C(12,1);" +/- ";C(12,2);" +/- ";C(12,3)
3856 PRINT @N:"C166 = ";C(13,1);" +/- ";C(13,2);" +/- ";C(13,3)
3857 PRINT @N:"C266 = ";C(14,1);" +/- ";C(14,2);" +/- ";C(14,3)
3858 PRINT @N:"C366 = ";C(15,1);" +/- ";C(15,2);" +/- ";C(15,3)
3860 PRINT @N:"C133,C233,C333,C123,C456 UNDETERMINED "
3870 PRINT @N:" "
3880 PRINT @N:"RECALCULATED VELOCITY DERIVATIVES USING FITTED TOEC'S"
3890 PRINT @N:"AND MAX. AND PROB. ERRORS IN SAME ORDER AS BEFORE"
3900 PRINT @N:"  "
3910 FOR I=1 TO 24
3920 PRINT @N:I;". ";H(I,3);" +/- ";H(I,4);" +/- ";H(I,5)
3930 NEXT I
3940 PRINT @N:"  "
3950 PRINT @N:"PERCENT DIFFERENCES, MAX. AND PROB. UNCERTAINTIES"
3960 PRINT @N:" "
3970 FOR I=1 TO 24
3980 PRINT @N:I;". ";V(I);T(I,1);T(I,2)
3990 NEXT I
3991 PRINT @N:"  "
3992 PRINT @N:"CONDITION # FOR INVERTING MATRIX IS: ";Z3
4000 RETURN
4010 END
```

REFERENCES

[1] F. D. Murnaghan, "Finite Deformation of an Elastic Solid," *Am. J. Math,* **49** (1937) pp. 235-260.

[2] F. Birch, "The Effect of Pressure Upon the Elastic Parameters of Isotropic Solids, According to Murnaghan's Theory of Finite Strain," *J. Appl. Phys.*, **9** (1938) pp. 279-288.

[3] M. Born, *Handbuch der Physik XXIV/2,* (Springer, Berlin, 1933) pp. 629-724.

[4] E. Madelung, *Zeits fur Physik* **11** (1910) p. 898.

[5] R. E. Green, Jr., "Ultrasonic Investigation of Mechanical Properties," *Treatise on Materials Science and Technology, Vol. 3,* H. Herman, ed., (Academic Press, New York, 1973) pp. 1-11, 73.

[6] A. A. Gedroits and V. A. Krasil'Nikov, "Finite Amplitude Elastic Waves in Solids and Deviations from Hooke's Law," *Soviet Physics J.E.T.P.*, **16** (1963) pp. 1122-1126.

[7] M. A. Breazeale and D. O. Thompson, " Finite Amplitude Ultrasonic Waves in Aluminum," *Appl. Phys. Let.*, **3** (1963) pp. 77-78.

[8] F. R. Rollins, Jr., "Interaction of Ultrasonic Waves in Solid Media," *Appl. Phys. Let.*, **2** (1963) pp.147-148.

[9] F. R. Rollins, Jr., L. H. Taylor, and P. H. Todd, Jr., "Ultrasonic Study of Three-phonon Interactions," *Phys. Rev.*, **136** (1964) pp. A597-A601.

[10] D. S. Hughes and J. L. Kelly, "Second Order Elastic Deformation of Solids," *Phys. Rev.*, **92** (1953) pp. 1145-1149.

[11] R. A. Toupin and B. Bernstein, "Sound Waves in Deformed Perfectly Elastic Materials, Acoustoelastic Effect," *J.A.S.A.*, **33** (1961) pp. 216-225.

[12] K. Brugger, "Thermodynamic Definition of Higher Order Elastic Coefficients," *Phys. Rev.*, **133** (1964) pp. A1611-A1612.

[13] K. Brugger, "Determination of Third-Order Elastic Coefficients in Crystals," *J. Appl. Phys.*, **36** (1965) pp. 768-773.

[14] R. N. Thurston and K. Brugger, "Third-Order Elastic Constants and the Velocity of Small Amplitude Elastic Waves in Homogeneously Stressed Media," *Phys. Rev.*, **133** (1966) pp.A1604-A1610.

[15] D. S. Hughes, E. B. Blankenship, and R. L. Mims, "Variation of Elastic Moduli and Wave Velocity with Pressure and Temperature in Plastics," *J. Appl. Phys.*, **21** (1950) pp. 294-297.

[16] H. J. McSkimin, "Measurement of Elastic Constants at Low Temperatures by Means of Ultrasonic Waves - Data for Silicon and Germanium Single Crystals, and for Fused Silica," *J. Appl. Phys.*, **24** (1953) pp. 988-997.

[17] H. J. McSkimin, "Use of High Frequency Ultrasound for Determining the Elastic Moduli of Small Specimen," Presented at the National Electronics Conference, 1956, Chicago, Illinois.

[18] J. Williams and J. Lamb, "On the Measurement of Ultrasonic Velocity in Solids," *J.A.S.A.*, **30** (1958) pp. 308-313.

[19] H. J. McSkimin, "Pulse Superposition Method for Measuring Ultrasonic Wave Velocities in Solids," *J.A.S.A.*, **33** (1961) pp. 12-16.

C-3

[20] J. E. May, Jr., *I. R. E. Nat. Conv. Rec.*, **6** (1958) pp. 134-142.

[21] E. P. Papadakis, "Ultrasonic Phase Velocity by the Pulse-Echo-Overlap Method Incorporating Diffraction Phase Corrections," *J.A.S.A.*, **42** (1967) pp. 1045-1051.

[22] E. P. Papadakis, "Absolute Accuracy of the Pulse-Echo-Overlap Method and the Pulse-Superposition Method for Ultrasonic Velocity," *J.A.S.A.*, **52** (1972) pp. 843-846.

[23] J. S. Heyman and Francis D. Stone, "Pulsed Phase Locked Loop Strain Monitor," *NASA Tech Briefs*, **6**, (1981) p. 68.

[24] J. S. Heyman and E. J. Chern, "Ultrasonic Measurement of Axial Stress," *J. of Testing and Evaluation*, **10** (1982) pp. 202-211.

[25] N. G. Einspruch and R. J. Manning, "Third-Order Elastic Moduli of Anisotropic Solids," *J. Appl. Phys.*, **35** (1964) pp.560-567.

[26] R. W. Benson and V. J. Raelson, "Acoustoelasticity," *Product Eng.*, **30** (1959) pp. 56-59.

[27] N. N. Hsu, "Acoustical Birefringence and the Use of Ultrasonic Waves for Experimental Stress Analysis," *Exp. Mech.*, **14** (1974) pp. 169-176.

[28] Y. Pao, W. Sachse, and H. Fukuoka, "Acoustoelasticity and Ultrasonic Measurements of Residual Stresses," *Physical Acoustics Vol. XVII.*, W. P. Mason and R. N. Thurston, ed., (Academic Press, New York, 1984) pp. 62-140.

[29] A. V. Clark, R. B. Mignona, and R. J. Sanford, "Acousto-elastic Measurement of Stress and Stress Intensity Factors Around Crack Tips," *Ultrasonics*, **21** (1983) pp.57-64.

[30] G. S. Kino, J. B. Junter, G. C. Johnson, A. R. Selfridge, D. M. Barnett, G. Hermann, and C. R. Steele, "Acoustoelastic Imaging of Stress Fields," *J. Appl. Phys.*, **50** (1979) pp. 2607-2613.

[31] J. S. Heyman, S. G. Allison, and K. Salama, "Influence of Carbon Content on Higher-Order Ultrasonic Properties in Steels," *IEEE Ultrasonics Symposium*, (1983) pp. 991-994.

[32] J. S. Heyman, and E. J. Chern, "Characterization of Heat Treatment in Aluminum Based on Ultrasonic Determination of the Second and Third Order Elastic Constants," *IEEE Ultrasonics Symposium*, (1981) pp. 936-939.

[33] H. Singh and A. W. Nolle, "Pressure Dependence of the Viscoelastic Behavior of Polyisobutylene," *J. Appl. Phys.*, **30** (1959) pp. 337-342.

[34] J. R. Assay, D. L. Lamberson, and A. H. Guenther, "Pressure and Temperature Dependence of the Acoustic Velocities in Polymethylmethacrylate," *J. Appl. Phys.*, **40** (1969) pp. 1768-1783.

[35] J. R. Assay, D. L. Lamberson, and A. H. Guenther, "Ultrasonic Technique for Determining Sound Velocity Changes in High-Loss Materials," *J.A.S.A.*, **45** (1969) pp. 566-571.

[36] D. L. Lamberson, Ph.D. dissertation, Air Force Institute of Technology, 1969.

[37] L. K. Zarembo and V. V. Shklovskaya-Kordi, "Generation of Harmonics During Propagation of Ultrasonic Longitudinal and Shear Waves in Solids," *Soviet Physics - Solid State*, **12** (1971) pp. 2960-2961.

[38] Y. Wada, A. Itani, T. Nishi, and S Nagai, "Gruneisen Constant and Thermal Properties of Crystalline and Glassy Polymers," *J. Poly. Sci.*, **7** (1969) pp. 201-208.

[39] D. L. Lamberson, J. R. Assay, and A. H. Guenther, "Equation of State of Polystyrene and Polymethylmethacrylate from Ultrasonic Measurements at Moderate Pressures," *J. Appl. Phys.*, **43** (1972) pp. 976-985.

[40] R. E. Hankey and D. E. Schuele, "Third Order Elastic Coefficients of Al_2O_3 ," *J.A.S.A.*, **48** (1970) pp. 190-202.

[41] E. H. Love, *On the Mathematical Theory of Elasticity,* (Cambridge University Press, New York, 1944).

[42] K. Brugger, "Pure Modes for Elastic Waves in Crystals," *J. Appl. Phys.*, **36** (1965) pp. 759-768.

[43] W. P. Mason, *Physical Acoustics and the Properties of Solids,* (Nostrand Co., Inc., Princeton, 1958) pp. 95-97.

[44] L. Y. Tu, J. N. Brennan, and J. A. Sauer, "Dispersion of Ultrasonic Pulse Velocity in Cylindrical Rods," *J.A.S.A.*, **27** (1955) pp. 550-555.

[45] R. D. Kriz and W. W. Stinchcomb, "Elastic Moduli of Transversely Isotropic Graphite Fibers and their Composites," *Experimental Mechanics,* **19** (1979) pp. 41-49.

[46] D. Hull, "An Introduction to Composite Materials," *Cambridge Solid State Science Series,* R. W. Cahn et al., ed., (Cambridge University Press, New York, 1981) p. 7.

[47] H. M. Ledbetter and D. T. Read, "Orthorhombic Elastic Constants of a NbTi/Cu Composite Superconductor," *J.A.P.*, **48** *(1977) pp. 1874-1879.*

[48] D. P. Garber, "Tensile Stress-Strain Behavior of Graphite/Epoxy Laminates," *NASA Contractor Report 3592 Contract NAS1-16000,* (1982) p. 21.

[49] J. H. Cantrell, Jr., "Anharmonic Properties of Solids from Measurements of the Stress Acoustic Constant," *J. of Testing and Evaluation,* **10** (1982) pp. 223-229.

Standard Bibliographic Page

1. Report No.	2. Government Accession No.	3. Recipient's Catalog No.
NASA CR-4100		

4. Title and Subtitle	5. Report Date
Ultrasonic Characterization of the Nonlinear Elastic Properties of Unidirectional Graphite/Epoxy Composites	October 1987
	6. Performing Organization Code
7. Author(s)	8. Performing Organization Report No.
William H. Prosser	
9. Performing Organization Name and Address	10. Work Unit No.
Center for NDE 102 Maryland Hall The Johns Hopkins University Baltimore, MD 21218	506-43-11-03
	11. Contract or Grant No.
	NGT 21-001-802
12. Sponsoring Agency Name and Address	13. Type of Report and Period Covered
National Aeronautics and Space Administration Langley Research Center Hampton, VA 23665-5225	Contractor Report
	14. Sponsoring Agency Code

15. Supplementary Notes

Langley Technical Monitor: Joseph S. Heyman
Final Report
The information presented in this report was offered as an essay in conformity with the requirements for the Master of Science in Engineering degree, The Johns Hopkins University, Baltimore, Maryland, March 1987.

16. Abstract

Because of their strength, stiffness, and light weight, fiber reinforced composite materials offer great potential for applications particularly in the aerospace industry. Early research has proven the usefulness of these materials, but the need to quantitatively characterize important material properties and develop applicable nondestructive evaluation techniques remains. Linear and nonlinear elastic properties are important physical properties in conventional materials in this respect. Nonlinear properties are important in the nondestructive determination of applied and residual stress as well as measuring the interatomic bonding forces in crystalline solids. Also, several investigations have established a possible relationship between nonlinear elastic properties and ultimate strength in aluminum and carbon steel.

This work presents the theoretical treatment of linear and nonlinear elasticity in a unidirectionally fiber reinforced composite as well as measurements for a unidirectional graphite/epoxy composite (T300/5208). Linear elastic properties were measured by both ultrasonic and strain gauge measurements. The nonlinear properties were determined by measuring changes in ultrasonic "natural" phase velocity with a pulsed phase locked loop interferometer as a function of stress and temperature. These measurements provide the basis for further investigations into the relationship between nonlinear elastic properties and other important properties such as strength and fiber-matrix interfacial strength in graphite/epoxy composites.

17. Key Words (Suggested by Authors(s))	18. Distribution Statement
Composites, Nonlinear Elasticity, Ultrasonic Velocity, Graphite/Epoxy, Nondestructive Tests	Unclassified - Unlimited Subject Category 24

19. Security Classif.(of this report)	20. Security Classif.(of this page)	21. No. of Pages	22. Price
Unclassified	Unclassified	198	A09

For sale by the National Technical Information Service, Springfield, Virginia 22161

NASA-Langley, 1987